Low-Complexity Multi-User MIMO Algorithms for mmWave WLANs

by

Khalid Aldubaikhy

A thesis
presented to the University of Waterloo
in fulfillment of the
thesis requirement for the degree of
Doctor of Philosophy
in
Electrical and Computer Engineering

Waterloo, Ontario, Canada, 2019

Examining Committee Membership

The following served on the Examining Committee for this thesis. The decision of the Examining Committee is by majority vote.

External Examiner:	Abdallah Shami Professor, Dept. of Electrical and Computer Engineering, Western University
Supervisor:	Xuemin (Sherman) Shen Professor, Dept. of Electrical and Computer Engineering, University of Waterloo
Internal Member:	Xiaodong Lin Adjunct Professor, Dept. of Electrical and Computer Engineering, University of Waterloo
Internal Member:	Zhou Wang Professor, Dept. of Electrical and Computer Engineering, University of Waterloo
Internal-External Member:	Raouf Boutaba Professor, David R. Cheriton School of Computer Science, University of Waterloo

Author's Declaration

I hereby declare that I am the sole author of this thesis. This is a true copy of the thesis, including any required final revisions, as accepted by my examiners.

I understand that my thesis may be made electronically available to the public.

Abstract

Very high throughput and high-efficiency wireless local area networks (WLANs) have become essential for today's significant global Internet traffic and the expected significant global increase of public WiFi hotspots. Total Internet traffic is predicted to expand 3.7-fold from 2017 to 2022. In 2017, 53% of overall Internet traffic used by WiFi networks, and that number is expected to increase to 56.8% by 2022. Furthermore, 80% of overall Internet traffic is expected to be video traffic by 2022, up from 70% in 2017. WiFi networks are also expected to move towards denser deployment scenarios, such as stadiums, large office buildings, and airports, with very high data rate applications, such as ultra-high definition video wireless streaming. Thus, in order to meet the predicted growth of wireless traffic and the number of WiFi networks in the world, an efficient Internet access solution is required for the current IEEE 802.11 standards.

Millimeter wave (mmWave) communication technology is expected to play a crucial role in future wireless networks with large user populations because of the large spectrum band it can provide. To further improve spectrum efficiency over mmWave bands in WLANs with large numbers of users, the IEEE 802.11ay standard was developed from the traditional IEEE 802.11ad standard, aiming to support multi-user MIMO. Propagation challenges associated with mmWave bands necessitate the use of analog beamforming (BF) technologies that employ directional transmissions to determine the optimal sector beam between a transmitter and a receiver. However, the multi-user MIMO is not exploited, since analog BF is limited to a single-user, single-transmission. The computational complexity of achieving traditional multi-user MIMO BF methods, such as full digital BF, in the mmWave systems becomes significant due to the hardware constraints. Our research focuses on how to effectively and efficiently realize multi-user MIMO transmission to improve spectrum efficiency over the IEEE 802.11ay mmWave band system while also resolving the computational complexity challenges for achieving a multi-user MIMO in mmWave systems.

This thesis focuses on MAC protocol algorithms and analysis of the IEEE 802.11ay mmWave WLANs to provide multi-user MIMO support in various scenarios to improve the spectrum efficiency and system throughput. Specifically, from a downlink single-hop

scenario perspective, a VG algorithm is proposed to schedule simultaneous downlink transmission links while mitigating the multi-user interference with no additional computational complexity. From a downlink multi-hop scenario perspective, a low-complexity MHVG algorithm is conducted to realize simultaneous transmissions and improve the network performance by taking advantage of the spatial reuse in a dense network. The proposed MHVG algorithm permits simultaneous links scheduling and mitigates both the multi-user interference and co-channel interference based only on analog BF information, without the necessity for feedback overhead, such as channel state information (CSI). From an uplink scenario perspective, a low-complexity user selection algorithm, HBF-VG, incorporates user selection with the HBF algorithm to achieve simultaneous uplink transmissions for IEEE 802.11ay mmWave WLANs. With the HBF-VG algorithm, the users can be selected based on an orthogonality criterion instead of collecting CSI from all potential users. We optimize the digital BF to mitigate the residual interference among selected users. Extensive analytical and simulation evaluations are provided to validate the performance of the proposed algorithms with respect to average throughput per time slot, average network throughput, average sum-rate, energy efficiency, signal-to-interference-plus-noise ratio (SINR), and spatial multiplexing gain.

Acknowledgments

My unreserved gratitude and praises are for Allah, the Most Compassionate and the Most Merciful. He has blessed me with his bounties, and He has given me the strength and courage to reach my goals during the course of this research.

I would like to express my deepest and sincerest gratitude to my supervisor, Professor Xuemin (Sherman) Shen, for his continuous guidance, inspiration, deep insight, invaluable advice, and support during my graduate studies at the University of Waterloo. His guidance and encouragement have inspired and motivated me throughout the completion of this thesis, and he has made my experience at the Broadband Communications Research (BBCR) Group worthwhile and enjoyable. I would also like to thank the examining committee members of this thesis, Professor Xiaodong Lin, Professor Zhou Wang, and Professor Raouf Boutaba. Their insightful comments have significantly improved the quality and presentation of my work. In addition, I would like to thank Professor Abdallah Shami for serving as my thesis external examiner and for his insights on my thesis with me.

Special thanks are due to my friends and colleagues at the BBCR group for their support and kindness, and for making my stay memorable. I would like to express special gratitude to Dr. Hassan Omar, Dr. Jian Qiao, Dr. Miao Wang, Dr. Ning Zhang, Dr. Qinghua Shen, Dr. Nan Cheng, Dr. Nizar Alsharif, Dr. Mohammed Alhasani, Dr. Omar Alhussein, Dr. Hesham Moussa, Dr. Manaf Ben-Yahya, and Dr. Wen Wu.

With great appreciation, I acknowledge the scholarship and financial support from my employer, Qassim University in the Kingdom of Saudi Arabia, for granting me the scholarship and giving me the opportunity to enhance my experience and education. Acknowledgment is also extended to the Saudi Cultural Bureau in Canada for their assistance. They have been very helpful in the administration of my scholarship during my academic journey in Canada.

Finally, my greatest thanks to my devoted parents, Ali Aldubaikhy and Latifah Alfallaj, my brothers, and my sisters, all of whom have constantly given me love, support, motivation, and sincere prayers. Last, but certainly not least, I would like to thank my beloved wife, Haifa Alsuwayyid, for her love, patience, and continued encouragement she

has provided me during my graduate study. Special thanks also go to my children, Faris and Judy, who fill my life with joy and happiness. Nothing would have been possible without Allah, the Creator and Lord of the universe, and my family support.

Dedication

This work is dedicated to my beloved parents, wife, children, and siblings for giving me love, support, and encouragement.

Table of Contents

List of Tables

List of Figures

Abbreviations

5G fifth-generation

A-BFT association beamforming training

ACK acknowledgement

ADC analog-to-digital converter

AP access point

ATI announcement transmission interval

AWV antenna weight vector

BC beam-combining

BF beamforming

BI beacon interval

BRP beam refinement protocol

BSS basic service set

BTI beacon transmission interval

CBAP contention-based access period

CCI co-channel interference

CN client-node

CSI channel-state information

CTS clear-to-send

D2D device-to-device

DAC digital-to-analog converter

DMG directional multi-gigabit

DN distribution-node

DTI data transfer interval

EDMG enhanced directional multi-gigabit

EDMG enhanced directional multi-gigabit

FTTx fiber-to-the x

FWA fixed wireless access

GP Grant period

GT guard time

HBF hybrid beamforming

I-TXSS initiator-transmit-sector-sweep

ID identification

IoT Internet of things

ISS initiator sector sweep

LOS line-of-sight

MAC medium access control

mDN mmWave distribution network

MHVG multi-hop virtual grouping

MID multiple-sector-identification-detection

MIDC multiple-sector-identification-detection and beam-combining

MIMO multiple-input multiple-output

mmWave millimeter wave

MUI multi-user interference

NLOS non-line-of-sight

OFDMA orthogonal frequency division multiple access

P2MP point-to-multipoint

P2P point-to-point

POP point-of-presence

PP polling period

QAM quadrature amplitude modulation

QoS quality of service

R-TXSS responder-transmit-sector-sweep

RF radio frequency

RSS responder sector sweep

RTS request-to-send

RX receiver

RXSS receive-sector-sweep

SID sector identification

SINR signal-to-interference-plus-noise ratio

SLS sector-level sweep

SNR signal-to-noise ratio

SP scheduled-service period

SSW sector sweep

TDD time division duplex

TDMA time-division multiple access

TX transmitter

TXOP transmission opportunity

TXSS transmit-sector-sweep

VG pre-defined virtual grouping

VS virtual sector

WLAN wireless local area network

WPAN wireless personal area network

WTTB wireless-to-the-building

WTTH wireless-to-the-home

ZF zero-forcing

Chapter 1

Introduction

In the foreseeable future, emerging data-hungry applications and the proliferation of wireless devices will substantially increase wireless data traffic. According to a report by Cisco [1], Internet traffic is predicted to expand 3.7-fold from 2017 to 2022, with 80% expected to be used by video traffic by 2022, up to 70% in 2017. Moreover, 53% of total Internet traffic was used by the current IEEE 802.11 wireless local area networks (WLANs) and is expected to be 56.8% by 2022. Thus, an efficient Internet access solution to the current IEEE 802.11 WLANs standards is required in order to meet the predicted growth of Internet traffic. In order to provide high-efficiency WLANs, there have been developments made to IEEE 802.11 WLANs. The IEEE 802.11ay is an enhanced WLAN standard that operates in the 60 GHz millimeter wave (mmWave) spectrum, which was developed based on modifications to the legacy IEEE 802.11ad standard. The IEEE 802.11ay standard aims to improve the spectrum efficiency and system throughput by supporting several technologies, such as multi-user multiple-input multiple-output (MIMO) and multi-channel operations [2, 3].

To satisfy the need for such an exponentially larger throughput gain, a number of advanced technologies will fall within the scope of academic and industrial research. MmWave

band communication resulting from a large spectrum swath is one potential solution that can provide multi-gigabit data-rate service for mobile devices. MmWave communication refers to a wireless system that transmits and receives signals using a band spectrum between 30 GHz and 300 GHz, with the system wavelength being in the millimeter range. The propagation characteristics of an mmWave, such as the high degree of path loss, mean that short-range directional transmission with the use of analog beamforming (BF) and beam tracking technologies must be considered in the design of medium access control (MAC) protocols. Analog BF is employed to conquer high path loss and select the best beam-sector pair between a transmitter (TX) and receiver (RX). In this way, mmWave communication can be exploited so that future WLANs can supply the predicted growth of wireless traffic.

To further improve spectrum efficiency over mmWave bands in WLANs with a large number of users, the massive MIMO available in the mmWave systems can be exploited to utilize a downlink multi-user MIMO technology. Current mmWave systems, such as the IEEE 802.11ad standard, are limited to single-stream transmissions and are considered single-user mmWave systems. Due to the narrow beams of mmWave directional antennas, simultaneous transmissions are possible based on the employment of a spatial reuse mechanism. Although multi-user MIMO is a promising technology, the user selection algorithm and BF mechanism need to be considered in an mmWave system with a large user population.

MmWave MIMO precoding for BF and multi-user transmission scenarios differs from that used with lower frequencies, since different hardware constraints are associated with mmWave bands, and require rethinking the MAC layer design and transceiver architectures. Implementing a fully digital BF is also complicated in mmWave systems. Digital BF requires a dedicated baseband, radio frequency (RF) hardware for each antenna element, and the acquisition of channel-state information (CSI). The IEEE 802.11ad standard involves only analog BF due to the significant power consumption of the analog-to-digital

converters (ADCs) in digital BF as well as the overhead associated with the CSI feedback of the digital BF in the mmWave. Enabling a simple multi-user transmission that employs, for example, only analog BF is desirable for facilitating future mmWave communication systems.

In this chapter, we first provide an overview of the mmWave technology and introduce the IEEE 802.11ay standard. Then, we discuss the research challenges of this thesis and our research objectives. Finally, we present the research contribution and an outline of this thesis.

1.1 MmWave

The mmWave band spectrum refers to the range of wavelengths from 1 to 10 millimeters (mm). The radio frequency range of these wavelengths is between 30 GHz and 300 GHz, referred to as the extremely high-frequency band, while the 3-30 GHz spectrum band is called the super high-frequency band. Since the wavelength of the mmWave is in the range of 1 to 10 mm, the mmWaves are shorter than radio waves or microwaves, for instance. However, they are longer than infrared waves or x-rays.

1.1.1 MmWave Channel Challenges and Characteristics

Although the mmWave wireless communication system is a very promising candidate for the next generation of wireless networks, the propagation characteristics of the mmWave create challenges. The main challenges regarding signal attenuation include free space propagation (path loss), atmospheric gaseous, and rain absorption. Other factors that affect the mmWave propagation are foliage blockage, scattering effects, low diffraction around obstacles, and penetration through objects [4].

1.1.1.1 Path Loss

The Friss transmission law in equation (1.1) indicates that the high carrier frequency of the mmWave communications will be affected by high path loss, because the path loss increases with the square of the wavelength (λ^2), the carrier frequency. However, high path loss will be realized assuming that the effective antenna aperture area increases with the wavelength. Therefore, more energy can be sent or received through narrow directed beams by applying array antennas into the same effective area at higher frequency carriers. It was found in [5] that the propagation loss is the same for both 3 GHz and 30 GHz carriers. Furthermore, the received power was found to be 20 dB when array antennas were used at 30 GHz, which is higher than the received power of the 3 GHz.

$$\frac{P_r}{P_t} = G_t \, G_r \, (\frac{\lambda}{4\pi R})^2 \tag{1.1}$$

where P_t and P_r are the transmitted and received power, respectively; G_t and G_r are the transmitter and receiver antenna gain, respectively; R is the distance between the transmitter and receiver in meters; and λ is the wavelength.

1.1.1.2 Atmospheric Gaseous

Atmospheric gaseous losses are the other type of signal attenuation for the mmWave transmission. These losses are due to the absorption of oxygen (O_2) molecules, water vapor (H_2O), and some other gaseous atmospheric elements. Fig. 1.1 shows the atmospheric absorption versus the frequency at altitudes of 4 km and at sea level [4, 6]. There are several attenuation peaks for different frequency bands because of the absorption of the radio signal by water vapor (H_2O) and oxygen (O_2). These peaks, such as 24 GHz and 60 GHz, will cause a high attenuation of the radio signal by reducing the propagation distance. However, less radio signal attenuation can be achieved in the other spectral regions of the

mmWave. The attenuation at the 57-64 GHz band for O_2 absorption is approximately 15 dB/km whereas at 28 GHz it is only 0.02 dB/km for the O_2 absorption and 0.09 dB/km for the H_2O absorption [4, 6].

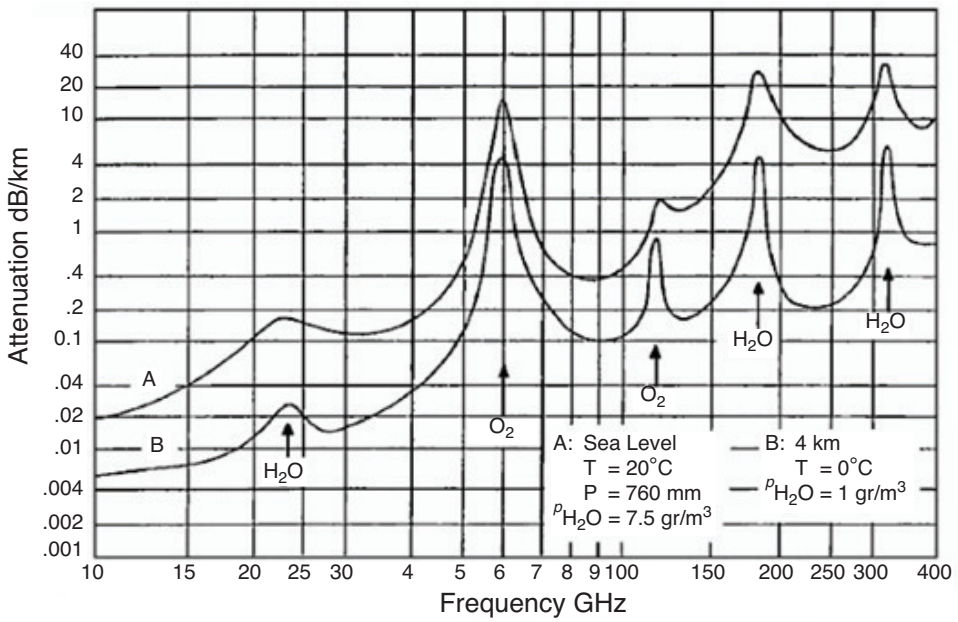

Figure 1.1: Average atmospheric absorption of mmWave.

1.1.1.3 Rain Losses

Another propagation characteristic challenge is rain losses, since the mmWave propagation suffers from rain absorption [4]. Raindrops cause the radio signal to scatter because the wavelength is approximately the same size as the raindrops. Fig. 1.2 shows the attenuation of rain in different rainfall rates [4]. For example, during heavy rainfall of 25 mm/hr, the rain attenuation is found to be about 7 and 10 dB/km for 28 GHz and 73 GHz, respectively. Nevertheless, it was found in [7] that the rain attenuation for the 28 GHz and 73 GHz are reduced to 1.4 and 2 dB/km, respectively, when considering a small-cell base station in the order of 200 m. Therefore, array antennas, spectral regions that have less gaseous losses,

and small-cell base stations or access points, especially in urban environments, might be promising future solutions for mmWave propagation due to the minimal impact of the free space propagation (path loss), atmospheric gaseous losses, and rain absorption.

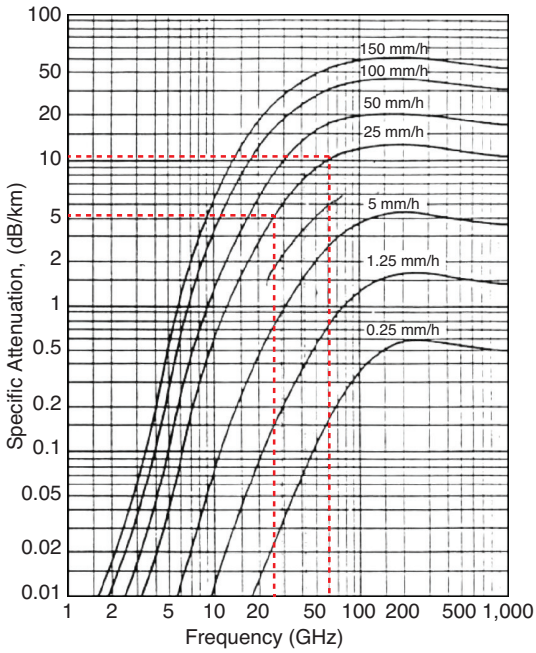

Figure 1.2: Rain attenuation in dB/km at various rainfall rates in mm/h.

1.1.2 MmWave and Multi-User Massive MIMO

Thanks to the very short mmWave wavelength, massive MIMO technology using large-scale antenna arrays can be implemented using BF and beam tracking technologies. In fact, massive MIMO is considered one of the enabling technologies for next-generation wireless systems, which has a higher spectrum and higher energy efficiency and will be secure and robust. Antenna arrays with a large-scale of antennas are used simultaneously in the massive MIMO in order to serve several terminals in the same time-frequency resource [8]. There are several benefits of the multi-user massive MIMO. These specific benefits include,

but are not limited to, the following [8]: (1) the capacity can be increased 10 times or more by using the multi-user MIMO; (2) the radiated energy efficiency can be improved by an order of 100; (3) multi-user MIMO has the advantage of low power and inexpensive components compared to conventional systems; and (4) the fading dips of wireless communications can be avoided with the BF technique and the law of large numbers of antennas of the massive MIMO. Thus, the latency on the air interface will be significantly reduced, since the performance is usually restricted by fading.

1.1.3 MmWave for Outdoor Communications

The challenges associated with the propagation characteristics of mmWaves present a serious obstacle to its implementation in outdoor applications. The small coverage area of a node that uses mmWave, such as small cell base station concept, is considered to have promising potential with respect to ensuring the efficiency of future wireless networks. A small mmWave node can be employed outdoor in an urban area by reducing the node coverage area, thereby exploiting spatial reuse, decreasing propagation losses, and increased data rate [7]. The deployment of the small mmWave node, in the order of 200 m, thus overcomes the issues related to the propagation characteristics of mmWaves [7]. Additionally, the very short wavelengths of mmWave technology enable the use of a small physical platform of several to hundreds of antenna array elements in a relatively smaller coverage. Both an mmWave node and a user can be equipped with a highly directional antenna to provide mmWave communication while simultaneous transmissions at an mmWave node can also be achieved. Thus, directional antennas and small mmWave nodes have the potential to provide effective solutions for addressing mmWave propagation challenges in outdoor applications [7, 9].

1.1.4 MmWave for Next Generation of WiFi

There are challenges for WLANs overcoming global data traffic growth, as driven by the emergence of the different bandwidth-intensive multimedia applications and the growth in the number and density of WiFi networks [10, 11]. Although there are efforts to support higher data rates in the current WLANs standards, massive data rate requirements are always required because of the emergence of different bandwidth-intensive multimedia applications and the need to access the Internet. Because of the exponential growth in global wireless data traffic and the large increase in the number of users every year, the current WiFi standards need to be enhanced to provide specifications for high-efficiency WLANs. Data rates up to gigabit-per-second are essential to support the significant increase in wireless data traffic. MmWave wireless communication technology is expected to play an essential role in the next generation of wireless systems because of the very large bandwidth allocations it can provide [7, 12, 13, 14]. This available bandwidth will deliver high-quality, low-latency video and multimedia applications by supporting higher connection speeds and higher traffic capacity to WLANs.

1.2 IEEE 802.11ay

The IEEE 802.11ay standard [2] is an advanced communication system that operates on the unlicensed 60 GHz band to enhance the user experience, in indoor and outdoor communications implementations where point-to-point (P2P) and point-to-multipoint (P2MP) are considered. The IEEE 802.11ay standard has been established to improve the legacy 802.11ad standard while guaranteeing backward compatibility for legacy users. The IEEE 802.11ay standard utilizes BF training and specific directional MAC, where multi-user MIMO and channel bonding and aggregation are supported to improve the spectrum efficiency and system throughput.

1.2.1 Channel Bonding and Aggregation

The 802.11ay [2] specifies up to six 2.16 GHz channels in the unlicensed 60 GHz frequency band. The center frequencies of these channels are 58.32, 60.48, 62.64, 64.80, 66.96, and 69.12 GHz. To enhance the channel utilization and achieve significant throughput gain, the IEEE 802.11ay standard supports the multi-channel approach by transmitting data over channels simultaneously [2, 15, 16]. The multi-channel transmission is not supported in the legacy IEEE 802.11ad even though coordinated channel access allocation is established to maintain a good quality of service (QoS). Channel bonding and aggregation are utilized to create a wider channel from multiple channels by combining two or more channels of 2.16 GHz. The difference between the two is that channel bonding combines two or more adjacent channels that have no channel spacing, while channel aggregation combines two or more adjacent or non-adjacent channels that are separated by a space. Users with enhanced directional multi-gigabit (EDMG) ability can use channel bandwidths containing 4.32, 6.48, or 8.64 GHz by combining two, three, or four 2.16 GHz channels, respectively. Therefore, EDMG users can utilize an aggregated or bonded channel to realize the required high transmission rate of the 802.11ay (at least 20 Gbps).

1.2.2 MIMO Channel Access

Another mechanism that can be combined with the multi-channel transmission is the MIMO channel access for the sake of realizing the required 20 Gbps or more. The IEEE 802.11ay standard can support the downlink multi-user MIMO to enable simultaneous transmissions for multiple users such that the spatial reuse and transmission robustness against link outages can be enhanced [2, 15, 16]. MIMO channel access can be initiated by checking the channel availability, where a TX and one or more RXs exchange request-to-send (RTS) and clear-to-send (CTS) frames among each other. In this process, a transmission opportunity (TXOP) must be gained first by the TX before accessing the

MIMO channel when either single-user MIMO or multi-user MIMO frames are intended to be sent. To enable MIMO channel access, physical carrier sensing, virtual carrier sensing, or clear channel assessment are implemented with specific MIMO backoff procedure. Thus, a TX is permitted to gain a TXOP for a downlink multi-user MIMO transmission when all the MIMO beams are sensed to be idle while the backoff procedure is satisfied. Multi-user MIMO can be achieved by employing an appropriate scheduling approach to select the perfect spatial users. The multi-user MIMO technique is considered in the upcoming IEEE 802.11ay standard to increase the throughput and reduce the BF operation time [17, 18, 19, 20].

1.2.3 Directional MAC

The IEEE 802.11ay directional MAC protocol includes a beacon interval (BI) access time that has four main components, where the functions of each are described as follows. First, during the beacon transmission interval (BTI), the BF training can be initiated by an access point (AP), where an Announce frame or EDMG-Beacon is transmitted. Second, during the association beamforming training (A-BFT), the BF training can be completed by users utilizing A-BFT slots. The number of A-BFT slots in IEEE 802.11ay is increased up to 16 slots using the extended A-BFT mechanism or up to 48 slots utilizing the multi-channel A-BFT method [2, 16]. Third, during the announcement transmission interval (ATI), exchanges in the request-response-based management and allocation information can be announced. Finally, during the data transfer interval (DTI), slot allocations are established by using either contention-based access periods or scheduled-service periods (SPs). Time division duplex (TDD) channel access allocation (TDD-SP) is another type of allocation that is utilized for the mmWave distribution network (mDN) use case during the DTI.

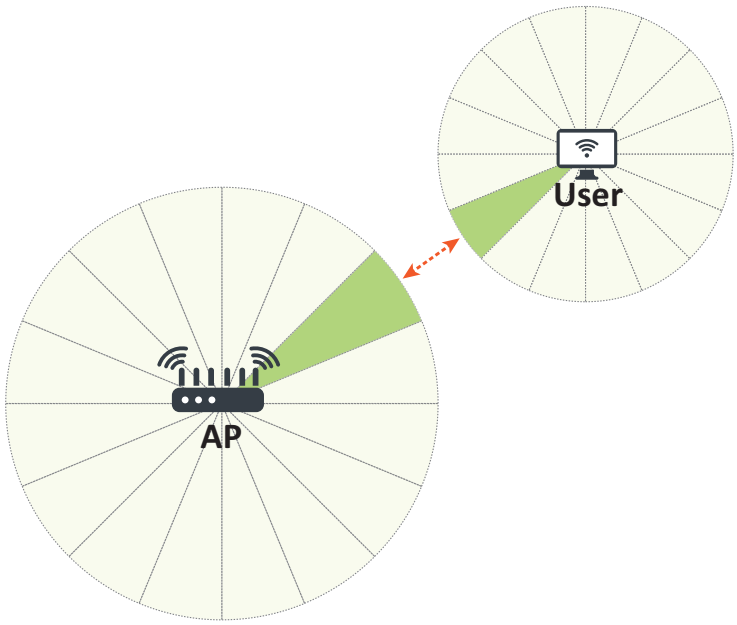

Figure 1.3: Virtual antenna sectors of the IEEE 802.11ay standard.

1.2.4 BF Training

BF training is utilized to establish a communication link between a TX and an RX in order to overcome the challenges that result from the directional transmission. The BF allows paired devices to have a highly directional signal focus by employing virtual antenna sectors using different antenna weight vectors (AWVs), where the antenna gain is focused in a certain direction based on the sector identification (SID), as shown in Fig. 1.3.

The IEEE 802.11ay BF training is similar to that of the legacy 802.11ad, except that it includes new stages that enhance the BF process. BF for multi-channel, BF for asymmetric links, BF for MIMO, and BF for the TDD channel access are the new BF training protocols, where the basic BF training of IEEE 802.11ay is a sector-level sweep (SLS) BF stage.

1.3 Research Challenges and Objectives

The objective of this thesis is to develop a set of efficient MAC layer algorithms in different scenarios for the mmWave WLANs based on the IEEE 802.11ay system in order to meet the very high throughput objective of the next generation wireless networks and to overcome the predicted global data traffic growth. Specifically, MAC layer algorithms are used to enable simultaneous transmission and mitigate the interference while keeping the computational complexity at a minimum level. In order to meet the objective, we aim to address the challenges of the simultaneous transmission for the IEEE 802.11ay WLANs in the following scenarios.

1.3.1 Single-Hop Multi-User Transmission: MUI Perspective

As discussed in Subsection 1.1.1, due to the nature of mmWave propagation characteristics, establishing effective communication and simultaneous downlink transmissions with mmWave requires a directional analog BF with large antenna arrays. However, analog BF is limited to single-user transmission, and multiplexing several data streams for different users cannot be achieved. Thus, a key consideration is to employ an appropriate BF mechanism to achieve simultaneous downlink transmission. The use of the digital BF for multi-user MIMO technology that has been widely applied in conventional lower-frequency systems (<6 GHz) is challenging in mmWave systems, since digital processing requires dedicated baseband and RF hardware for each antenna element [21, 22]. Because mmWaves entail a considerable number of antenna array elements, the implementation of a vast number of RF chains can be costly. Further, designing the precoding matrices in a digital BF requires acquiring CSI. However, obtaining CSI in an mmWave system is difficult because of the large number of antennas and the very low SNR [21, 22]. Hybrid beamforming (HBF), which combines digital BF with analog BF, can reduce the complexity of the hardware

constraints to realize simultaneous downlink transmission [23, 24, 21]. Although HBF is proposed for multi-user MIMO to mitigate the multi-user interference (MUI) and to realize simultaneous downlink transmission in mmWave systems, digital processing in HBF is still challenging for the following reasons [21]:

- CSI feedback overhead increases with the number of antennas and the number of users. Imperfect channel knowledge can affect performance because multi-user MIMO with mmWaves requires more CSI at the transmitter, where HBF performance gain is achievable only with perfect knowledge of the CSI at the transmitter [22].
- Digital precoding schemes, such as zero-forcing, require very frequent sounding and feedback because of the short wavelength of mmWaves.
- The signal-to-noise ratio (SNR) received over an mmWave channel is very low because the bandwidth of an mmWave is very large.
- Performing channel estimation is difficult because part of the precoder in an HBF is RF precoding.

Since the IEEE 802.11ay standard implements directional beams for transmission due to the characteristics of the mmWave band, simultaneous transmission can be achieved due to the potential spatial reuse, where the most desirable spatial users can be scheduled for simultaneous downlink transmissions. Thus, an appropriate scheduling scheme for the simultaneous downlink transmission is needed to overcome this challenging problem and to improve the system efficiency while keeping the overhead at a minimum level.

1.3.2 Multi-Hop Multi-User Transmission: CCI Perspective

In the foreseeable future, emerging data-hungry applications and the proliferation of wireless devices will substantially increase wireless data traffic. Wireless networks are expected

to move toward denser deployment scenarios, such as stadiums, large office buildings, and airports, with very high data rate applications, such as ultra-high definition video wireless streaming [10, 11].

Maintaining efficient utilization of ultra-dense wireless networks requires spatial and spectrum reuse, which negatively affects the end-user experience at coverage boundaries due to co-channel interference (CCI) [25, 26, 27]. Since wireless devices are increasingly deployed in dense environments that are characterized by several APs, the CCI between neighboring devices could reduce the performance experienced by individual users. CCI and adjacent channel interference may cause either transmission delays or even transmission failure, and network performance can be affected due to the high density of wireless devices. CCI occurs when multiple APs are employed utilizing the same frequency channel in dense deployment environments, where neighboring APs' coverage can overlap.

Although the directional beam transmissions of the mmWave have the advantage of spatial reuse with a very small chance of interference [28], there is a possibility of CCI among neighboring APs and therefore needs to be managed. It is worth noting that to mitigate the CCI using traditional lower frequency systems, numerous mechanisms have been proposed in the literature, mainly using digital BF methods such as zero-forcing BF [29]. Nevertheless, for mmWave communications, these methods introduce significant overhead and extreme computational complexity [21, 22]. The size of the channel state information feedback increases with the number of antennas and the number of devices. Furthermore, extra antennas are needed on each TX node for digital BF to mitigate the CCI.

In the densely deployed and partially overlapped WLANs, CCI challenges resulting from neighboring APs needs to be addressed by carefully planning and tuning the network. New and efficient, low-complexity methods for managing interference and radio resources must be developed for ultra-dense IEEE 802.11ay WLANs. How to mitigate interference

in different neighboring APs' coverage to allow for spatial reuse while simultaneously performing transmissions is an important and challenging issue.

1.3.3 Low-Complexity Uplink Multi-User MIMO Algorithm

MmWave communication technology is expected to play a crucial role in future wireless networks with large user populations because of the large spectrum band it can provide [16, 7, 30, 31, 32]. To further improve spectrum efficiency over mmWave bands in WLANs with a large number of users, the IEEE 802.11ay standard was developed from the traditional IEEE 802.11ad standard, aiming to support multi-user MIMO. Moreover, network throughput can be improved significantly by using uplink multi-user MIMO transmissions in ultra-dense networks. Although uplink multi-user transmission is a promising technology, both the user selection algorithm and the BF mechanism need to be considered in an mmWave system with a large user population.

User selection in large-scale multi-user MIMO is crucial due to the MUI and the potential collection of CSI to find the best group of users [33, 34]. In particular, the orthogonality of the instantaneous channels among selected users can affect the achievable rates where the users are coupled [35, 36, 37, 38]. The literature has used several criteria for user selection or user grouping to solve the problem of selecting a subset of users. An explicit solution is to find an optimal subset of users by deploying an exhaustive search over all users. However, in dense deployment scenarios, this requires formidable CSI overhead, and its complexity can grow significantly with the number of users. Other criteria [35, 36, 37] have been used to simplify the user selection problem into sub-optimal algorithms by utilizing the orthogonality criterion as a selection metric, such as the largest principal angle [39], subspace collinearity [40], and chordal distance [41]. Thus, user selection is essential in multi-user MIMO, especially when the number of users is large.

Employing traditional digital BF in an mmWave system is challenging due to high

feedback overhead and the power consumption of the mixed signal processing components [42, 24]. A potential solution is to exploit the concept of HBF in the mmWave systems by combining analog BF and digital BF. The literature proposes several approaches that split the BF process into two stages, analog BF and digital BF optimization, to simplify finding a joint optimal solution in the HBF [24, 23, 43, 44, 45, 46]. However, the existing HBF algorithms do not consider the user selection algorithm, even though the user selection needs to be jointly considered with the HBF algorithm when there is a high number of users. Thus, computational complexity can be significant in dense deployment scenarios. Specifically, there can be high power consumption due to the increased demand for RF chains, with the number of simultaneous transmissions limited to the RF chain number. The assumption that the system can serve users up to the total number of RF chains without considering user selection to maximize the data rate is not realistic in an mmWave system with a large number of users. Also, CSI acquisition overhead from all the potential users can be considerable. Even though there have been substantial research efforts on existing HBF algorithms, to the best of our knowledge, the user selection algorithm in dense user scenarios has not been incorporated into the HBF algorithm for uplink multi-user MIMO mmWave systems.

1.4 Research Contributions

The main contributions of this thesis are as follows:

- **Single-Hop Multi-User Transmission: MUI Perspective:** We propose a practical and efficient MAC protocol algorithm for IEEE 802.11ay in densely deployed WLAN scenarios to achieve simultaneous downlink transmission. Specifically, in order to mitigate the MUI generated from the simultaneous downlink transmissions and to avoid collecting the CSI matrices, a pre-defined virtual grouping (VG) al-

gorithm is proposed to select the perfect spatial users based on the information of the best SID of the analog BF. The backward compatibility with the legacy IEEE 802.11ad standard is maintained in the proposed VG algorithm. Two methods for the downlink transmission are developed for the proposed VG algorithm to realize and select the simultaneous users without the necessity for feedback overhead, such as CSI. A signal-to-interference-plus-noise ratio (SINR) evaluation from the point of view of the directed beam-width angle of each simultaneous link is conducted to investigate the successful simultaneous transmission. We demonstrate via simulation that the proposed VG algorithm can considerably improve the average throughput and save on transmission time allocation without adding extra feedback overhead to the system.

- **Multi-Hop Multi-User Transmission: CCI Perspective:** We propose a low-complexity simultaneous downlink scheduling algorithm to enhance the network performance while mitigating the interference by taking advantage of the spatial reuse in a dense mDN. Specifically, a multi-hop virtual grouping (MHVG) algorithm is proposed to expand the VG algorithm in the first scenario to cancel both the MUI within a single hop and the CCI generated from the multi-hop simultaneous downlink transmissions scenario. The MHVG algorithm focuses on exploiting spatial reuse while mitigating the interference by utilizing the analog BF information without the need for digital BF, where the complexity and overhead are kept at minimum levels. We evaluate the performance of the MHVG algorithm by analyzing the spatial multiplexing gain. The spatial multiplexing gain represents the number of concurrent transmissions allowed over the same mmWave channel in a given area from the perspective of spatial reuse. The results of the evaluative simulations conducted demonstrate the superior performance offered by the proposed MHVG algorithm with respect to average throughput per time slot and spatial multiplexing gain.

- **Low-Complexity Uplink Multi-User MIMO Algorithm:** We propose a low-complexity user selection algorithm for an uplink multi-user transmission in mmWave WLAN. We first formulate the user selection problem, taking HBF, an NP-hard problem, into consideration. We then develop a three-step HBF algorithm, denoted by HBF-VG, that incorporates user selection. Specifically, users can be selected based on the semi-orthogonality criterion of the VG algorithm instead of collecting CSI from all potential users. We optimize the digital BF to mitigate residual interference among the selected users. Furthermore, we provide analytical validation for the proposed user selection algorithm and study the impact of angle correlation, analog beam pattern, and beamwidth on the achievable rate of selected users. We then analyze the computational complexity of the proposed algorithm in comparison with the optimal user selection solution. We also evaluate the energy efficiency performance of the proposed HBF-VG algorithm and examine the effect of the RF chains implementation. Extensive simulations validate the performance of the proposed HBF-VG algorithm when compared with existing solutions.

1.5 Thesis Outline

The remainder of this thesis is organized as follows: Chapter 2 presents the preliminaries and introduces a comprehensive overview of related literature on simultaneous transmission and mmWave wireless communications. In Chapter 3, we present the proposed VG algorithm designed to achieve simultaneous downlink transmission for mmWave WLANs. In Chapter 4, we present the second algorithm, the MHVG, where simultaneous downlink transmission is considered in a multi-hop scenario. In Chapter 5, we present our third algorithm, the HBF-VG, where a low-complexity user selection algorithm for an uplink multi-user transmission in mmWave WLAN is proposed. Finally, Chapter 6 concludes the thesis and introduces the future research directions relevant to the work in this thesis.

Chapter 2

Background

This chapter introduces BF and simultaneous transmission in mmWave systems. First, we review BF mechanisms and the mDN use case of the IEEE 802.11ay standard that we leverage to design the proposed algorithms. Then, we comprehensively survey the literature on BF and simultaneous transmission in mmWave systems.

2.1 IEEE 802.11ay BF Background

Since this thesis aims to enhance throughput and improve spectrum efficiency over the mmWave band based on the upcoming IEEE 802.11ay standard, the following subsections review the BF mechanisms of IEEE 802.11ay in detail.

2.1.1 DMG BF Mechanisms

A pair of devices employ an analog BF mechanism to achieve an appropriate directional multi-gigabit (DMG) link budget by finding the optimal sector beam between each other.

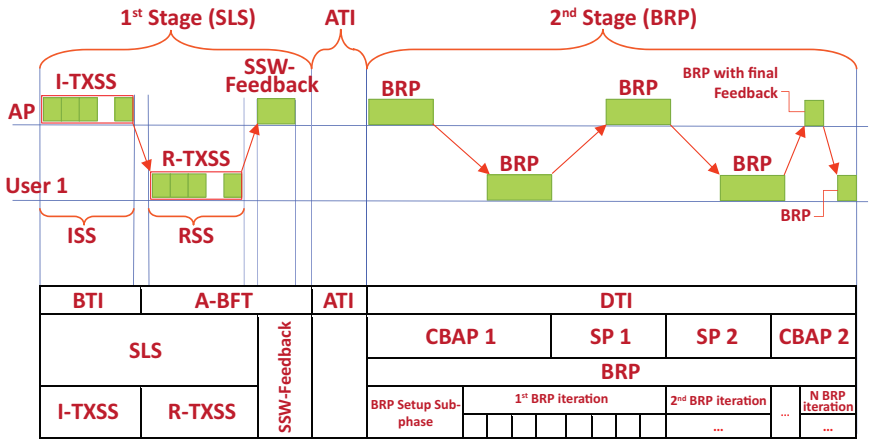

Figure 2.1: The BF training procedure of the IEEE 802.11ay.

In order to allow each device to resolve a proper AWV setting, BF training is used bidirectionally for both transmission and reception. In IEEE 802.11ay, an initiator is an AP or user that commences the BF training, while a responder is a peer user that participates in the BF training with the initiator. As shown in Fig. 2.1, the BF training procedure in IEEE 802.11ay is divided into two main stages: (1) first, a SLS stage that selects the best sector pair by transmitting AWVs training with a quasi-omni antenna pattern between the initiator and the responder; (2) subsequently, a beam refinement protocol (BRP) stage in which the initiator and responder refine their sectors by iteratively refining the AWVs of both the initiator and responder [2, 3].

2.1.1.1 The SLS BF stage

The SLS stage includes the following phases: initiator sector sweep (ISS), responder sector sweep (RSS), sector sweep (SSW)-Feedback, and SSW-acknowledgement (ACK); however, the SSW-ACK phase is skipped when the BF is carried out during A-BFT. As shown in Fig. 2.2, the AP, the initiator, starts the ISS phase by sending out an initiator-transmit-sector-sweep (I-TXSS) during the BTI with quasi-omni antenna patterns. The responders

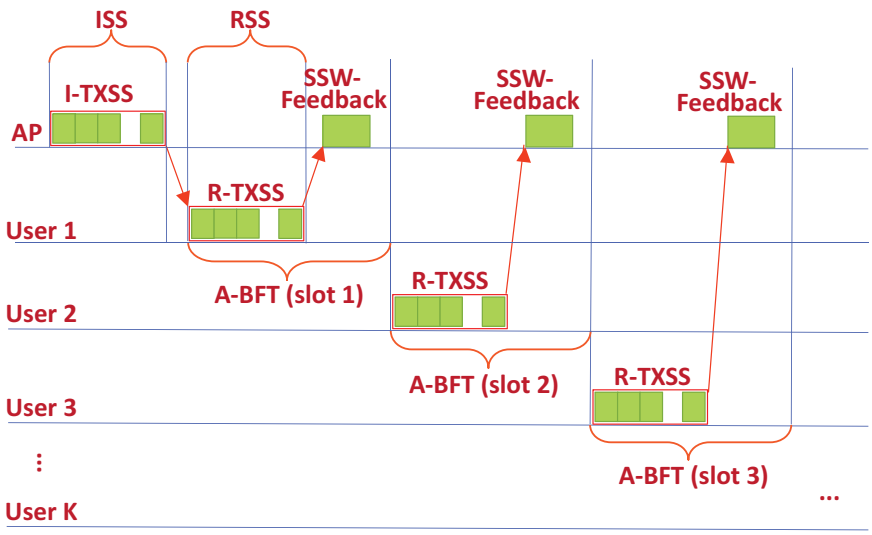

Figure 2.2: The SLS stage of the BF process.

(users) follow with an RSS by transmitting a responder-transmit-sector-sweep (R-TXSS) during the A-BFT. Users can thus be associated to the AP in multiple slots during the A-BFT, as shown in Fig. 2.2. Then, during SSW-Feedback phase, the AP decides whether a user is to be associated based on the information received from the R-TXSS for each user. The best SID detected during ISS will be reported during the R-TXSS phase, while the best SID detected during RSS will be reported during SSW-Feedback. Then, the initiator (AP) and responders (users) will have their best SIDs, and the first stage (SLS) is complete [2, 3].

It is worth noting that users randomly contend for a slot during A-BFT. A collision can occur if a slot is selected by two or more users. Therefore, a high collision probability is expected in dense deployment scenarios, since there are no more than 8 A-BFT slots available in IEEE 802.11ad [47]. However, the number of A-BFT slots in IEEE 802.11ay increases to 16 when using the extended A-BFT mechanism [48, 49] or 48 when using the multi-channel A-BFT approach [50], which reduces severe collision issues during the A-BFT [2].

SSW and SSW-Feedback Procedure Example: As mentioned above, the SSW and SSW-Feedback frames are used between an initiator and responder in the SLS and during the A-BFT period in order to conduct coarse BF training. This subsection will provide an example of this procedure between the AP (initiator) and a user (responder), in terms of the details of both the SSW and SSW-Feedback frame formats [2, 3]. A summary is shown in Fig. 2.3.

- First, the AP sends an I-TXSS containing several SSW frames, as shown in Fig. 2.3. Fig. 2.4 shows the detailed frame format of each SSW exchanged between the AP and the user. While the AP is transmitting the I-TXSS in this example, BF information is included in each SSW frame. The Frame Control and Duration sub-fields are set first. Then, the MAC addresses of both the AP and user are transmitted. The direction of the transmission is identified, indicating that this SSW is sent by the AP (initiator). The total number of SIDs for the AP, the SID for each SSW frame, and the DMG antenna identification (ID) that the AP is using are all transmitted, until the best SID is found. Then the specific ID number of the DMG antenna for the following RSS is transmitted.

- Second, the user responds to the AP by sending an R-TXSS, as shown in Fig. 2.3. The process is the same as for the I-TXSS, except that the SSW-Feedback sub-field considers a responder (not an initiator), as shown in Fig. 2.4. The Frame Control and Duration sub-fields are set first. Then, the MAC addresses of both the user and the AP are transmitted. The direction of the transmission is identified to show this SSW is sent by the user (responder). The SID for each SSW frame and the DMG antenna ID that the AP is using are also transmitted. The R-TXSS reports the best SID received, along with its SNR value, and the best antenna ID. In the Poll Required sub-field, the user indicates whether a communication link needs to be initiated to the AP.

- Third, after receiving the R-TXSS from the user, the AP transmits an SSW-Feedback frame to associate the user. It sets the Frame Control and Duration sub-fields first. Then, it transmits the MAC addresses of both the AP and the user, as well as the total number of sector IDs for the AP. The number of receive DMG antennas for the following RSS is reported, and the BRP request sub-field and Beamformed Link Maintenance sub-field are both performed if needed. Note that both the initiator and the responder can send either a transmit-sector-sweep (TXSS) or a receive-sector-sweep (RXSS) to train the transmitter and receiver side, respectively.

2.1.1.2 The BRP BF stage

This stage uses an iterative approach to refine the beams by improving the antenna arrays of the users during the DTI. Both the initiator and responder can request training to receive or transmit antenna patterns. The AWVs for phased antenna arrays are predicted and optimized during the BRP using an iterative approach. The imperfection of coarse BF (quasi-omni antenna patterns) is eliminated by evaluating a set of directional transmit or receive patterns against the best SID obtained earlier during the SLS. By increasing the beam training at this stage, a reliable link between users and extra throughput can be obtained [2, 3].

There are several sub-phases in the BRP stage, as shown in Fig. 2.6: BRP setup, multiple-sector-identification-detection (MID), beam-combining (BC), and beam refinement transactions. Together, the MID and BC sub-phases are known as the multiple-sector-identification-detection and beam-combining (MIDC) sub-phase. Information is exchanged in the BRP setup sub-phase in order to proceed to the next sub-phases. If there are better AWVs than the best found during the SLS stage, this is resolved between users in the MIDC sub-phase. The initiator and responder can use two types of beam refinement training by sending the BRP frame: 1) transmit request beam refinement training

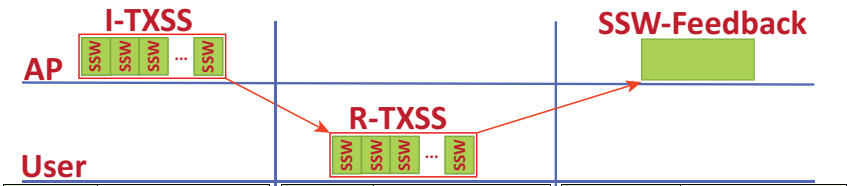

Frame Control & Duration	The Frame Control and Duration are set first
RA & TA	MAC address of the AP and user are transmitted
Direction	Is sent by the AP (initiator)
Sector ID	Sector ID for each SSW frame is transmitted
DMG Antenna ID	DMG Antenna ID that the AP is using is transmitted
Total Sectors	Total # of Sector ID of the AP is transmitted
# of RX DMG Ant.	Specific # of receive DMG antenna for the following RSS is transmitted

Frame Control & Duration	The Frame Control and Duration are set first
RA & TA	MAC address of user and AP are transmitted
Direction	Is sent by the user (responder)
Sector ID	Sector ID for each SSW frame is transmitted
DMG Antenna ID	DMG Antenna ID that the user is using is transmitted
Sector Select	Best-quality Sector ID received is reported
DMG Ant. Select	Best-quality Antenna ID received is reported
SNR Report	Value of SNR frame that was received with the best quality of the best sector
Poll Required	Is sent to indicate whether user needs the AP to initiate communication

Frame Control & Duration	The Frame Control and Duration are set first
RA & TA	MAC address of the AP and user are transmitted
Total Sectors	Total # of sectors of the AP
# of RX DMG Ant.	Send the # of receive DMG antenna for the following RSS
BRP Request	BRP request frame is initiated
Beamformed Link Maintenance	Beamformed Link Maintenance is performed

Figure 2.3: Example of coarse BF training between the AP (initiator) and a user (responder).

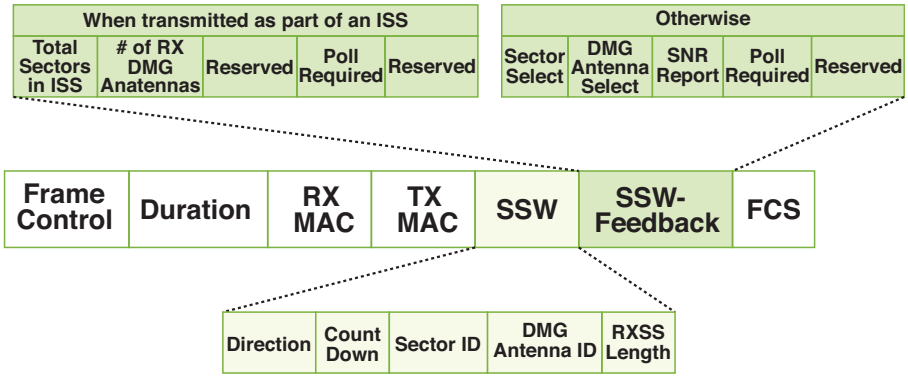

Figure 2.4: The SSW frame format.

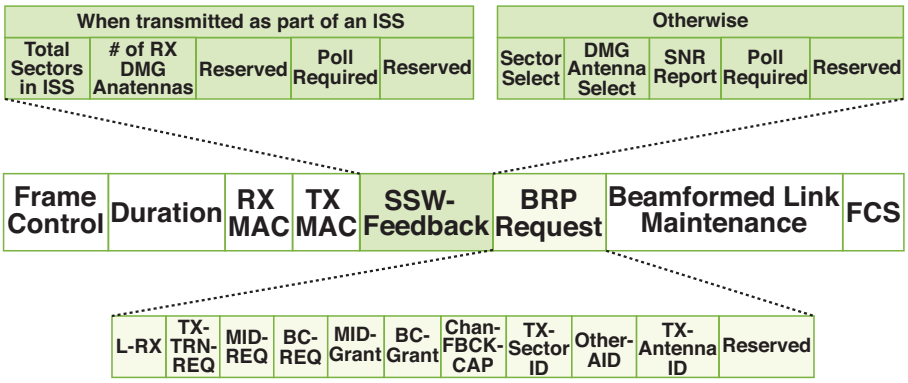

Figure 2.5: The SSW-Feedback frame format.

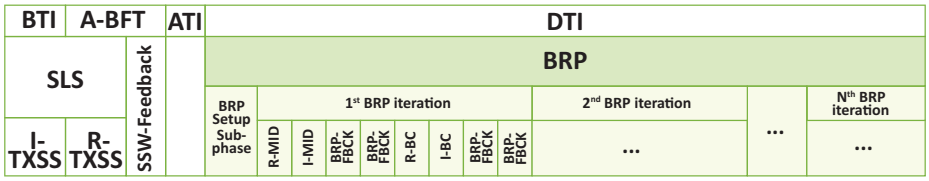

Figure 2.6: Example of time allocation for the BRP stage of the BF process.

and 2) receive request beam refinement training. If both the initiator and the responder use only a TXSS in the SLS stage, then the receive side will now be refined using RXSS. For either transmit or receive beam refinement training, the requesting or responding users send a BRP frame with the request or response in the training field, using either transmit or receive beam refinement training. The reply from the responding user with the best receive quality is then reported. For this process, the request-response frame of the BRP continues until the responder sets the capability-request field to 0, at which point neither user has a request for training. The second stage of BF training is completed when neither initiator nor responder request such training [2, 3].

2.1.2 The TDD BF Training

The IEEE 802.11ay standard defines a new TDD-SP allocation for the mDN use case (a multi-hop scenario) in order to achieve fair communication with no interference. New TDD channel access rules are specified [2]. Since the BF training protocol in the SLS and BRP uses specific interframe-space times to separate BF frames, it is not appropriate for TDD channel access times using new guard time (GT) interframes. Therefore, a new form of TDD BF training is defined for the mDNs by considering TDD channel access. IEEE 802.11ay includes two types of TDD BF training (TDD individual BF training and TDD group BF training), with antenna reciprocity for transmitter and receiver assumed in both. There are three types of TDD BF frame (TDD-SSW, TDD-SSW-Feedback, and TDD-SSW-ACK), and TDD BF training is performed during TDD-SP allocation in the DTI. The following subsections describe the TDD-SP allocation training procedures of TDD individual and group BF training.

2.1.2.1 TDD Individual BF

In TDD individual BF, only one user can perform BF training with an AP during assigned TDD-Slots. This involves unicast TDD BF frames that are repeated for each user in order to complete the training. The TDD individual BF procedure is illustrated in Fig. 2.7(a).

i) An AP sends several TDD-SSW frames while a user utilizes all receive sectors. The TDD-SSW frame is sent repeatedly to span all the AP's SIDs and specifies the time offset for the upcoming TDD-SSW-Feedback and TDD-SSW-ACK transmission.

ii) The user transmits a TDD-SSW-Feedback frame using the sector with the best quality (best SID).

iii) The AP sends a TDD-SSW-ACK frame after receiving TDD-SSW-Feedback, in order to acknowledge the received configuration.

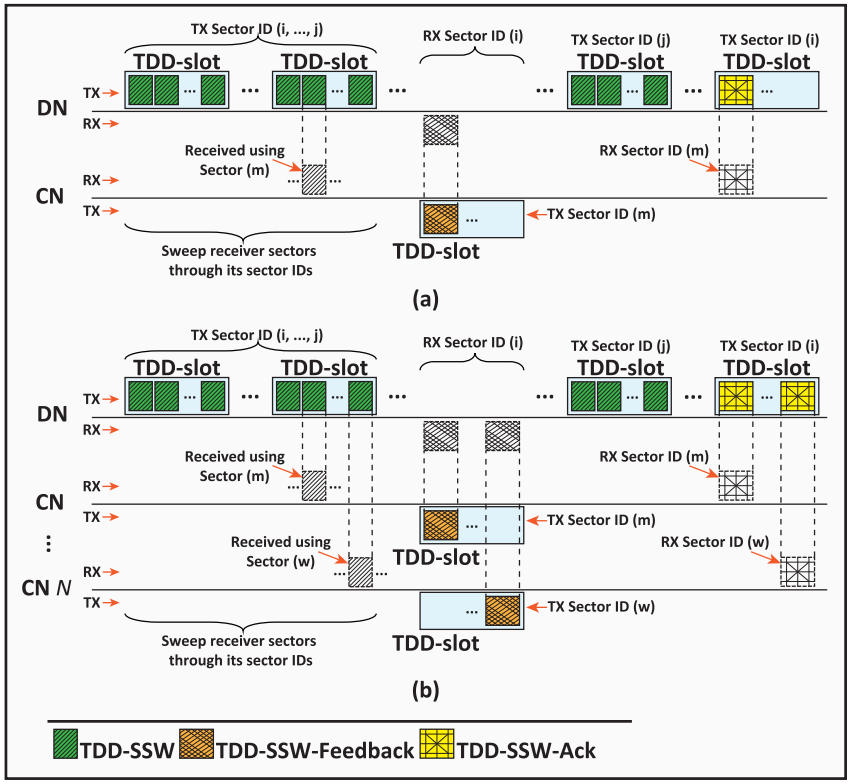

Figure 2.7: TDD BF training procedure: (a) TDD individual BF (b) TDD group BF.

This process can be repeated if needed, unless the AP specifies that the TDD individual BF is to end during the TDD-SSW-ACK.

2.1.2.2 TDD Group BF

In order to increase TDD BF efficiency by reducing BF training overhead, IEEE 802.11ay introduces TDD group BF, performing BF training for multiple users instead of repeating it individually for each user. BF training time is hence reduced, since a certain number of users are trained simultaneously. As shown in Fig. 2.7(b), the TDD group BF procedure is similar to that of TDD individual BF, with the following modifications.

i) An AP sends multiple TDD-SSW frames for multiple users, using the broadcast MAC address subfield, to initiate the TDD group BF. The TDD-SSW frames specify the number of users to be trained. Responder ID subfields for each user are generated using a predefined scheme known by the AP.

ii) TDD-SSW-Feedback frames are sent by each user in different time allocations, using the sector with the best link quality among the TDD-SSW frames sent.

iii) After receiving the TDD-SSW-Feedback frames, the AP transmits several TDD-SSW-ACK frames to each user in different time allocations, in order to transmit the sector used by the AP, the sector used by the user, the measured SNR, the Announce frames, and an indication of whether the BF training is complete.

2.2 mmWave Distribution Network Use Case

IEEE 802.11ay supports the mDN use case, which can provide a promising, cost-efficient and high-performance solution for fiber broadband networks [2, 51, 52]. Recently, fifth-generation (5G) fixed wireless access (FWA) has received considerable attention from both academia and service providers because of the reduced cost of network infrastructure and because of its high speeds compared to fiber-to-the x (FTTx) networks. The mDN has the potential to build denser urban networks capable of connecting more people everywhere in the world thanks to various emerging applications. The mDN is also considered one of the first 5G deployments, since it may be able to provide a fast time to market. The following subsections first introduce 5G FWA and then present the architecture, applications, and benefits of mDN.

2.2.1 What is 5G FWA?

FWA is a broadband network that provides Internet access to customers using wireless technology instead of a wired network, such as the fiber broadband network. In the past, FWA used earlier cellular generations and standards derived from the Wi-Fi family. However, the speeds and latency of these approaches cannot compete with fiber broadband networks. With new advanced technologies such as mmWave BF and small cell base stations [7, 9], 5G FWA can deliver Internet access to homes with fiber-like speeds. Something else that makes 5G FWA essential is that many houses around the globe do not have reliable broadband access; it can be expensive and time-consuming to deploy fiber broadband network everywhere. This provides an opportunity for operators and service providers to adopt 5G FWA.

2.2.1.1 5G FWA Deployments

The industry has conducted several 5G FWA trials to demonstrate the potential of both licensed and unlicensed mmWave technologies. In 2017, Verizon started pre-standard 5G trials to provide 5G FWA and thereby launched this service, which they called 5G-Home, in limited locations in the United States. Another 5G FWA trial was recently launched in Canada by Huawei and TELUS, using Huawei 5G products entirely based on 3GPP standards. Facebook, Deutsche Telekom, and Qualcomm are working together on the Facebook Terragraph project based on mDN, which operates in the unlicensed 60 GHz band. Furthermore, SiKlu launched a P2MP mmWave system, another 5G FWA trail based on the unlicensed 60 GHz band.

2.2.1.2 5G FWA Advantages

The main advantages of 5G FWA based on either licensed or unlicensed mmWave spectrum are as follows:

- High speeds and very low latency, due to the mmWave spectrum.
- Reduced cost of network infrastructure when compared to fiber broadband networks.
- Faster time to market, enabling quick and cheap Internet access.
- Ubiquitous connectivity to rural areas where wired access infrastructure is unavailable.

2.2.2 mDN Architecture

As illustrated in Fig. 2.8, the mDN is based on the concept of mesh networking topology, where each node not only sends and receives its own data (within its coverage area) but also acts as a relay node, in order to have a direct and dynamic connection with other nodes in the network [51]. The mDN is connected to the provider network through point-of-presence (POP), using an optical fiber link. The distance between the distribution-nodes (DNs) is up to 1000 m and 300 m for rooftops and street poles, respectively, while the distance between a DN and client-node (CN) is up to 100 m. The mDN can enable neighboring outdoor DNs to construct and preserve non-overlapping data transmission and control allocations dynamically over multi-hops.

2.2.3 mDN Applications

The primary purpose of the mDN is to create a wireless backhaul network and provide P2MP mmWave access to the CNs, in order to achieve 5G fiber-replacement applica-

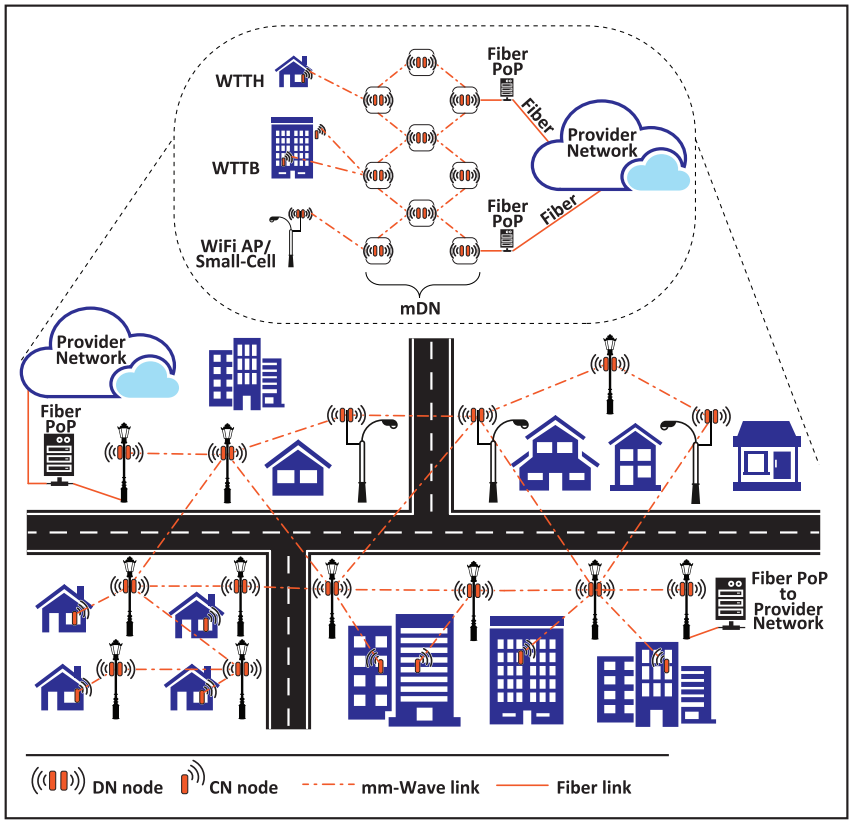

Figure 2.8: The network topology of the mDN.

tion scenarios. These application scenarios include wireless-to-the-home (WTTH) access, wireless-to-the-building (WTTB) access, WiFi DN backhauling, and small-cell backhauling. An additional and optional indoor wireless or wired network can be used in the WTTH and WTTB scenarios, using different frequency bands from the mmWave links for backhauling.

2.2.4 mDN Benefits

Communication network data traffic in cities is growing exponentially, demanding a tremendous amount of bandwidth per km^2 to support new smart city applications such as smart

utility meters, traffic cameras, a massive number of sensors, and smart parking meters. Although optical fiber cable solutions can offer a tremendous amount of bandwidth, the infrastructure cost of the fiber network is expensive, and it can be slower to implement in certain locations. Therefore, an efficient solution, such as the mDN, can provide Internet access everywhere and improve quality of life. The main benefits of the mDN are that (i) high-speed access (with fiber-like speed) can be achieved, based on the 60 GHz of the IEEE 802.11ay; (ii) a significant lower-cost network infrastructure is offered for fixed access networks; (iii) faster time to market can be delivered, with small mDN access points (DNs) implemented on pre-existing street poles or buildings without the need to spend time securing permission; (iv) ubiquitous coverage with high speeds can be realized where the service can reach areas that can be difficult for fiber network infrastructure in urban and suburban areas.

2.3 Related Works

The following subsections discuss BF techniques, multi-user HBF, simultaneous users' orthogonality, device-to-device (D2D) simultaneous transmission, simultaneous transmission in multi-hop scenarios, and simultaneous uplink transmission proposals in the mmWave literature.

2.3.1 MmWave MIMO BF

Conventional omni-directional transmission technology can be very challenging for mmWave communications due to the propagation characteristics of the mmWave bands. Hence, mmWave systems use directional transmission technology with narrow beams for long-distance communications. However, deafness can arise in the mmWave as a direct consequence of directional transmission links between the TX and RX. Several studies [53,

54, 55, 56, 57, 58] address this issue by using a beam-searching procedure to establish communication links when the main beams of the TX and intended RX are not aligned.

[58] proposes a simple and efficient AWV algorithm for mmWave wireless local area networks. Only one AWV feedback is used for this algorithm, in order to obtain the best transmission and reception AWV pair. [56] proposes a BF protocol that reduces BF set-up time and decreases the effect of the high path loss of the mmWave wireless personal area network (WPAN) systems. This BF protocol employs sector-level and beam-level searching mechanisms. [54] presents a low complexity, codebook-based BF scheme. To determine the best transmission/reception beam pattern and reduce the setup time, it uses a multi-level heuristic searching algorithm. [57] presents a BF approach for mmWave that employs an adaptive codebook to reduce complexity and uses a sub-array method with squinting angles to develop an adaptive beam width BF technique. [53] and [55] propose another beam search procedure by performing an exhaustive search over all possible combinations of transmission and reception directions through a sequence of pilot transmissions, in order to further reduce the alignment overhead. They offer this procedure as a replacement for the two-stage exhaustive search proposed elsewhere.

The analog BF training procedure in the IEEE 802.11ay [2], IEEE 802.11ad [3], and IEEE 802.15.3c [59] standards is divided into two main stages to reduce the overhead of the beam searching procedure and allow each device to resolve proper AWV settings. The first stage of the analog BF training procedure in both IEEE 802.11ad and IEEE 802.11ay is the SLS stage, where the best sector pair can be resolved by transmitting BF training frames with a quasi-omni directional antenna. The second stage is the BRP, an optional BF training phase that refines the sectors between the TX and RX, if necessary, using an iterative refinement protocol.

2.3.2 HBF for Multi-User mmWave

As mentioned earlier, due to the characteristics of mmWave propagation, establishing effective communication and simultaneous transmission with mmWaves requires directional BF with large antenna arrays. An appropriate BF mechanism for achieving simultaneous transmission is thus a key consideration.

The use of digital BF for multi-user MIMO technology, which has been widely applied in conventional lower-frequency systems (<6 GHz), is challenging in mmWave systems since digital processing requires dedicated baseband and RF hardware for each antenna element [24, 23, 60, 61, 21, 22]. Because mmWaves entail a considerable number of antenna array elements, implementing a vast number of RF chains can be costly. Also, designing the precoding matrices in digital BF requires CSI, but obtaining CSI in an mmWave system is difficult because of the large number of antenna elements and the very low SNR [24, 23, 21, 22, 62].

To overcome the challenges associated with using digital BF with mmWaves, analog BF can be used instead of baseband approaches. Analog BF, such as that identified in IEEE 802.11ay and 802.11ad, has been implemented in the RF domain, with a group of analog phase shifters applied to control the phase of the signal in each antenna. However, analog BF is limited to single-stream transmission, and multiplexing several data streams or employing multi-user transmission is difficult. HBF, which combines digital BF with analog BF, can reduce the complexity of the hardware constraints to attain simultaneous transmission [23, 24, 21]. HBF offers a trade-off between performance and complexity, with both analog and digital domains used in the design of the precoder.

The literature proposes several HBF approaches [24, 23, 60, 61, 62, 63] to overcome the challenges of mmWaves and achieve simultaneous transmission. [24] proposes a downlink multi-user mmWave system that uses the hybrid precoding technique under the assumption of limited feedback. Analog and digital beamformers are taken from different codebooks

to reduce the need for training and feedback. [63] considers an HBF with a multi-user multi-carrier system, proposing QR[1]-based factorization of the set of digital BF matrices over all subcarriers. In this work, only one phase shifter per antenna is assumed for each RF chain. [62] employs HBF to overcome the problem of multi-user uplink mmWave channel estimation. A layered pilot transmission approach and a decomposition-based method, CANDECOMP/PARAFAC, jointly estimate channels from multiple users to the base station.

Highlights of Challenges and Limitations of the HBF: Even though HBF is the preferred approach for multi-user MIMO technology in mmWave systems, digital processing remains challenging for the following reasons [21]:

- CSI feedback overhead increases with the number of users and antennas in the system.
- Digital precoding schemes, such as zero-forcing, require frequent sounding and feedback because of the short wavelength of mmWaves.
- The SNR received over an mmWave channel is very low because of the high bandwidth of an mmWave.
- Performing channel estimation is difficult because the precoder in the HBF approach involves RF precoding.

To address the challenges related to channel estimation and signal training design, [21] proposes an alternative solution based on the sparse nature of mmWave channels in the angular domain. This method allows channel estimation by implementing compressed sensing; however, random and unknown antenna array geometries are not considered when

[1]QR factorization decomposes a matrix into a product in which Q stands for an orthogonal matrix and R is an upper triangular matrix.

robust mmWave channel estimation algorithms are needed [21]. The performance gain is also achievable only with perfect knowledge of the CSI at the transmitter [22]. Imperfect channel knowledge can affect performance because multi-user MIMO with mmWaves requires more CSI at the transmitter. The HBF approach therefore incurs significant additional overhead to obtain reliable multi-user MIMO. Thus, an appropriate analog BF scheme with limited digital processing is crucial [21].

2.3.3 User Selection and Users' Orthogonality in MIMO

Multi-user MIMO is a set of multiple-input and multiple-output technologies for wireless communication that allows a set of links to be transmitted simultaneously. Thus, network throughput is improved due to the multi-user MIMO technique. However, user selection in large-scale multi-user MIMO is crucial due to MUI and the potential collection of CSI to find the best group of users [33, 34]. In particular, the orthogonality of the instantaneous channels between selected users can affect achievable rates when users are coupled [35, 36, 37, 38]. The literature uses several criteria for user selection or user grouping, to solve the problem of selecting a subset of users. An explicit solution is to find an optimal subset of users by deploying an exhaustive search over all users. However, in dense deployment scenarios, this requires formidable CSI overhead, and its complexity can grow significantly with the number of users. Other criteria [35, 36, 37] can simplify the user selection problem into sub-optimal algorithms by utilizing the orthogonality criterion as a selection metric. These criteria include the largest principal angle [39], subspace collinearity [40], and chordal distance [41]. Thus, user selection is essential in multi-user MIMO, especially when the number of users is large.

[38] proposes a distributed multi-user MIMO protocol named Signpost, which uses a two-dimensional prioritized contention mechanism for the lower frequencies (but not for mmWaves) to achieve distributed user selection. This approach uses local CSI for each user

to estimate orthogonality, instead of collecting CSI for all users. [38] shows that the channel quality of a single transmission link depends on the angles between the other links' channel coefficients. Channel quality increases when the angle between two simultaneous links is almost orthogonal, and decreases when the angle is small. Thus, selecting orthogonal users is essential to maintaining strong channel orthogonality. However, this assumes there is local CSI and channel estimation, which can be challenging for mmWave systems since they require digital processing.

Traditionally, multi-user MIMO systems involve a direct orthogonality evaluation approach. An optimal set of users is selected by collecting CSI for all users and then evaluating the orthogonality of each possible user. However, this mechanism will introduce significant overhead and high computational complexity [17, 38]. Data in CSI feedback increases with the number of antenna elements and the number of users. Moreover, this approach produces very significant overhead for mmWave wireless communication, due to the short wavelength of 60 GHz, which requires frequent sounding and feedback [17]. Also, Qualcomm found in [64], after intensive measurement analysis, that the best multi-user MIMO performance in the IEEE 802.11ac system involves three simultaneous users. To achieve such performance, the set of most effective simultaneous users must first be selected and scheduled in a coordinated manner. This supports the idea of having centralized APs and scheduling the most spatially effective simultaneous users.

2.3.4 D2D Simultaneous BF

Both the IEEE 802.15.3c and IEEE 802.11ad standards and the mmWave BF protocols surveyed in subsection 2.3.1 are mainly designed to train sequentially transmitter and receiver BF and schedule a single transmission per time slot. They use directional transmissions due to the propagation loss of the mmWave, and can thus exploit simultaneous transmissions because of spatial reuse. However, the throughput of simultaneous commu-

nication links in a short coverage area can be affected due to MUI from the simultaneous transmissions. According to [28, 65, 66], designing transmission scheduling and efficient MAC protocols will solve the problems of spatially multiplexed simultaneous links. The following proposals are among the few that consider the simultaneous transmission option.

[67] proposes an iterative searching algorithm to realize sub-optimal simultaneous transmission/reception beam sets, formulating an optimization problem in order to maximize the sum rates of simultaneous transmissions by considering MUI. This simultaneous-BF iterative searching algorithm activates an additional link in each time slot if its contribution to the total throughput is greater than the interference it causes. [55] proposes a joint beam-width selection and power allocation problem for BF search and employs multiple concurrent transmissions. This approach maximizes the effective network throughput for short-range mmWave networks through an optimization problem. Since the computation of this optimization problem is complicated, [55] uses two approximation solution algorithms. [68] proposes a multi-path multi-hop scheduling scheme for mmWave WPANs, based on the spatial multiplexing structure in HBF. This technique shows spatial reuse can be improved through optimum path selection, traffic distribution, and transmission scheduling. [69] proposes a scheduling approach for multiple coexisting P2P links in the mmWave WPAN system, presenting the SINR analysis for various antenna configurations, including omni-directional and directional ones. They also apply the first-come-first-serve link scheduling algorithm using both the SINR and the BF information from IEEE 802.11ad.

Highlights of the D2D Simultaneous BF: The proposals in [55, 67, 68] introduce significant overhead on top of the BF overhead already applied in the WPAN IEEE 802.11ad standard because of their greedy iterative searching algorithms. In addition, they are not compatible with the current IEEE 802.11ad MAC protocol, so the whole MAC protocol would need to be revised in order to adopt them. [69] proposes concurrent mmWave transmissions for IEEE 802.11ad; however, they are specifically designed for the P2P wireless

communication scenario instead of the downlink multi-user scenario. On the other hand, scheduling simultaneous downlink transmission while mitigating MUI is necessary for simultaneous downlink BF/transmission for the IEEE 802.11ay.

2.3.5 Simultaneous Transmission in Multi-Hop Scenarios

Since wireless devices are increasingly deployed in dense environments characterized by several APs, interference between different devices in neighboring basic service sets (BSSs) could harm individual users' performance and network throughput: inefficient BF may cause transmission delays or even failure of transmission. Inter-BSS interference occurs when using multiple BSSs with dense deployment environments in which neighboring BSSs can overlap. Due to the high density of wireless devices, data transmission in such environments can cause interference and reduce network performance.

The literature has employed several techniques to cancel inter-BSS interference in a multi-hop network by exploiting a digital BF technique [70, 29, 71, 72] such as the zero-forcing precoder. [70] uses two-step optimization for coordinated inter-BSS interference cancellation. [71] deploys an inter-BSS interference mitigation scheme in overlapping BSS, based on a power threshold and zero-forcing precoder. [72] proposes cooperative interference management by employing digital BF with analog BF and power control to reduce interference.

Highlights of Simultaneous Transmission in Multi-Hop Scenarios: However, the above-surveyed techniques [70, 29, 71, 72] introduce significant overhead on top of the existing BF overhead applied in the IEEE 802.11ad standard. This is because they use digital BF, which requires CSI at all APs and users to cancel the inter-BSS interference. In mmWave communication, digital precoding schemes, such as zero-forcing, require very frequent sounding and feedback because of the short wavelength of the mmWave bands

[21, 23, 60]. Also, the precoding matrices in a digital BF require CSI. However, obtaining CSI in an mmWave system is difficult because of the large number of antenna elements and the very low SNR [21, 22]. To realize digital BF and cancel the inter-BSS interference requires additional antennas on each AP.

2.3.6 Simultaneous Uplink Transmission

Recently, internet traffic has changed from very light web browsing and file transfer to a rich amount of user-uploaded content because of the recent emergence of applications such as ultra-high definition video wireless streaming and augmented reality/virtual reality headsets. The IEEE Task Group ay has included augmented reality/virtual reality headsets and other high-end wearables as usage models for the upcoming IEEE 802.11ay standard, with a 20 Gbps data rate required [2, 52]. Thus, to improve MAC efficiency and meet the requirements of the current and upcoming dense deployment usage scenarios, uplink multi-user transmission (or uplink multi-user MIMO) is considered a potential future solution for next-generation WiFi technologies, such as the IEEE 802.11ax and IEEE 802.11ay [2, 73, 74].

Simultaneously transmitted uplink signals from users need to be separated by the AP to avoid MUI. A solution to this issue is to coordinate user selection by the AP to have perfect spatial characteristics among all the selected users [73, 75]. Joint scheduling decision, a scheme to choose a set of users to uplink their transmissions to the AP, is key to designing simultaneous uplink MAC protocols [73, 75]. Joint scheduling decision among spatially distributed users is a challenging issue, and users need to be separated spatially to avoid MUI [73, 75].

2.3.6.1 Simultaneous Uplink Transmissions in Traditional WLAN

There are two types of scheduling in simultaneous uplink transmission, namely coordinated and un-coordinated. In un-coordinated scheduling, such as that in [76, 77, 78], simultaneous uplink transmission decisions are made by users through the random MAC mechanism. In coordinated scenarios, on the other hand, such as the proposals in [75, 79, 80, 81], the simultaneous uplink scheduling decision is made by the AP, or the AP notifies the users who have won the channel contention. This section reviews simultaneous uplink transmission proposals in the literature for both the coordinated and un-coordinated scenarios.

Simultaneous Un-Coordinated Uplink: [76] proposes an un-coordinated uplink multi-user MIMO approach. This approach assumes all users are orthogonal, so users can be differentiated by the AP using the channel coefficients. The zero-forcing (ZF) scheme then differentiates the received signals. [77] proposes an un-coordinated uplink spatial multiple access scheme for WLANs, using a distributed MAC scheme called Carrier Counting Multiple Access to employ simultaneous uplink transmissions. To detect other users frame preambles, each user employs a transmission counter and then decides whether to contend for the channel. [78] proposes another un-coordinated asynchronous uplink throughput analytical model, based on the Bianchi Markov chain model. To set the maximum number of users that will transmit in parallel, the AP sends an announcement beacon. Then, ZF with successive interference cancellation decodes parallel data streams.

Simultaneous Coordinated Uplink: [79] proposes a coordinated-scheduled uplink MAC protocol using code-division multiple access to separate the compound frames. Users can be scheduled by the current CSI and by the capability of the AP when the user's back-off counter reaches zero. This approach assumes that the CSI is obtained from the downlink transmission and that the data have the same length. [80] proposes a coordinated-

unscheduled uplink distributed MAC protocol with spatial-division multiple access support for the WLANs. For channel estimation and user synchronization, the authors use a dual-mode clear-to-send responding technique. The MAC procedure in this technique is divided into two stages, random access and data transmission. [75] presents a coordinated uplink multi-user MIMO protocol for the IEEE 802.11 WLANs. This protocol uses both a synchronized access scheme coordinated by the AP and an orthogonal frequency-division multiple access scheme. The selection of the users for uplink transmission is based on the CSI calculated by the AP.

Highlights of the Coordinated and Un-Coordinated Uplink: Un-coordinated simultaneous uplink transmissions do not exploit spatial separation, because they are mainly based on the randomness of the IEEE 802.11 backoff mechanism. Moreover, next generation WiFi will likely use coordinated uplink scenarios, since the AP can schedule a group of users to achieve high network performance [73]. In addition, since the AP gathers BF information from all users and can make the best scheduling decision, uplink multi-user MIMO in the next WiFi generation is expected to follow a coordinated and scheduled approach controlled by the AP [73]. Therefore, the challenges of simultaneous uplink scheduling, such as the multi-user detection problem, need to be addressed in order to achieve simultaneous uplink transmission in the 802.11 WLANs [73, 75]. Simultaneously transmitted uplink signals from users need to be separated by the AP in order to avoid MUI. A possible solution to this issue is to coordinate user selection by the AP for the perfect spatial characteristics among all selected users [73, 75].

2.3.6.2 Uplink Multi-User MIMO Systems Using HBF:

Several HBF algorithms that specifically consider the uplink scenario in multi-user MIMO mmWave systems have been proposed for mmWave bands [43, 44, 45, 46]. These exploit a

near-optimal solution using the HBF approach. [43] proposes a uplink multi-user MIMO mmWave system for the joint HBF approach, employing an orthogonal matching pursuit algorithm for the analog precoder while using a mean square error measure for the digital BF. [44] considers an uplink of large-scale multi-user MIMO for the mmWave systems. The HBF joint optimization problem is addressed to maximize the sum rate, by considering the transmit power, analog phase shifter, and receive antenna selection matrix. [45] proposes a near maximum likelihood detector to deal with a challenge inherent in uplink multi-user massive MIMO systems, namely the power consumption of the ADCs. It considers one-bit ADCs and proposes a two-stage algorithm to solve the problem. [46] proposes an HBF algorithm for the uplink multi-user MIMO scenario, using the Gram-Schmidt method and the minimum mean square error method in the analog and digital stages, respectively.

Highlights of Uplink Multi-User MIMO Systems Using HBF: The existing HBF algorithms do not consider the user selection algorithm, even though user selection needs to be jointly considered along with HBF when there are many users. Thus, computational complexity can be significant in dense deployment scenarios. Specifically, there can be high power consumption due to the increased demand for RF chains, with the number of simultaneous transmissions limited to the RF chain number. The assumption that the system can serve users up to the total number of RF chains without considering user selection to maximize the data rate is not realistic in an mmWave system with many users. Also, CSI acquisition overhead from all the potential users can be considerable. Even though there have been substantial research efforts on existing HBF algorithms, to the best of our knowledge, the user selection algorithm in dense user scenarios has not been incorporated into the HBF algorithm for uplink multi-user MIMO mmWave systems.

Chapter 3

Single-Hop Multi-User Transmission: MUI Perspective

High frequency and very high throughput WLANs are an essential need due to the substantial global increase in WiFi public hotspots and existing internet traffic. Due to the challenges arising from this increase, an efficient solution is required for the current IEEE 802.11 standards to meet the predicted growth of wireless traffic and in the number of WiFi networks in the world.

This chapter proposes a practical and efficient simultaneous downlink transmission MAC layer algorithm for mmWave WLANs based on the IEEE 802.11ay standard. Specifically, it proposes a VG algorithm to schedule simultaneous downlink links in a single-hop scenario by using information from the analog BF training. The VG algorithm can successfully handle and select simultaneous users while mitigating MUI with no additional computational complexity to the system. After introducing the proposed algorithm, we evaluate the SINR and antenna directivity of each simultaneous link to investigate the successful simultaneous transmission and spatial multiplexing gain of the VG algorithm. We also demonstrate via simulations that the proposed VG algorithm can enhance average

throughput and save allocation time for the scheduled data transmission without adding extra feedback overhead.

3.1 System Model

For the system model, we use the IEEE 802.11ay mmWave WLANs to describe the simultaneous downlink transmission of the VG algorithm. The following subsections describe the network model, the IEEE 802.11ay directional MAC protocol, and the directional antenna model.

3.1.1 Network Model

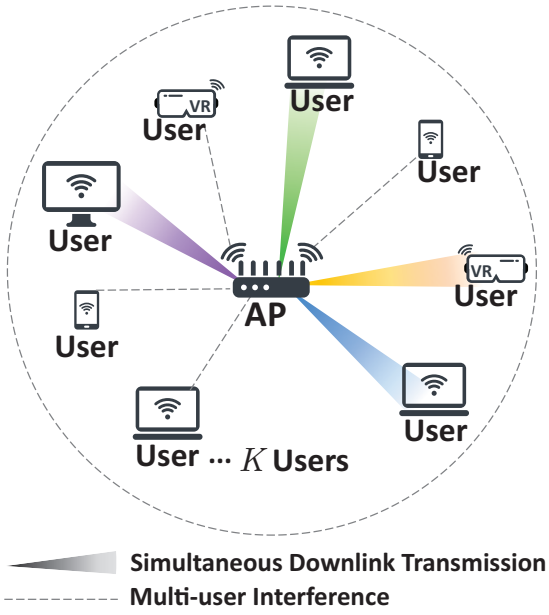

Figure 3.1: Simultaneous downlink transmission scenario in a single-hop mmWave WLAN.

The system model in this proposal is an mmWave single-hop WLAN that considers

simultaneous downlink transmission, as shown in Fig. 3.1. This single-hop WLAN contains an AP and K users. The AP and users have EDMG antennas. This network model also considers MUI generated by simultaneous transmissions in the single-hop WLAN, as shown in Fig. 3.1.

3.1.2 Timing Structure for Directional MAC

As shown in Fig. 3.2, the timing structure of the IEEE 802.11ay directional MAC protocol includes a unique BI access time with four main components. First, during the BTI, the AP can initiate the BF training with an Announce frame or by transmitting an DMG-Beacon. Second, during the A-BFT, users can complete the BF training by using A-BFT slots. Third, during the ATI, exchanges in the request-response-based management and allocation information can be announced. Finally, during the DTI, the protocol establishes slot allocations using either contention-based access periods (CBAPs) or scheduled SPs. TDD channel access allocation (TDD-SP) is also used for the mDN use case during the DTI. This thesis only considers the scheduled allocations, and we assume that the length of the transmission frames during the DTI is equal.

It is worth noting that users randomly contend for a slot in the A-BFT, and a collision can occur if a slot is selected by two or more users. Therefore, dense deployment scenarios involve a high probability of collision since no more than 8 A-BFT slots are available in IEEE 802.11ad [47]. However, in IEEE 802.11ay, there can be up to 16 A-BFT slots using the extended A-BFT mechanism [48, 49] or up to 48 slots using the multi-channel A-BFT approach [50], which reduces the severe collision issue during the A-BFT.

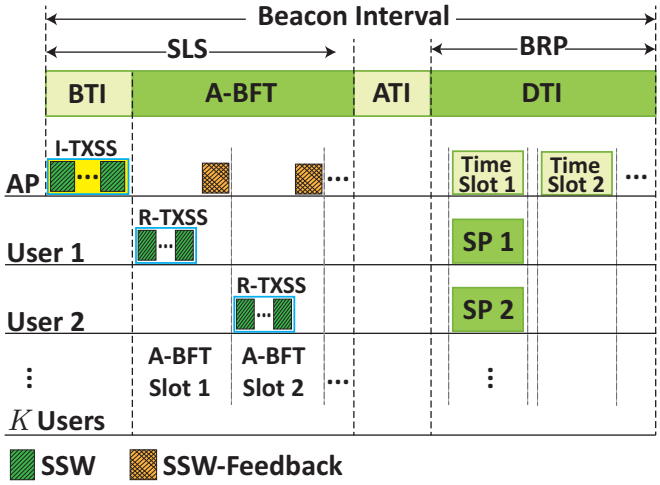

Figure 3.2: The BI timing structure of IEEE 802.11ay and the analog BF training MAC protocol.

3.1.3 Analog BF Training Process

BF training can establish a communication link between a TX and an RX to overcome the challenges arising from directional transmission. BF training for 802.11ay is similar to that for the legacy 802.11ad but includes new BF training stages, such as single-user MIMO BF and multi-user MIMO BF, to enhance the BF process [82]. As shown in Fig. 3.2, the analog BF training for IEEE 802.11ay is divided into two main stages, the SLS and the BRP. The BF training is first done in the SLS and can then be performed again with an optional iterative BF process in the BRP. The BF process in the SLS stage is as follows:

1. The AP transmits SSW frames during the I-TXSS phase of the BTI, using multiple enhanced directional multi-gigabit (EDMG) Beacon frames with different sector beams (multiple sectors in different directions); each user receives these frames in quasi-omni mode.

2. During A-BFT, each user transmits SSW frames with different sector beams during the R-TXSS phase for association with the AP, and the AP receives them in quasi-

omni mode. During this process, each SSW frame includes information about the best SID in the AP (which means the best sector beam).

3. The AP feeds the best SID, i.e., that with the highest SNR, to every associated user during the SSW-Feedback frame by using the best SID from the previous step.

3.1.4 Antenna Model

The antenna pattern functions of the directional antenna are characteristic of that antenna since they measure the power gain G(θ,ϕ), where θ and ϕ are the spherical elevation and azimuthal angle coordinates, respectively. We consider a circular array and approximate it with a sectored, flat-top directional antenna model for simplicity and generality. The literature on interference analysis considers this model a useful idealization [28, 67]. By assuming a horizontal plane, the directional antenna model is given by

$$g(\phi) = \frac{G(0,\phi)}{G_{max}}, \tag{3.1}$$

where $G_{max} = \max_{\phi} G(\phi)$. Then, the sectored, flat-top directional antenna model can be represented as

$$g(\phi) = \begin{cases} 1, & |\phi| \leq \frac{\Delta\phi}{2} \\ 0, & otherwise, \end{cases} \tag{3.2}$$

where $\Delta\phi$ is the beam angle. The antenna directivity of this model is calculated as follows:

$$D = \frac{4\pi}{\omega}, \tag{3.3}$$

where $\omega = \int_{\theta=0}^{\pi} \int_{\phi=-\pi}^{\pi} G_n(\theta,\phi)\ sin\theta\ d\theta\ d\phi$ is the beam solid angle and $G_n(\theta,\phi)$ is the normalized power pattern. Let the sector width for the 3-D flat-top antenna to be $\Delta\phi$.

Then, $G_n(\theta, \phi)$ is

$$G_n(\theta,\phi) = \begin{cases} 1, & -\pi \leq \phi \leq \pi, \quad 0 \leq \theta \leq (\Delta\phi/2) \\ 0, & otherwise. \end{cases} \tag{3.4}$$

Then,

$$\begin{aligned} \omega &= \int_{\theta=0}^{\pi} \int_{\phi=-\pi}^{\pi} G_n(\theta,\phi) \sin\theta (d\theta)(d\phi) \\ &= \int_{\theta=0}^{\Delta\phi/2} \int_{\phi=-\pi}^{\pi} \sin\theta (d\theta)(d\phi) \\ &= 2\pi \left(1 - \cos\left(\frac{\Delta\phi}{2}\right)\right). \end{aligned} \tag{3.5}$$

By substituting equation (3.5) into equation (3.3), the directivity D becomes

$$D = \frac{2}{1 - \cos\left(\frac{\Delta\phi}{2}\right)}. \tag{3.6}$$

Therefore, for different beam widths ($\Delta\phi$), we have different directivity (D). For example, for $\Delta\phi = 14.4°$, $30°$, $45°$, $60°$, $90°$, $135°$, and $180°$, the directivity $D = 24$, 17.7, 14.2, 11.7, 8.3, 5.1, and 3 dB, respectively.

3.2 Details of the Proposed VG algorithm

Analog BF and beam steering are essential in the mmWave system to establish a high-quality communication link, even though they are not required in conventional systems that operate in the lower frequency bands. Thanks to this analog BF mechanism, users

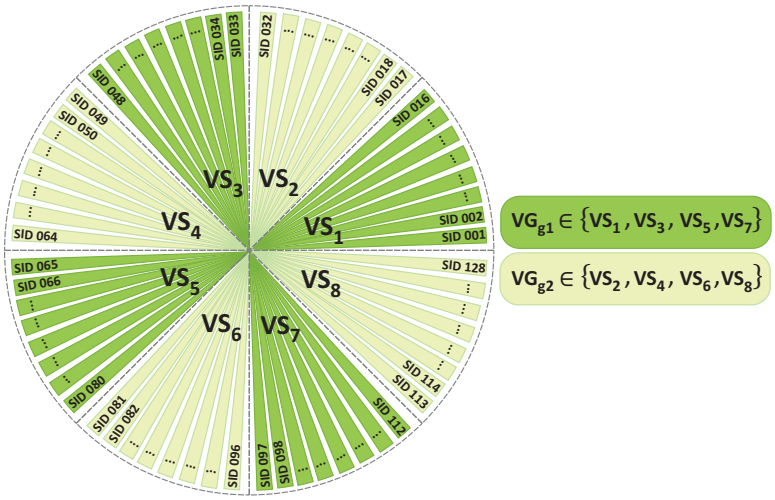

Figure 3.3: The pre-defined directional antenna SID and VG algorithm concept when $A = 8$ and $p = 128$.

can be selected using information from the analog BF training in order to reduce the complexity and feedback overhead.

After the analog BF training, and thus after reporting the best SIDs and exchanging them among the AP and users, the VG algorithm divides the coverage area into virtual sectors (VSs) using information about the best SID, as shown in Fig. 3.3. Two orthogonal groups, VG_{g1} and VG_{g2}, are defined to divide users into orthogonal groups and achieve simultaneous transmission without needing to find an optimal set of users by collecting the CSI for all users. Then, based on the SID, VG_{g1} and VG_{g2} can be constructed from the following equations, respectively:

$$\left(\frac{A + 2pq - 2p}{A}\right) \leq \text{SID} \leq \left(\frac{2pq - p}{A}\right) \tag{3.7}$$

$$\left(\frac{A + 2pq - p}{A}\right) \leq \text{SID} \leq \left(\frac{2pq}{A}\right), \tag{3.8}$$

Table 3.1: The best SID information after user association during the A-BFT period for the example in Fig. 3.4a.

VG_{g1}			
VS number	SID	Users' best SID	User number
1	1 to 16	7	12
3	33 to 48	43	8
5	65 to 80	72	9
7	97 to 112	No user associated	n/a
VG_{g2}			
2	17 to 32	29	2
4	49 to 64	60 & 52	4 & 5
6	81 to 96	88	6
8	113 to 128	118	7

where m is the total number of SIDs defined in the system, A is the total number of VSs, and $q = \{1, 2, ..., A/2\}$. Fig. 3.3 shows the VG algorithm. Eight VSs are used in this example to construct the first group, $VG_{g1} \in \{VS_1, VS_3, VS_5, VS_7\}$, and the second group, $VG_{g2} \in \{VS_2, VS_4, VS_6, VS_8\}$.

Fig. 3.4 illustrates the proposed VG algorithm: in Fig. 3.4a, the area is divided into eight VSs ($A = 8$), while in Fig. 3.4b, it is divided into sixteen ($A = 16$). In Fig. 3.4a, 12 users are uniformly randomly distributed in a single hop WLAN. As shown in Fig. 3.4a, suppose that 8 of the 12 users are associated at the A-BFT, with the best SIDs of each user reported in Table 3.1. Then, only user 8, user 9, and user 12 can be selected for the simultaneous transmission at VG_{g1}, based on their SIDs; user 2, user 4, user 5, user 6, and user 7 can be selected for VG_{g2}. However, a non-spatial orthogonal problem exists if more than one user is located in the same VS, as shown in VS_4 in Fig. 3.4a. Hence, a proper scheduling algorithm is required for the non-spatial orthogonal problem.

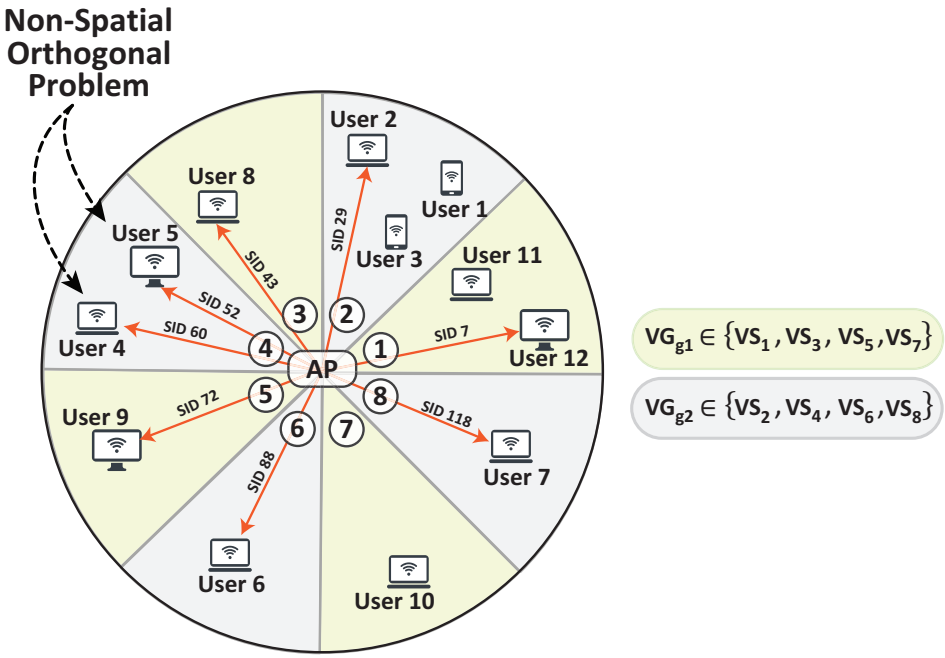

(a) $A = 8$.

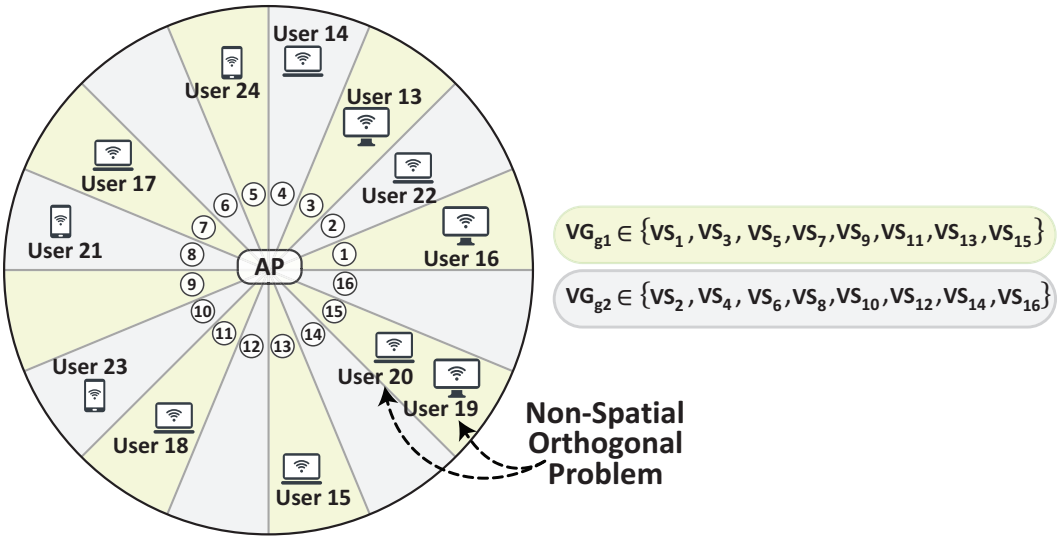

(b) $A = 16$.

Figure 3.4: Simultaneous transmission selection examples using the VG algorithm.

To accomplish simultaneous downlink transmission, we consider two methods for the VG algorithm. Depending on the length of the DTI period in each BI and the time allocation available, these two methods can be employed in IEEE 802.11ay. The non-spatial orthogonal problem and the algorithms for the two methods appear in the following subsections.

3.2.1 Non-Spatial Orthogonal Problem

According to the VG algorithm, if the best SID of a user is located in a VS of VG_{g1} or VG_{g2}, this user will be selected for a simultaneous transmission. However, we expect there to sometimes be more than one user in the same VS, especially in dense deployment scenarios, as shown in Fig. 3.4.

Therefore, if there is more than one user in the same VS, the AP selects only one of them, based on a scheduling mechanism. The remaining users can be allocated sequentially (not concurrent transmission), as shown in Fig. 3.5. For simplicity and tractability, we consider the mmWave path loss model in [83] for the performance evaluation. The path loss model [83] is as follows:

$$PL[dB] = C + 20 \cdot log_{10}(f) + 10 \cdot n \cdot log_{10}(d), \tag{3.9}$$

where $C = 45.5$ and n is the path loss exponent, equal to 1.4. Both C and n are set for a non-line-of-sight (NLOS) environment. $f = 60GHz$ is the central frequency, and d is the transmission distance.

The algorithm for this process is as follows. If the AP receives the best SID information during the A-BFT period, it will check if there is another user in the VS identified for one of the VG algorithm groups. If there is, the AP selects only the one user with the lowest path loss among the users in this specific VS, and schedules the remaining users sequentially.

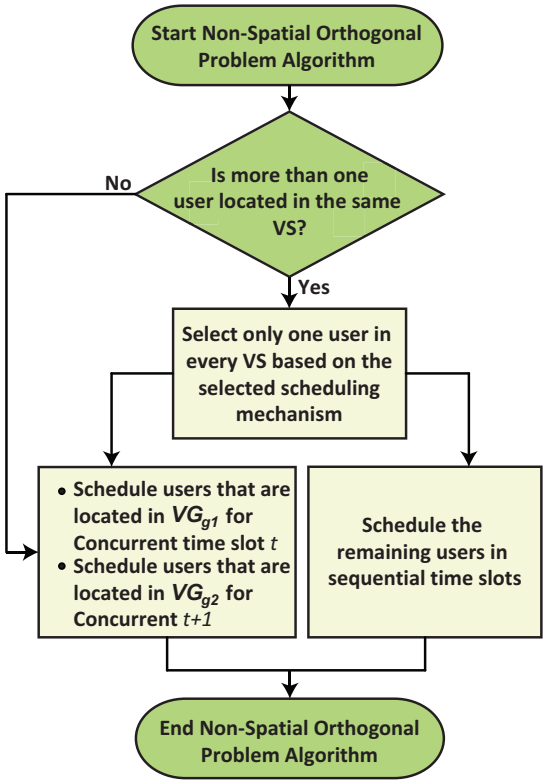

Figure 3.5: Non-spatial orthogonal problem algorithm flow chart.

Otherwise, if there is no more than one user in the same VS, it continues to the next stage and sends out the concurrent transmission.

3.2.2 VG Algorithm: Method A

After all the best SIDs for the associated users are reported, the VG algorithm starts. For every BI, there will be a simultaneous transmission time slot for only one VG group (VG_{g1} or VG_{g2}), as shown in Fig. 3.6a. If VG_{g1} is assigned for simultaneous transmission in the first BI, then VG_{g2} will be in the next BI. This process will take place for every BI, and each will have a different VG_g from the next, as described in detail in Algorithm 1.

Algorithm 1: Method A of the VG algorithm

Begin:
  for $SID = 1$ *to* p **do**
    if $mod(BI, 2) = 1$ (first BI) **then**
      if $user_i \in \left\{\left(\frac{A+2pq-2p}{A}\right) \leq SID \leq \left(\frac{2pq-p}{A}\right)\right\}$ **then**
        select user$_i$ and $\mapsto VG_{g1}$
      if *there is more than one user in* VS_1, VS_3, VS_5, *or* VS_7 **then**
        select only the one user that has $min\{PL_i[dB]\}$ and allocate unselected users sequentially in advanced sequential time slots
    else if $mod(BI, 2) = 0$ (next BI) **then**
      if $user_i \in \left\{\left(\frac{A+2pq-p}{A}\right) \leq SID \leq \left(\frac{2pq}{A}\right)\right\}$ **then**
        select user$_i$ and $\mapsto VG_{g2}$
      if *there is more than one user in* VS_2, VS_4, VS_6, *or* VS_8 **then**
        select only the one user that has $min\{PL_i[dB]\}$ and allocate unselected users sequentially in advanced sequential time slots

For instance, as shown in Fig. 3.4a, user 8, user 9, and user 12 are selected for simultaneous transmission in the first BI, where only VG_{g1} is considered. Then, for the next BI, only VG_{g2} is considered, where user 2, user 5, user 6, and user 7 are selected for simultaneous transmission.

3.2.3 VG Algorithm: Method B

The upcoming IEEE 802.11ay standard should support 20 Gbps or higher throughput, which should be scalable to a large number of users. Thus, in order to meet the requirements of the usage scenarios for IEEE 802.11ay, the first method can be improved by considering two time slots for simultaneous transmissions in every BI, instead of only one time slot. Since the analog BF and the best SID information are available for all associated users, both VG_{g1} and VG_{g1} can be allocated in two different time slots in the same BI.

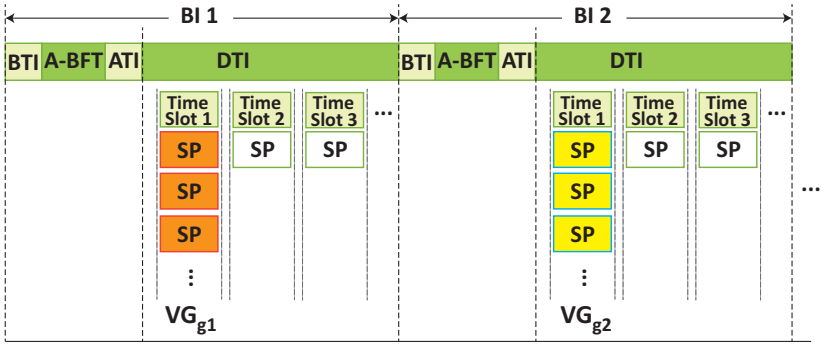

(a) Method A of the VG algorithm.

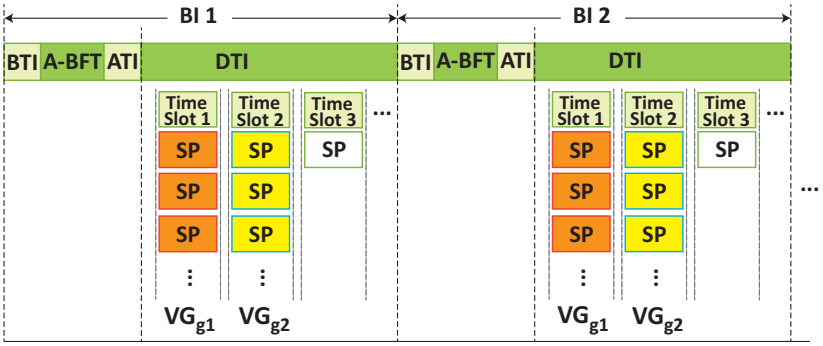

(b) Method B of the VG algorithm.

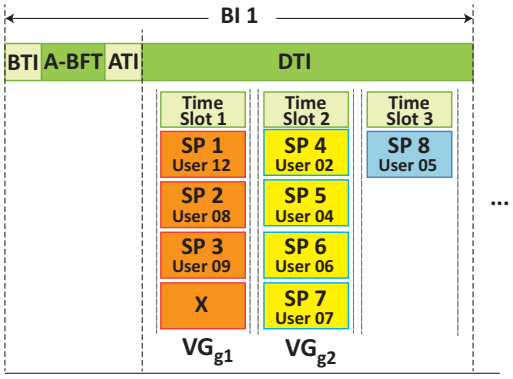

(c) Time allocation example for Fig. 3.4a.

Figure 3.6: Time allocation examples for the VG algorithm during the DTI.

Furthermore, IEEE 802.11ay with EDMG ability can allocate data transmission frames using the SP allocation approach (non-contention based). As a result, higher throughput is expected in method B of the VG algorithm, since it uses two time slots for simultaneous transmission in every BI. In addition, the number of channel accesses and the overhead associated with short packets can be reduced significantly compared with the equivalent figures for method A. In short, the main difference between method A and method B of the VG algorithm is that method B considers two time slots for simultaneous transmission in each BI in order to improve performance, instead of considering only one time slot.

The procedure will remain the same as in the VG algorithm, except that each BI will have two time slots for two different simultaneous transmissions, as described in Algorithm 2. For every BI, the procedure considers both VG_{g1} and VG_{g2} simultaneously, as shown in Fig. 3.6b. With this method, more throughput can be gained and more time slots can be saved, while the MUI can be mitigated.

Using the same example as in Fig. 3.4a and Table 3.1, Fig. 3.6c shows the time allocation of method B, with both VG_{g1} and VG_{g2} used in the same BI. In addition, since VS_4 in this example has two active users (user 4 and user 5), we can see that only user 4 is selected for simultaneous transmission for VG_{g2}, while user 5 is allocated in a different time slot to solve the non-spatial orthogonal problem, as shown in Fig. 3.6c.

3.3 Performance Evaluation

In this section, we describe the performance evaluation methodology and provide the simulation results for the proposed VG algorithm, as compared to the single-stream of IEEE 802.11ad. We evaluate the performance of the VG algorithm in terms of average throughput per time slot, average percentage of the time allocation that has been saved, SINR, and spatial multiplexing gain.

Algorithm 2: Method B of the VG algorithm

Begin:
  Repeat (for every BI)
    for $SID = 1$ *to* p **do**
      if $user_i \in \left\{\left(\frac{A+2pq-2p}{A}\right) \leq SID \leq \left(\frac{2pq-p}{A}\right)\right\}$ **then**
        select user$_i$ and $\mapsto VG_{g1}$
      if *there is more than one user in* VS_1, VS_3, VS_5, *or* VS_7 **then**
        select only the one user that has $min\{PL_i[dB]\}$ and allocate unselected users sequentially in advanced sequential time slots
      if $user_i \in \left\{\left(\frac{A+2pq-p}{A}\right) \leq SID \leq \left(\frac{2pq}{A}\right)\right\}$ **then**
        select user$_i$ and $\mapsto VG_{g2}$
      if *there is more than one user in* VS_2, VS_4, VS_6, *or* VS_8 **then**
        select only the one user that has $min\{PL_i[dB]\}$ and allocate unselected users sequentially in advanced sequential time slots

3.3.1 Simulation Setup

We simulate a typical mmWave WLAN environment with the AP in the center and K users uniformly randomly distributed within the coverage of the AP, as shown in Fig. 3.7. In this simulation, we assume there are 8 random active users to associate in every BI. Then, during the polling periods (PPs) and Grant periods (GPs) of the ATI, these active users can be allocated for downlink data transmission by the AP, with some scheduled simultaneously based on the VG algorithm. According to the IEEE 802.11ad standard [3], the throughput of the IEEE 802.11ad system is up to 6.75 Gbps, using 64-quadrature amplitude modulation (QAM) modulation and approximately 2 GHz of spectrum at 60 GHz. For comparison purposes, we assume that the maximum throughput that can be achieved is 6.75 Gbps per time slot. In the following, we provide simulation results for methods A and B of the VG algorithm, the SINR, and the spatial multiplexing gain.

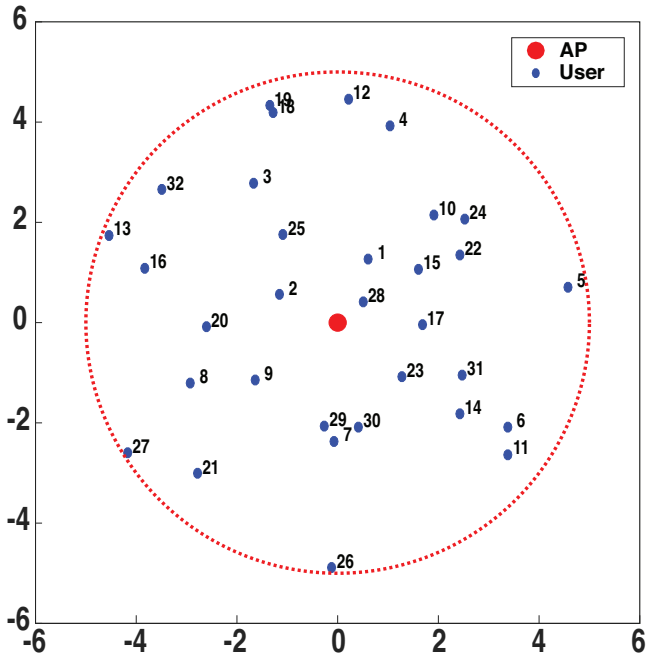

Figure 3.7: Simulation area layout for different numbers of users.

3.3.2 Average Throughput Performance

Fig. 3.8 and Fig. 3.9 show the simulation results of the throughput for each time slot in order to compare the throughput performance of a single transmission in IEEE 802.11ad and the proposed VG algorithm when using method A and method B, respectively, for each BI. This simulation considers 10 total BIs and 16 users. Since the SPs are allocated sequentially in IEEE 802.11ad, the throughput of a single transmission is 6.75 Gbps for each time slot, as shown in both Fig. 3.8 and Fig. 3.9. By applying simultaneous transmission using the VG algorithm, the throughput increases to 8.79 for method A and 11.4 Gbps for method B. In addition to the throughput, the number of time allocation slots can be saved, depending on the direction of each user and the randomness of the 8 users contending for association during the A-BFT period, which can reduce the overhead from the BRP during

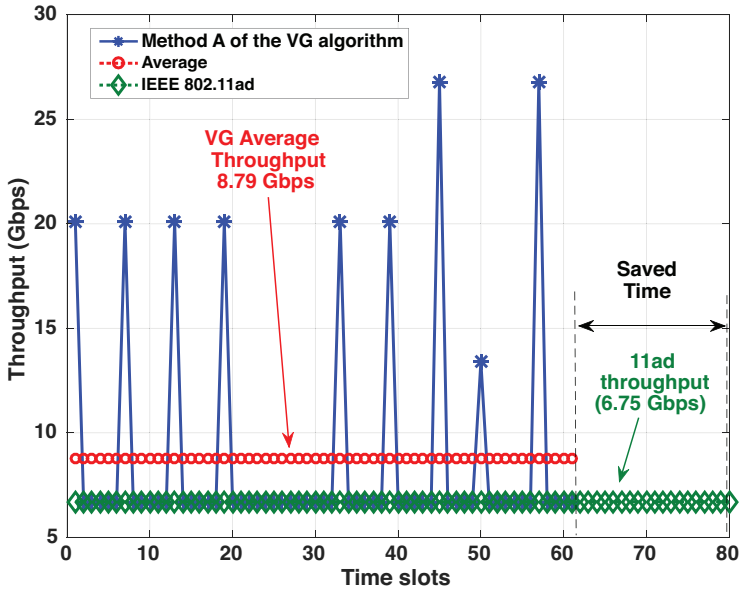

Figure 3.8: Throughput performance comparison using method A of the VG algorithm.

the DTI. Fig. 3.10 shows how both methods in the VG algorithm can reduce the number of time slot allocations for 100 BIs: 18 % of time slot allocations are saved using method A and 48 % using method B.

We simulate different numbers of users to get accurate results for the above scenarios. This demonstrates the average throughput of the proposed VG algorithm, the available time allocations that can be saved, and the performance of the algorithm in dense deployment scenarios. We evaluate the efficiency of our proposed algorithm for different network topologies by randomly generating user location information 10,000 times, with 10,000 BIs for each time. Then, this simulation is repeated for a different number of users (from 16 to 256), as shown in Fig. 3.11.

First, for method A, which only considers one simultaneous VG slot in each BI, the average throughput per time slot for different numbers of user increases from 6.75 Gbps

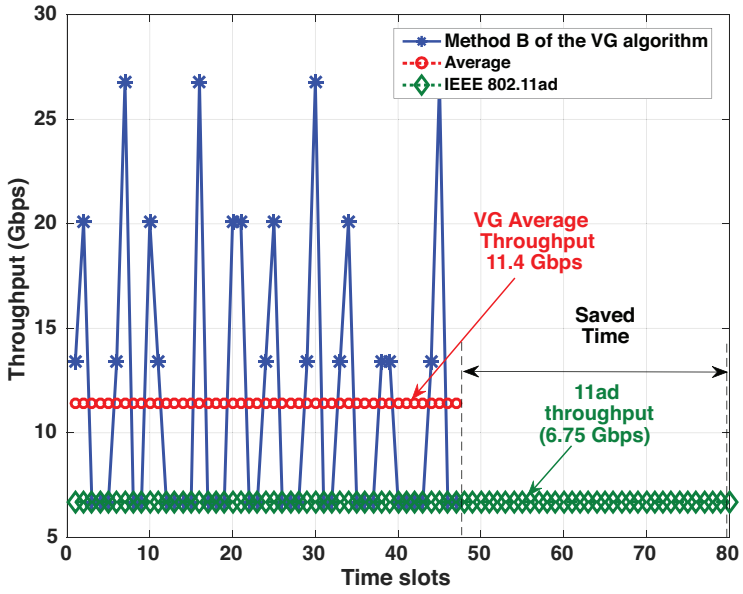

Figure 3.9: Throughput performance comparison using method B of the VG algorithm.

to around 8.2 Gbps when $A = 8$ and to 8.9 Gbps when $A = 16$, as shown in Fig. 3.11. This increase is to be expected since every BI has one slot with simultaneous transmission. Second, for method B, the average throughput per time slot for different numbers of users increases significantly, from 8.2 to 10.6 Gbps when $A = 8$ and from 8.9 to 12.9 Gbps when $A = 16$, as shown in Fig. 3.11. This significant increase in throughput is also as expected, since the chance to have simultaneous transmission is increased over two adjacent time slots rather than only one.

In addition to the gain in throughput, time can also be saved, thus improving performance and reducing the overhead of the BRP procedure during the DTI. As shown in Fig. 3.12, using method A saves an average of 18% and 20% of scheduled SPs when $A = 8$ and when $A = 16$, respectively. For method B, the average percentages increase to 36% and 40% when two VG_g groups are assigned in two consecutive time slots for simultaneous transmission during each BI. The efficiency increases because the second method saves

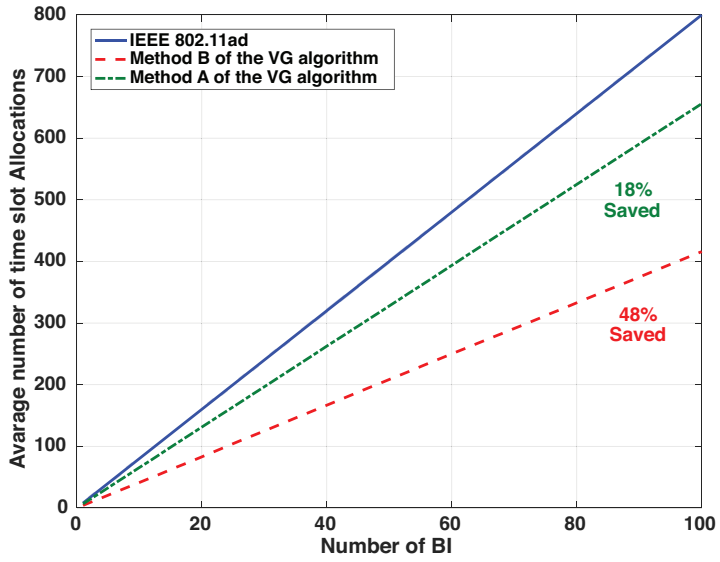

Figure 3.10: Average number of time slot allocations for methods A and B.

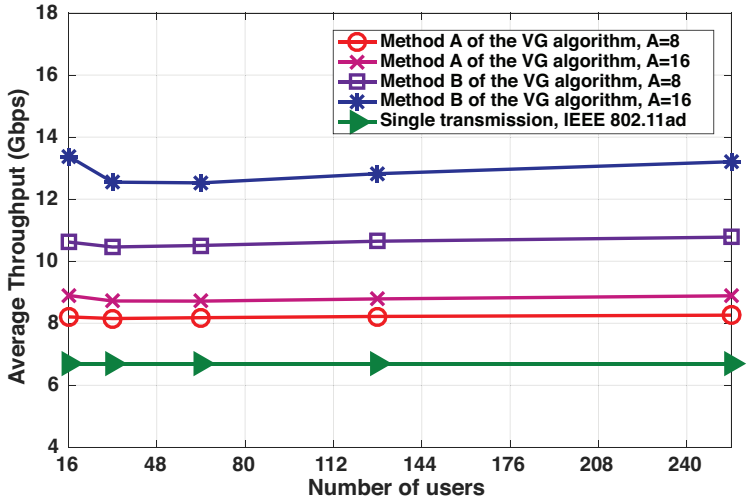

Figure 3.11: Average throughput performance.

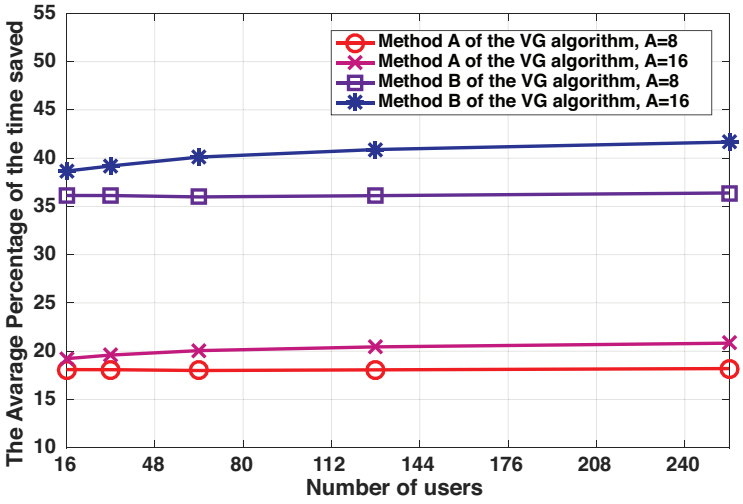

Figure 3.12: Average percentage of the time saved.

approximately 40% of the scheduled time when two simultaneous VG slots are used in the same BI.

Therefore, both methods of the proposed VG algorithm not only improve the throughput of the system but also save time slot allocations used for the downlink SP transmission. The VG algorithm strategy avoids the need to solve an optimal selection, as in digital BF and iterative search. Significant overhead can be expected in mmWave communication with the latter methods, as the complexity can increase significantly if the number of users is large. From this result, we can see that our proposal is independent on the number of users regardless of whether there are 16 or 256 users in the area, because the VG algorithm selects only one user in each VS out of all associated users in every BI. Furthermore, this proposal considers fairness, since all associated users that report their SIDs are allocated for downlink transmission sequentially or simultaneously for every BI, regardless of whether the number of users is small or large. We acknowledge that the effect of the contention mechanism of A-BFT is not considered in this simulation, with the number of associated users decreasing in dense deployment scenarios due to the probability of collision; however,

both a single transmission in IEEE 802.11ad and the proposed VG strategy will be affected by this issue, since all request-to-send, clear-to-send, and downlink time allocations happen after the user has been associated.

3.3.3 Impact of Beamwidth on Proposed VG Algorithm

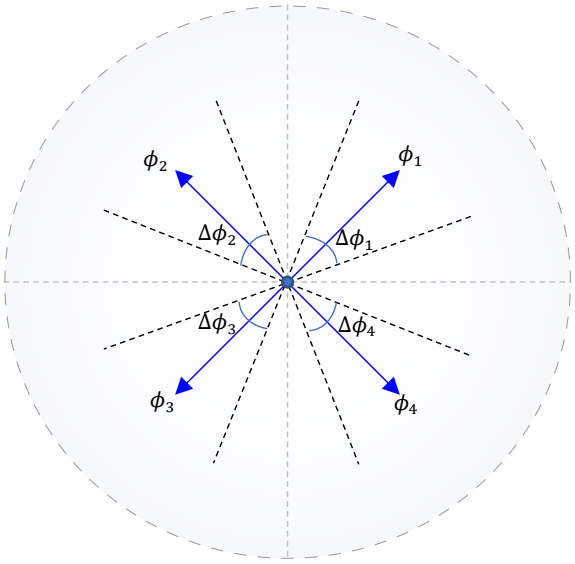

Figure 3.13: The SINR analysis with the directional antenna.

The beamwidth of the beam pattern under consideration can influence the performance of the proposed VG algorithm or the spatial multiplexing gain. We analyze the latter from the point of view of beamwidth, defining it as the number or ratio of available, successful concurrent links after determining the SINR by eliminating interfering links. Since we are studying the effect of beamwidth on the proposed VG algorithm, we consider a circular array and approximate it with a sectored, flat-top directional antenna model for simplicity and generality, as described in Subsection 3.1.4.

As shown in Fig. 3.13, the impact of the beamwidth of the user selection algorithm can

be evaluated by measuring the SINR for each selected user in order to analyze the spatial multiplexing gain. Let P_{tx}, G_{tx}, G_{rx}, D, and n be the transmit power, transmitter antenna gain, receiver antenna gain, transmission distance, and path loss exponent, respectively. Then, from the *Friis* transmission formula, the power of the received signal for the i-th user is given by

$$P_{rx,i} = P_{tx,i} G_{max}^2(\phi_i) \left(\frac{\lambda}{4\pi}\right)^2 D_i^{-n}, \tag{3.10}$$

where $G_{max} = G_{tx} = G_{rx}$ is defined as the maximum antenna gain by assuming that the transmitter and receiver are within each other's beams (the same assumption as in [28]). The SINR can then be written as

$$\gamma_i = \frac{P_{tx,i} G_{max}^2(\phi_i) \left(\frac{\lambda}{4\pi}\right)^2 D_i^{-n}}{\sum_{j \neq i} P_{tx,i} G_{max}^2(\phi_j)\ \psi_i \left(\frac{\lambda}{4\pi}\right)^2 D_j^{-n} + N_o B_w}, \tag{3.11}$$

where N_o is the background noise power density and B_w is the system bandwidth. $\psi = 1$ if the interferer and the receiver are within each other's beam; otherwise, $\psi = 0$.

Thus, the achievable rate for the i-th user can be written as

$$R_i = B_w \cdot \log_2 (1 + \gamma_i)\,. \tag{3.12}$$

The propagation parameters are shown in Table 3.2.

Fig. 3.14 shows the impact of beamwidth using the average data rate from a Monte Carlo simulation of the proposed VG algorithm for various beamwidths and different path loss exponents. The beamwidth and antenna directivity are evaluated using the SINR in (3.11). We can see that average data-rate performance is affected by interference and increases with beamwidth. For different path loss scenarios, this simulation uses exponents measured for the indoor environment in [84]. These path loss exponent values are for the

Table 3.2: SINR Simulation Parameters

Parameters	Value
Central frequency (f)	60 GHz
System bandwidth (B_w)	2.16 GHz
Transmission power (P_{tx})	0.1 mW
Background noise (N_o)	-134 dBm/MHz
Path loss exponent (Corridor) (n)	1.64
Path loss exponent (LOS) (n)	2.17
Path loss exponent (NLOS) (n)	3.01

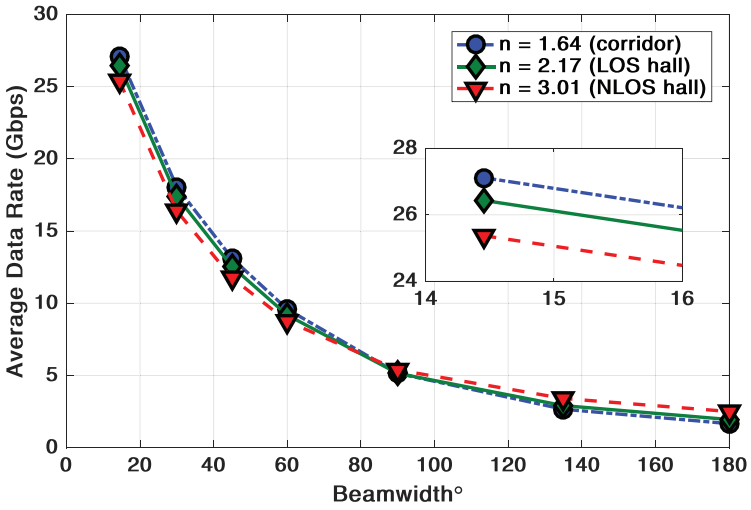

Figure 3.14: Data rate performance for various beamwidths.

corridor, line-of-sight (LOS) hall, and NLOS hall. Note that performance is not significantly affected by the path loss exponent values. The path loss depends on the frequency and is independent of the transmitted power and the antenna gain. Therefore, better performance can be achieved when the beamwidth is narrower, and the effect of the path loss exponent scenarios is insignificant to overall performance.

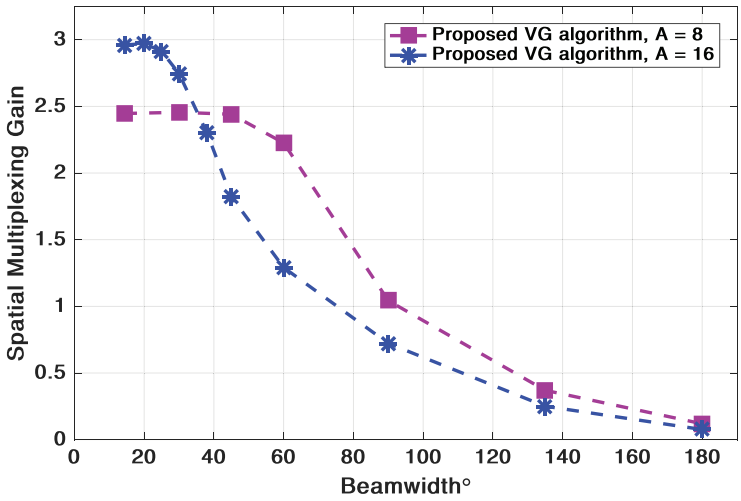

Figure 3.15: Spatial multiplexing gain performance for different beamwidths when the total number of VSs is 8 and 16.

Fig. 3.15 shows the impact of beamwidth using spatial multiplexing gain from a Monte Carlo simulation of the proposed user selection algorithm for various beamwidths. We can see that when beamwidths are narrow (e.g., below 45°), the user selection algorithm attains a higher spatial multiplexing gain. Higher performance can be achieved when the number of VSs is large ($A = 16$), due to the increased number of simultaneous users. Nevertheless, a trade-off exists between performance and beamwidth. Thus, better performance is achievable as long as the latter is kept sufficiently narrow.

3.4 Summary

This chapter has proposed a VG algorithm for the IEEE 802.11ay mmWave WLANs to realize simultaneous downlink transmission and mitigate MUI by using information from analog BF training. It develops two ways for the proposed VG algorithm to attain and select simultaneous users without adding any further computational overhead to the system. The simulation results show that the proposed VG algorithm can considerably improve the average throughput and save the scheduled allocation time for data transmission without extra feedback overhead. Furthermore, based on the SINR performance evaluation, the proposed VG algorithm can achieve high spatial multiplexing gain and simultaneous transmission without causing MUI, as long as the directivity of mmWave communication and the VG algorithm are utilized.

Chapter 4

Multi-Hop Multi-User Transmission: CCI Perspective

In the foreseeable future, the emergence of data-hungry applications and proliferation of wireless devices will substantially increase wireless data traffic. Wireless networks are expected to move toward denser deployment scenarios, such as stadiums, large office buildings, and airports, with very high data rate applications, such as ultra-high definition wireless video streaming. Since wireless devices are increasingly deployed in dense environments characterized by several APs, interference between different devices at neighboring APs could harm both performance for individual users and network throughput. CCI can occur when using multiple APs with dense deployment environments, as APs can overlap. Due to the high density of wireless devices, data transmission in neighboring APs can cause interference and reduce network performance.

In this chapter, we propose a novel multi-hop simultaneous downlink scheduling algorithm in ultra-dense networks based on the analog BF training information. Specifically, we propose a MHVG algorithm by expanding our initial findings from Chapter 3 to mitigate both the MUI within a single hop and the CCI generated from the multi-hop simultaneous

downlink transmission scenario. We use the MHVG algorithm to select the most perfect spatial users, based on the information from analog BF training, so simultaneous downlink transmissions can be realized without the need for digital BF in order to minimize complexity and overhead. We evaluate the performance of the MHVG algorithm by analyzing the spatial multiplexing gain. The spatial multiplexing gain represents the number of concurrent transmissions allowed over the same mmWave channel in a given area from the perspective of spatial reuse. Extensive simulations show the effectiveness and efficiency of the proposed MHVG algorithm.

4.1 System Model

We use IEEE 802.11ay mDN to describe the MHVG algorithm. The following subsections describe the network model, mDN protocol, and directional antenna model.

4.1.1 Network Topology

We consider a dense wireless network, such as a stadium, park area, or university campus, with mesh networking topology, in which multiple neighboring APs partially overlap, as shown in Fig. 4.1. The users are densely deployed in an mDN, and can communicate with the APs using directional antennas by performing analog BF training of the IEEE 802.11ay system. We consider TDD BF training in order to realize an appropriate link budget between a TX and RX before transmitting data, and assume antenna reciprocity for both the TX and RX. This network model considers both MUI and CCI. The MUI is generated from the simultaneous transmission within a single hop, while the CCI is generated from simultaneous transmission from neighboring APs. This model considers only one channel frequency. This increases the spectral efficiency because the reduced footprint of the mmWave directional antennas offers the potential for spatial reuse.

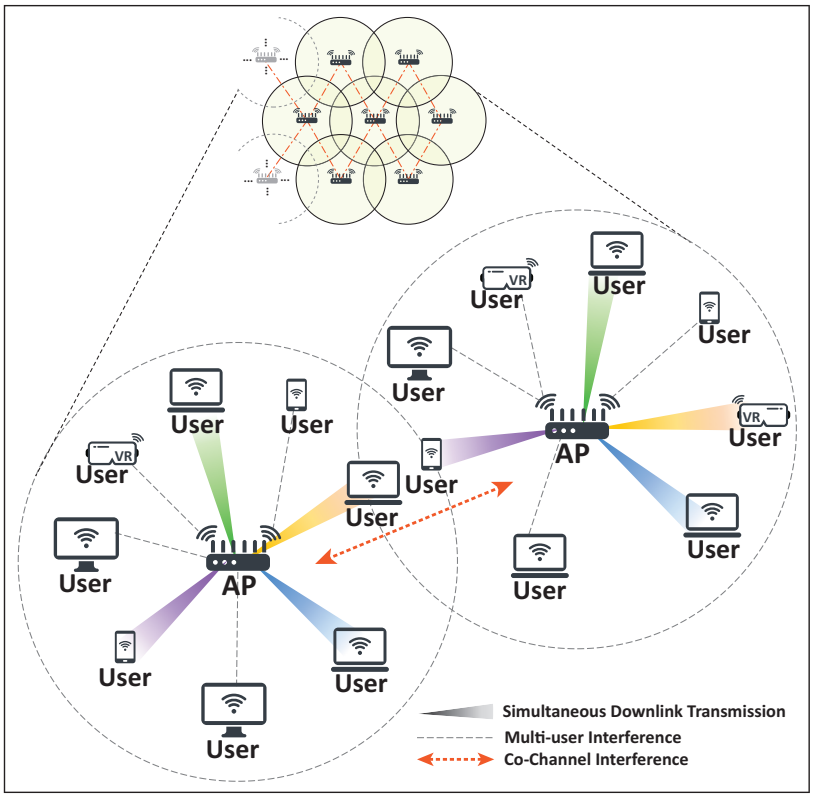

Figure 4.1: Network model considered.

4.1.2 mDN Protocol

The IEEE 802.11ay standard defines a distributed scheduling protocol specifically for mDNs in which two or more neighboring APs partially overlap to enhance spatial sharing and interference mitigation, where two or more of the channels used in these APs are similar [2]. This protocol aims to arrange dynamic, non-overlapping allocations and assure fair resource scheduling among APs using TDD channel access by considering a highly dynamic network with delay sensitive traffic. The main aspects of the mDN scheduling protocol are as follows.

- A distributed scheduling protocol can be established during an Announce frame

in order to initiate TDD channel access. The Announce frame contains two subfields, *TDD-Slot-Structure-Element* and *TDD-Slot-Schedule-Element*, that describe the structure of the TDD channel access and address the access time assignments using a TDD bitmap schedule, respectively. To enable the distributed scheduling protocol and identify the upcoming transmission schedules of neighboring APs, each AP must listen for Announce frames from its neighbors and may need to listen in different channels.

- For a specific channel, each AP needs to divide its BI duration by the number of neighboring APs that it has discovered in order to distribute channel resources. To maintain fairness among APs with the same channel in the same coverage area, the maximum access time allocation for each AP is (BI duration)/(number of discovered neighboring APs +1).

- The APs in an mDN exchange information between one another using mesh networking topology or via a method such as the following.

  - A wireless medium between APs using a different channel or via an associated user located in the mDN.
  - Wired communication among APs, such as a wired local network.
  - A combination of a distribution service and external network.

4.1.2.1 TDD Channel Access

To achieve fair communication with no interference in mDNs, a TDD-SP allocation method is used to specify the TDD channel access rules. As shown in Fig. 4.2, a TDD-SP consists of consecutive TDD-Intervals, each of which in turn consists of consecutive TDD-Slots separated by new GTs. During both the TDD-SP and a TDD-Interval, the allocation time

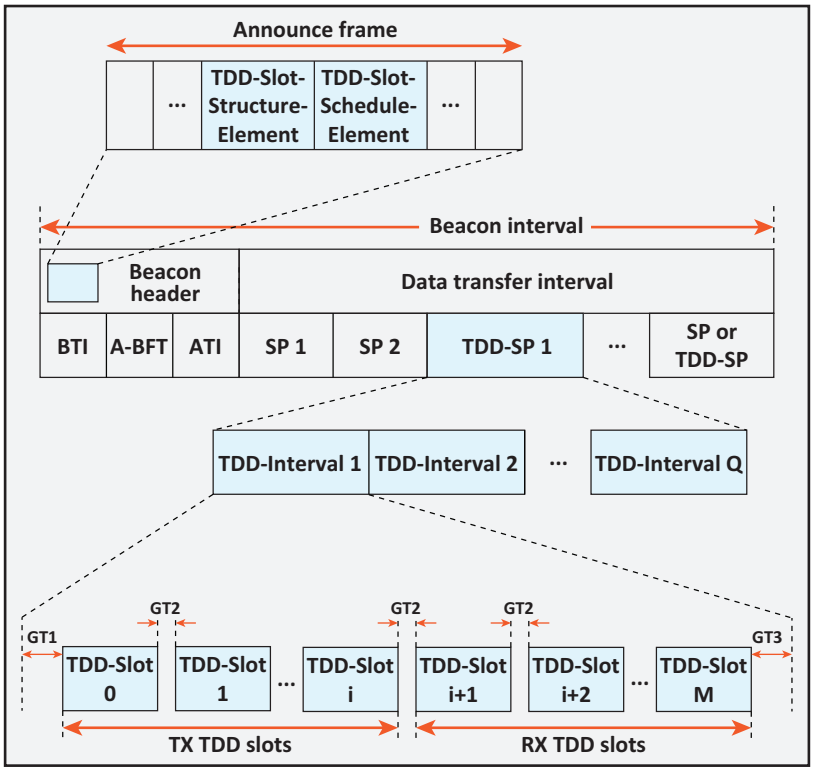

Figure 4.2: The allocation structure of TDD channel access.

may contain one or more slots. A TDD bitmap schedule is used to indicate the allocation type, e.g., TX or RX allocation, and the access permissions. During the Announce frame, each AP transmits the bitmap information to its neighbors in unicast messages. Moreover, it identifies the allocation category, such as a control, management, or Data-only frame.

4.1.2.2 mDN BF Training Protocol

Regular BF training is not appropriate for TDD channel access allocations because it uses different interframes to separate the BF frames. Therefore, IEEE 802.11ay defines a new form of TDD BF training for mDNs by considering new GT interframes. There are the two types of TDD BF training, namely TDD individual and group BF training. We consider

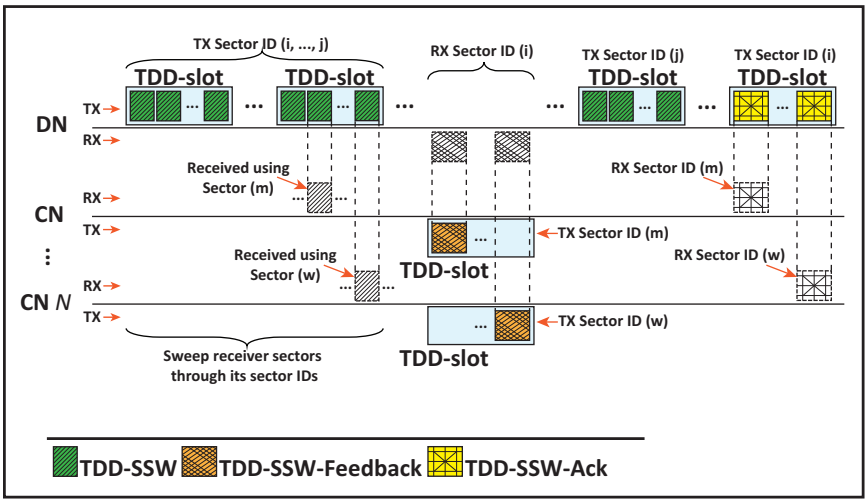

Figure 4.3: TDD BF training procedure.

group BF training in this chapter, since it can increase TDD BF efficiency by reducing the BF training overhead: BF training time is reduced since a certain number of users are trained simultaneously. As shown in Fig. 4.3, the procedure of the TDD group BF is as follows.

i) An AP sends multiple TDD-SSW frames for multiple users by using the broadcast MAC address subfield to initiate the TDD group BF. During this process, the number of users to be trained is specified.

ii) Each user sends TDD-SSW-Feedback frames in different time allocations using the sector with the best link quality (the best SID).

iii) After receiving the TDD-SSW-Feedback frames, the AP transmits several TDD-SSW-Ack frames to each user in different time allocations in order to transmit the SID used by the AP, the SID used by the user, and information about whether the BF training is completed.

4.2 MHVG Algorithm

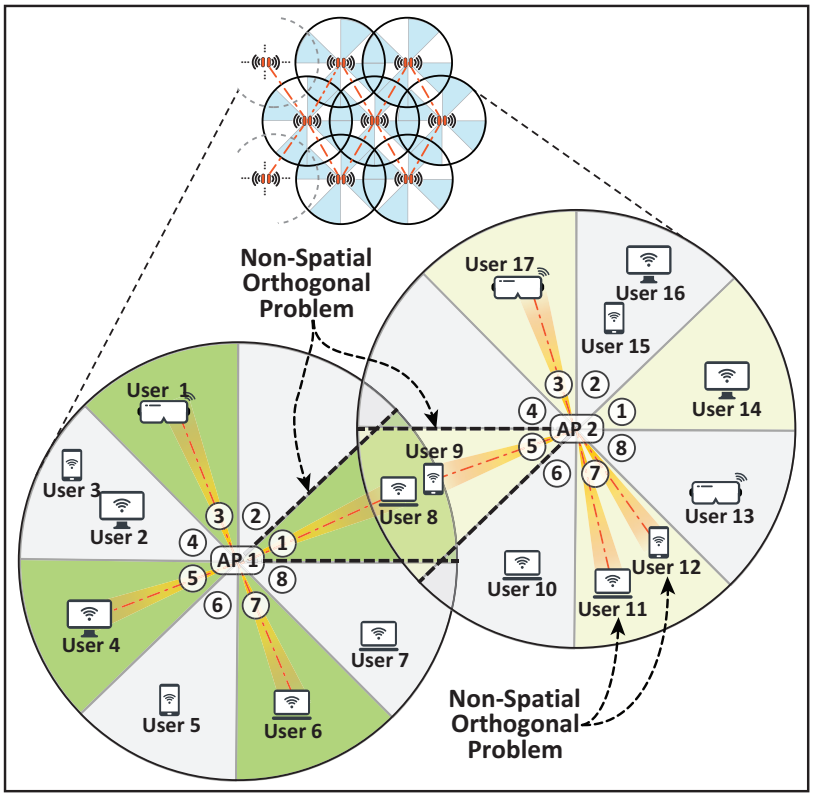

Figure 4.4: Multi-hop simultaneous downlink transmission example.

The VG algorithm in Chapter 3 is extended here to realize simultaneous downlink transmission and mitigate the CCI when two or more APs are deployed, instead of mitigating only the MUI in a single hop. The MHVG algorithm allows simultaneous downlink transmissions and can cancel both the MUI and the CCI without pre-coding schemes or CSI feedback information. As shown in Fig. 4.4, the MHVG algorithm is similar to the VG algorithm, with the following modifications. The MHVG algorithm divides the coverage area of each AP into VSs in order to mitigate the MUI and the CCI. These VSs are divided based on the beam direction associated with the optimal SID, determined when the users report their SID during the TDD BF training. Then, these VSs are divided into

two orthogonal groups (VG_{g1} and VG_{g2}) so as to achieve simultaneous transmission in separate time slots for each group. To mitigate the interference among overlapping users in the same active VS, we propose a Spatial-Reuse condition as an essential prerequisite before transmission can be granted. This helps avoid the non-spatial orthogonal problem (discussed in Section (3.2.1)). As illustrated in Fig. 4.4, this problem occurs when more than one user is reported in the same VS within a single hop, or when the VS used will incur CCI to any active users within the coverage of other APs. Specifically, the simultaneous downlink transmission can start when the Spatial-Reuse condition is fulfilled; otherwise, the algorithm terminates simultaneous transmission and schedules the intended user sequentially in a different time slot, if necessary.

Suppose the VSs for AP 1 and AP 2 for a particular time are as shown in Fig. 4.4. We can see there is CCI because user 8 is in the same VS coverage as user 9: that associated with AP 2. In this situation, AP 1 cannot transmit simultaneously with user 8 because of the non-spatial orthogonal problem, but can do so with user 1, user 4, and user 6, as they would not interfere with respect to AP 2. Note that user 11 and user 12 suffer from the non-spatial orthogonal problem with AP 2. Only one of these users is selected for simultaneous transmission, and the other is sequentially scheduled in a different time slot.

The proposed MHVG algorithm for simultaneous downlink transmissions is shown in Fig. 4.5 and runs as follows.

1. An AP initiates an Announce frame to establish TDD channel access. Each AP listens to identify the upcoming transmission schedules of neighboring APs so the maximum permitted BI duration and bitmap information can be exchanged.

2. After the BF training is completed, all APs check and announce the best SID information exchanged among all associated users.

3. Upon reception of the best SID information, the AP examines both the MUI and the

CCI before granting simultaneous data transmission allocations as follows.

(a) If the Spatial-Reuse condition is not satisfied when more than one user is reported in the same VS within a single hop, the one user with the highest SNR will be picked for simultaneous transmission. During the TDD-Interval, the selected user will be allocated in time slot t if located in VG_{g1} and or in $t+1$ if in VG_{g2}. The remaining users will be sequentially allocated in different time slots.

(b) If the Spatial-Reuse condition is not satisfied when the choice of VS will incur CCI to any active users in partially overlapped APs, the intended simultaneous transmission in this specific VS for the corresponding user will be terminated and sequentially rescheduled in a different time slot.

4. Finally, both simultaneous and sequential TDD-Slots will be started during TDD-Interval allocations, where these allocations are announced.

4.3 Performance Analysis

The main idea of the proposed MHVG algorithm is to mitigate CCI and allow simultaneous transmission by exploiting the spatial reuse that results from the virtual grouping when the coverage zones are separated into VSs. Spatial reuse is an essential metric for evaluating MAC protocol performance in wireless mesh networks. As shown in Fig. 4.6, we investigate the proposed MHVG algorithm in this section from the spatial reuse point of view, in a static mesh network where simultaneous downlink transmissions are considered inside a given region (a). The analysis considers different powers or coverage areas for each AP, as shown in Fig. 4.7.

Specifically, we evaluate the performance of the MHVG algorithm by analyzing the spatial multiplexing gain, which represents the number of simultaneous transmissions al-

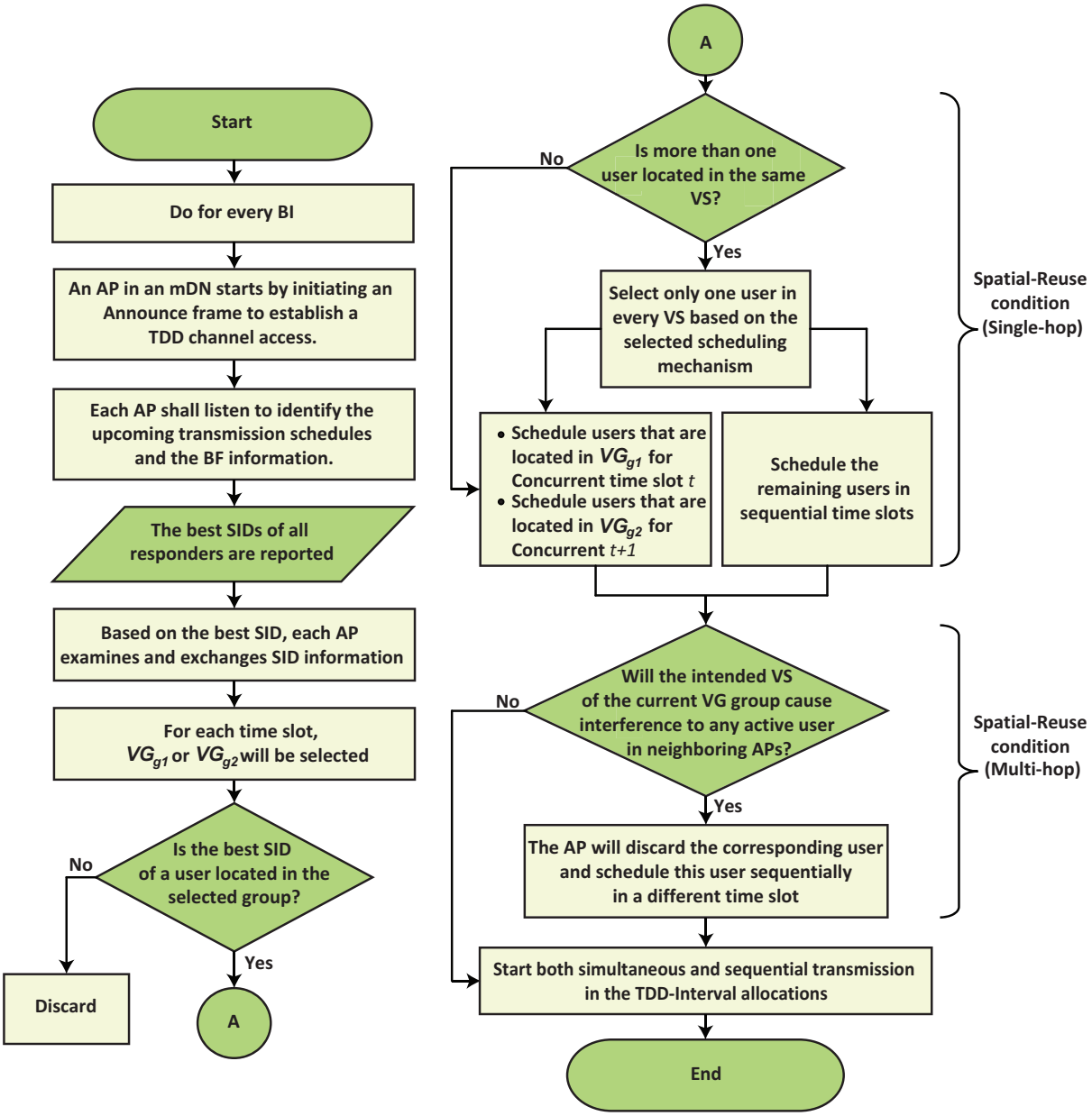

Figure 4.5: Flow chart of the MHVG algorithm.

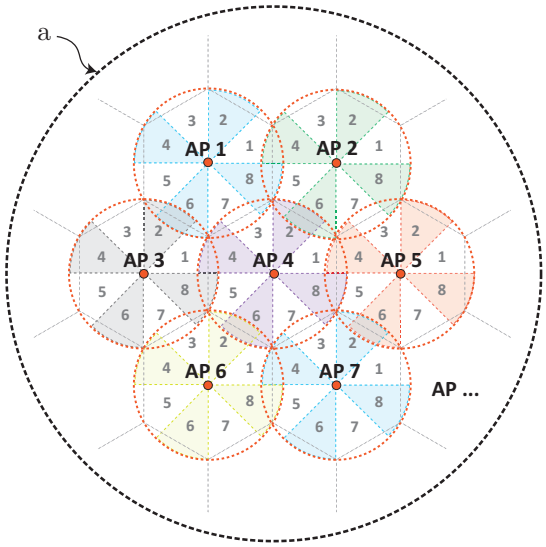

Figure 4.6: Example of the spatial reuse of the MHVG algorithm in a wireless mesh network.

lowed over the same mmWave channel in a given area from the perspective of spatial reuse. The throughput and delay characteristics at each AP in a wireless multi-hop network can be severely affected by CCI if the spatial reuse is not managed appropriately. Moreover, the probability of achieving simultaneous transmissions depends on the coverage area and the VS angle: interference occurs when the active VSs overlap.

For simplicity, we consider a traceable case, as shown in Fig. 4.8, where a is the area of a circle with radius r. There are two or more APs with coverage area of radius x_i randomly distributed in a. Let b_1 and b_2 denote the areas of the active VSs of AP 1 and AP 2, respectively. Then, the probability (P_1) that b_2 does not overlap with b_1 is

$$P_1 = 1 - \frac{x_1^2}{2r^2}, \tag{4.1}$$

The probability (P_2) that b_1 does not overlap with b_2 is

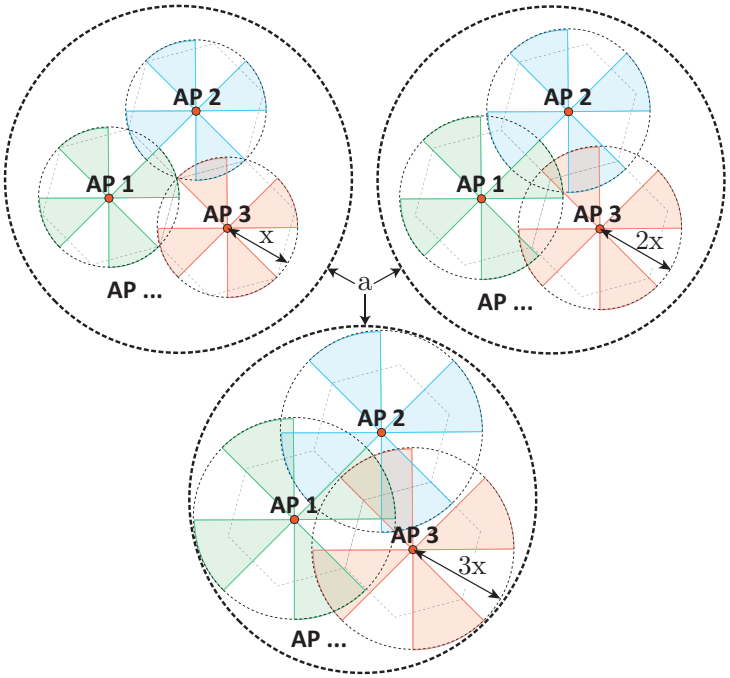

Figure 4.7: Example of MHVG algorithm considering different power or coverage area of each AP.

$$P_2 = 1 - \frac{x_2^2}{2r^2}, \tag{4.2}$$

Thus, the probability (Q) that neither AP 1 nor AP 2 interfere with each other is

$$Q = P_1 P_2, \tag{4.3}$$

Fig. 4.9 shows the numerical results of the probability Q versus the radius coverage of AP 1 and AP 2 ($x_1 = x_2$), considering different VS angles (θ). It can be seen that a higher spatial multiplexing gain can be achieved when both the radius and angle are relatively small, while the spatial multiplexing gain decreases when the angle and radius are larger. Therefore, simultaneous transmission can be realized and interference can be mitigated

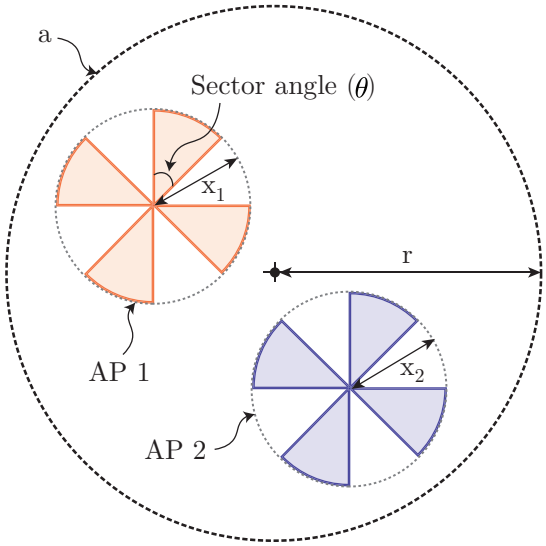

Figure 4.8: Example of the simultaneous transmission scenario in an mDN.

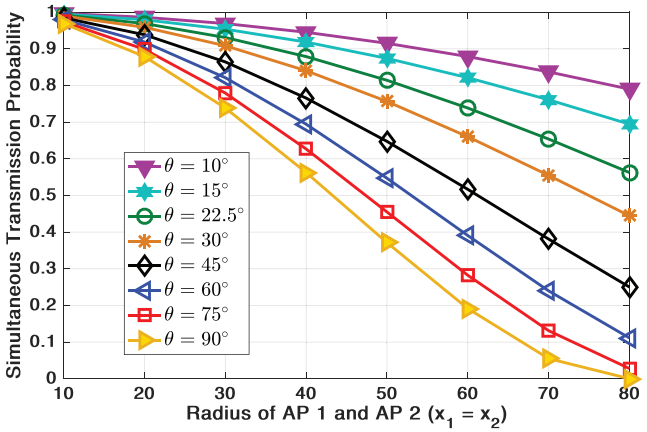

Figure 4.9: Probability Q versus the radius of AP 1 and AP 2 ($r = 80m$).

when using the proposed MHVG algorithm and when ensuring that the radius coverage of the APs is sufficiently small.

Fig. 4.10 shows the numerical results of the probability Q versus the number of APs when considering different VS angles (θ) and radius coverage (x), assuming all APs

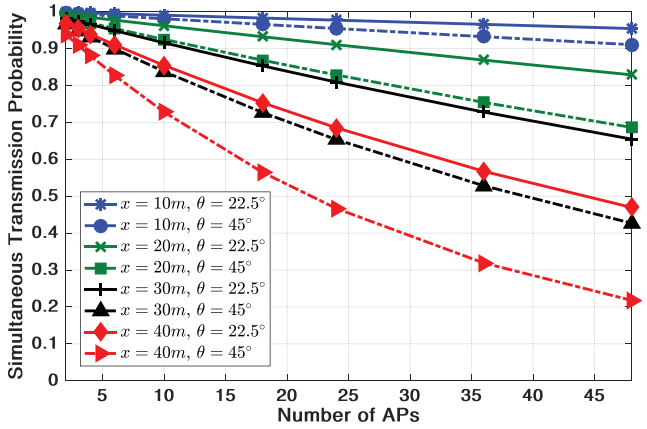

Figure 4.10: Probability Q versus the number of APs ($r = 160m$).

have the same x at every time. Fig. 4.10 shows how separating the coverage zone into VSs can increase the channel utilization efficiency and interference mitigation, as long as the coverage area of each AP is small enough. More spatial gain can be realized when the VS angle (θ) is reduced. Therefore, simultaneous transmission can be realized and interference can be mitigated while considering the footprint of the VSs, especially in dense deployments.

4.4 Performance Evaluation

In this section, we provide the simulation results for the proposed MHVG algorithm, as compared to the time-division multiple access (TDMA) method.

4.4.1 Simulation Setup

We consider a mesh networking topology where each AP is in the center of its coverage and all K users are uniformly, randomly distributed in this area, as shown in Fig. 4.11.

All transmitters and receivers have directional antennas and use the same transmission power. The contention problem of the A-BFT is not considered in this simulation, and we assume that there are always 8 random active users to associate in every BI. We evaluate the MHVG algorithm in terms of average throughput per time slot; the throughput of the IEEE 802.11ad system is up to 6.75 Gbps, using 64 quadrature amplitude modulation and 2.16 GHz of spectrum at 60 GHz. We evaluate the performance of our proposed MHVG algorithm by randomly generating user location information 10,000 times for each AP, simulating 2,000,000 BIs. Then, this simulation is repeated for a different number of APs in order to demonstrate the average network throughput performance in dense deployment scenarios.

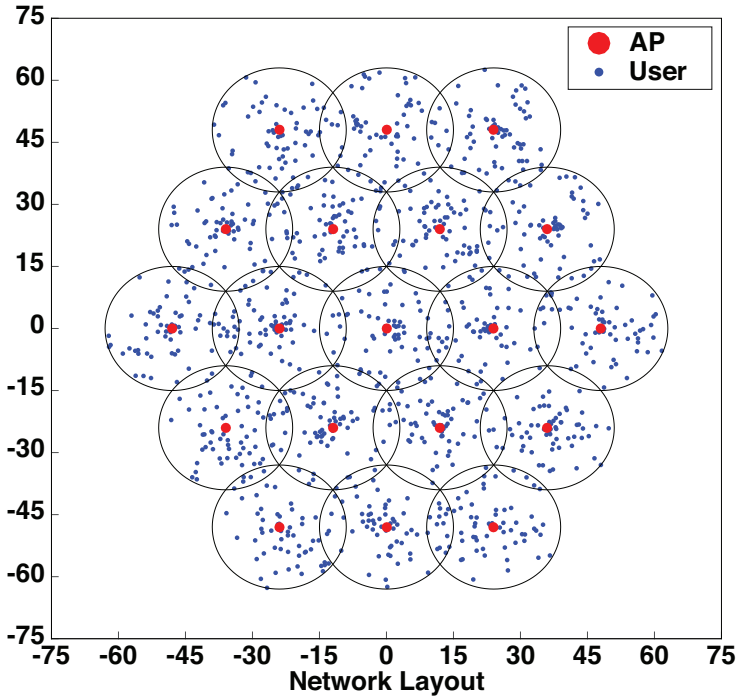

Figure 4.11: Simulation network layout.

4.4.2 Average Network Throughput Performance

Fig. 4.12 shows how the unique spatial reuse of the MHVG algorithm can be exploited for simultaneous downlink transmission, as compared to the TDMA method of TDD channel access. For TDD channel access, the APs divide the data transmission among themselves using a time division method. At each AP, there is at most one transmission link in any time slot. The simultaneous transmissions enabled by the proposed MHVG algorithm increase the average network throughput significantly and improve the spatial reuse. This significant increase in throughput is expected due to the two-time slots in VG_{g1} and VG_{g2}, which can realize simultaneous transmission. Simulation results demonstrate that it is possible to achieve both interference mitigation and simultaneous transmission without complex precoding methods.

For further performance evaluation, we also evaluate the scenario in which both interfering VSs are excluded from simultaneous transmissions, so both users are eliminated if either causes CCI for the other. The two users are then sequentially allocated in two different time slots. For example, in Fig. 4.4, user 8 and user 9 will not be considered for simultaneous transmission. The results in Fig. 4.12 show the average network throughput decreases insignificantly when the interfering VSs of both APs are excluded from simultaneous transmissions. However, it still maintains a significantly better average network throughput than the TDMA method due to the spatial reuse provided by the MHVG algorithm.

Fig. 4.13 shows the average network throughput of the MHVG algorithm versus the number of users for different numbers of APs when one or both interfering VSs are eliminated. It can be seen that there is no significant effect when the number of users increases. This is similar to the findings in Chapter 3, in which the MHVG algorithm is independent on the number of users because it selects only one user in each VS out of the associated users in every BI. Therefore, simultaneous transmission can be achieved without

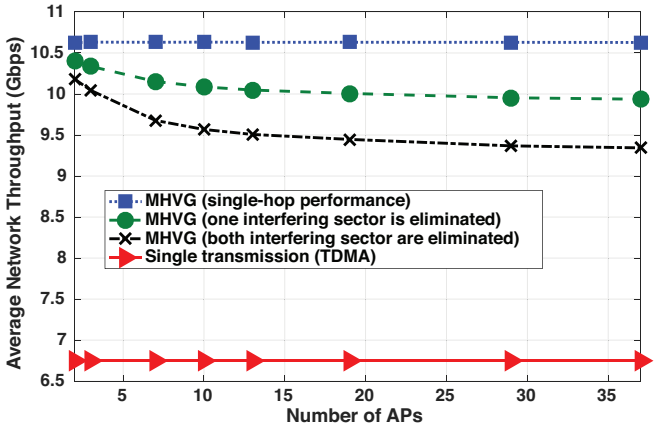

Figure 4.12: Average network throughput versus the number of APs.

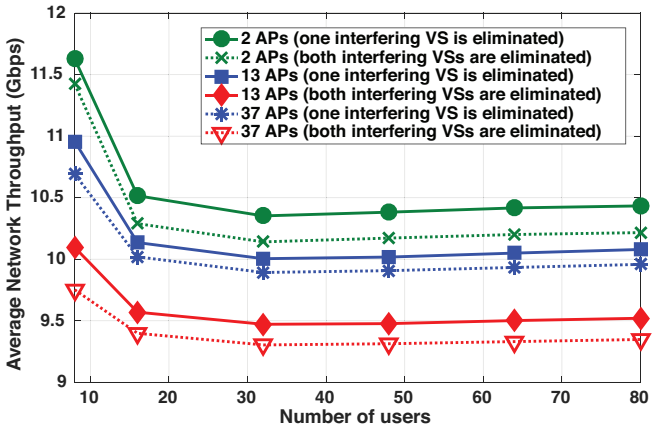

Figure 4.13: Average network throughput versus the number of users.

adding any further overhead or complexity to the system.

4.5 Summary

This chapter proposes an MHVG algorithm for simultaneous downlink transmission links in overlapping APs scenarios. Based on only the analog BF information, the MHVG

algorithm can mitigate CCI without adding extra overhead, such as CSI feedback, to the system. Simulation results show that the average network throughput can significantly improve on the TDMA scheme in IEEE 802.11ad. Furthermore, the proposed MHVG algorithm can achieve high performance and attain simultaneous transmission without causing interference, as long as the directivity of the mmWave communication is applied.

Chapter 5

Low-Complexity Uplink Multi-User MIMO Algorithm

MmWave communication technology is expected to play a crucial role in future wireless networks with large user populations because of the large spectrum band it can provide. To further improve spectrum efficiency over the mmWave bands in WLANs with a large number of users, an uplink multi-user MIMO transmission can be exploited in ultra-dense networks. Although uplink multi-user transmission is a promising technology, both the user selection algorithm and the BF mechanism need to be considered in an mmWave system with a large user population.

In this chapter, we propose a low-complexity user selection algorithm for an uplink multi-user transmission in mmWave WLAN. The proposed algorithm can achieve simultaneous uplink transmissions when the number of users is large while keeping the computational complexity as low as possible. This chapter offers three main contributions:

1. We develop a three-step HBF algorithm, HBF-VG, to combine user selection with the HBF algorithm while keeping the computational complexity low. Specifically,

we propose a low-complexity user selection algorithm in which semi-orthogonality is exploited as a selection metric based on analog BF information rather than seeking full CSI from all users. In addition, we optimize the digital BF by maximizing the SINR to further enhance system performance instead of utilizing the traditional ZF method.

2. We analyze the influence of angle correlation, analog beam pattern, and beamwidth on the proposed user selection algorithm. We then determine the computational complexity of the proposed algorithm as compared to the optimal user selection solution.

3. We evaluate the energy efficiency of the proposed HBF-VG algorithm and examine the effect of RF-chain implementation. We carry out extensive simulations to validate the performance of the proposed algorithm with respect to both energy efficiency and the average sum rate of the system, as compared to the existing HBF algorithms.

5.1 System Model

We use the IEEE 802.11ay mmWave system architecture to describe the uplink multi-user MIMO BF problem, while achieving backward compatibility with traditional IEEE 802.11ad. As shown in Fig. 5.1, simultaneous uplink transmissions are considered in this model, with the benefits of the spatial dimension of the channel applied by using the physical layer mechanism of the multi-user MIMO. In this scenario, we consider one AP and K users. The AP and users are all equipped with steerable directional antennas and can use enhanced-DMG, as defined in IEEE 802.11ay.

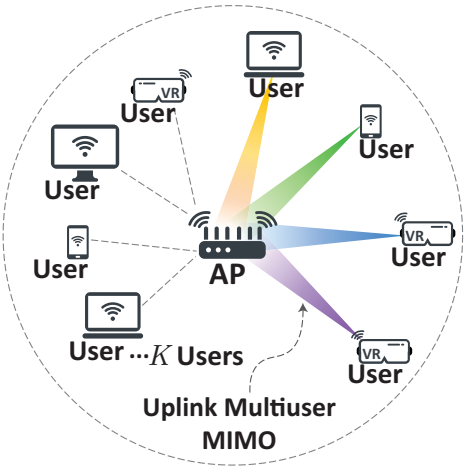

Figure 5.1: Network model.

5.1.1 HBF Model

We consider an uplink multi-user HBF system for a subset of users. The AP is equipped with N_r antennas, and each user is equipped with N_t antennas, as shown in Fig. 5.2. We assume there are N_f RF chains at the AP, to support multiple users simultaneously, while a single RF chain is available for each user. We assume that the number of users, K, is larger than the number of available RF chains at the AP, N_f ($K >> N_f$). User selection is necessary because the HBF approach requires a limited number of RF chains at the AP to reduce complexity and power consumption. Let $\Omega = \{1, ..., K\}$ be the set of all potential users, and $\mathcal{G} \subseteq \Omega$ be the subset of selected users served by the AP simultaneously. For ease of representation, let S be the cardinality of the subset $\mathcal{G}$ ($S = |\mathcal{G}|$).

Both AP and user are assumed to use predefined analog beams due to the constraints of the RF hardware: the RF phase shifters can take only quantized angles. Thus, the analog BF vector at the i-th user is represented by $\mathbf{u}_i \in \mathbb{C}^{N_t \times 1}$, where $\mathbf{u}_i$ is an element of the analog transmitter BF vectors $\mathcal{F}_t$ with quantized phases and constant magnitude items. Similarly, the analog BF vector at the i-th RF chain at the AP is denoted by

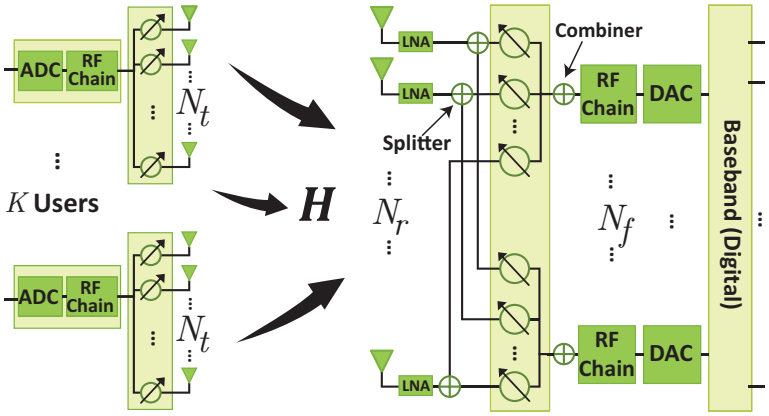

Figure 5.2: HBF architecture.

$\mathbf{v}_i \in \mathbb{C}^{N_r \times 1}$, where $\mathbf{v}_i$ is an element of the analog receiver BF vectors $\mathcal{F}_r$. Note that $\mathbb{E}[\|\mathbf{u}_i\|^2] = \mathbb{E}[\|\mathbf{v}_i\|^2] = 1$. We assume that each user is transmitting a single uplink data stream. Therefore, the transmitted signal of the i-th user is

$$\mathbf{s}_i = \sqrt{P}\mathbf{u}_i x_i, \tag{5.1}$$

where x_i and P are, respectively, the data symbol and transmit power for the i-th user, such that $\mathbb{E}[x_i] = 0$ and $\mathbb{E}[|x_i|^2] = 1$. To simplify analysis, we assume all users employ the same transmit power [24, 44]. For traceability, we also assume a block-fading channel model, in which the AP observes the received signal as

$$\mathbf{r} = \sum_{i=1}^{S} \sqrt{P}\mathbf{H}_i \mathbf{u}_i x_i + \mathbf{n}, \tag{5.2}$$

where $\mathbf{H}_i \in \mathbb{C}^{N_r \times N_t}$ is the channel matrix from the i-th user to the AP, and $\mathbf{n} \in \mathbb{C}^{N_r \times 1}$ is the additive white Gaussian noise vector at the AP, with zero mean and variance per element σ^2 .

The mmWave MIMO channel can be illustrated using the broadly applicable Saleh-

Valenzuela model [85] with L limited scatters in user i's channel. Therefore, we adopt this model to construct the uplink channel matrix $\mathbf{H}_i$ from the i-th user to the AP:

$$\mathbf{H}_i = \sqrt{\frac{N_t N_r}{L_i}} \sum_{l=1}^{L_i} g_{i,l} \mathbf{a}_r(\theta_{i,l}) \mathbf{a}_t(\phi_{i,l})^H, \tag{5.3}$$

where $\mathbf{a}_t(\phi_{i,l})$ and $\mathbf{a}_r(\theta_{i,l})$ are the antenna array response vectors for the i-th user and the AP, respectively. $\theta_{i,l}$ and $\phi_{i,l} \in [0, 2\pi]$ denote the angles of arrival and departure, respectively, of the l-th path. $g_{i,l}$ denotes the channel gain of the l-th path. A uniform antenna array is adopted in this chapter even though our algorithms and results can be revised to work with other antenna arrays. Thus, the $\mathbf{a}_t(\phi_{i,l})^H$ and $\mathbf{a}_r(\theta_{i,l})$ can be written as

$$\mathbf{a}_r(\theta_{i,l}) = \frac{1}{\sqrt{N_r}} [1, e^{j\frac{2\pi}{\lambda} d \sin(\theta_{i,l})}, ..., e^{j(N_r-1)\frac{2\pi}{\lambda} d \sin(\theta_{i,l})}]^T, \tag{5.4}$$

$$\mathbf{a}_t(\phi_{i,l}) = \frac{1}{\sqrt{N_t}} [1, e^{j\frac{2\pi}{\lambda} d \sin(\phi_{i,l})}, ..., e^{j(N_t-1)\frac{2\pi}{\lambda} d \sin(\phi_{i,l})}]^T, \tag{5.5}$$

where λ represents the mmWave signal wavelength and $d = \lambda/2$ denotes the distance between antenna elements.

We consider a unitary Discrete Fourier Transform (DFT) codebook similar to that in the IEEE 802.11ad/ay standard [82, 86] to define the analog BF codebooks, $\mathcal{F}_t$ and $\mathcal{F}_r$. Let δ_t and δ_r be the antenna separations normalized by λ at the i-th user and AP, respectively. Then, $\mathcal{F}_t$ and $\mathcal{F}_r$ are given by

$$\mathcal{F}_t = [\mathbf{a}_t(0), \ \mathbf{a}_t\left(\tfrac{1}{N_t\delta_t}\right), \ \cdots \ \mathbf{a}_t\left(\tfrac{N_t-1}{N_t\delta_t}\right)], \tag{5.6}$$

$$\mathcal{F}_r = [\mathbf{a}_r(0), \ \mathbf{a}_r\left(\tfrac{1}{N_r\delta_r}\right), \ \cdots \ \mathbf{a}_r\left(\tfrac{N_r-1}{N_r\delta_r}\right)], \tag{5.7}$$

where $N_t\delta_t$ and $N_r\delta_r$ are the normalized lengths of the transmit and receive antenna arrays, respectively. The elements of each codebook indicate the steering angles (or sectors).

The signal received after multiplying by the analog BF matrix at the AP can be expressed by

$$\begin{aligned}\mathbf{y} &= \mathbf{V}^H\mathbf{r}, \\ &= \mathbf{V}^H\sum_{i=1}^{S}\sqrt{P}\mathbf{H}_i\mathbf{u}_i x_i + \mathbf{V}^H\mathbf{n}, \\ &= \sqrt{P}\mathbf{V}^H\mathbf{H}_i\mathbf{u}_i x_i + \sqrt{P}\underbrace{\sum_{j\neq i}^{S}\mathbf{V}^H\mathbf{H}_j\mathbf{u}_j x_j}_{\text{interference}} + \mathbf{V}^H\mathbf{n},\end{aligned} \tag{5.8}$$

where $\mathbf{V} = [\mathbf{v}_1, \mathbf{v}_2, ..., \mathbf{v}_S]$ is the analog BF matrix comprised of S analog BF vectors. The MUI generated by $S-1$ transmitting users is demonstrated in the second item of (5.8).

Digital BF is then employed to mitigate the MUI. Let $\mathbf{F} = [\mathbf{f}_1, \mathbf{f}_2, ..., \mathbf{f}_S] \in \mathbb{C}^{S\times S}$ be the digital BF at the AP such that $\|\mathbf{f}_i\|^2 = 1$. Then, $\mathbf{f}_i$ is utilized to decode x_i for the i-th user. Thus, the decoded symbol can be expressed as

$$\hat{x} = \sqrt{P}\mathbf{f}_i^H\mathbf{V}^H\mathbf{H}_i\mathbf{u}_i x_i + \sqrt{P}\underbrace{\sum_{j\neq i}^{S}\mathbf{f}_i^H\mathbf{V}^H\mathbf{H}_j\mathbf{u}_j x_j}_{\text{interference}} + \mathbf{f}_i^H\mathbf{V}^H\mathbf{n}. \tag{5.9}$$

Given the decoded symbol at the AP in (5.9), the SINR of the i-th user is given by

$$\gamma_i = \frac{P|\mathbf{f}_i^H\mathbf{V}^H\mathbf{H}_i\mathbf{u}_i|^2}{P|\sum_{j\neq i}^{S}\mathbf{f}_i^H\mathbf{V}^H\mathbf{H}_j\mathbf{u}_j|^2 + \sigma^2}. \tag{5.10}$$

Thus, the achievable rate for the i-th user can be written as

$$R_i = \log_2\left(1 + \frac{P|\mathbf{f}_i^H\mathbf{V}^H\mathbf{H}_i\mathbf{u}_i|^2}{P|\sum_{j\neq i}^{S}\mathbf{f}_i^H\mathbf{V}^H\mathbf{H}_j\mathbf{u}_j|^2 + \sigma^2}\right). \tag{5.11}$$

5.1.1.1 Problem Formulation

The sum rate (R_{sum}) of the uplink multi-user network can be maximized. The optimal HBF can be determined by finding the optimal analog BF, optimal digital BF, and optimal subset of users. The optimization problem can be formulated as

$$\mathcal{P}1 : \max_{\mathbf{U},\mathbf{V},\mathbf{F},\mathcal{G}} \quad R_{sum} = \sum_{i=1}^{S} R_i \tag{5.12a}$$

$$\text{s.t.} \quad \mathbf{u}_i \in \mathcal{F}_t, \forall i \in \mathcal{G}, \tag{5.12b}$$

$$\mathbf{v}_i \in \mathcal{F}_r, \forall i \in \mathcal{G}, \tag{5.12c}$$

$$\|\mathbf{f}_i\|^2 = 1, \forall i \in \mathcal{G}, \tag{5.12d}$$

$$\mathcal{G} \subseteq \Omega, \tag{5.12e}$$

$$|\mathcal{G}| \leq N_f. \tag{5.12f}$$

The optimization problem ($\mathcal{P}1$) is a mixed integer programming problem. This is a non-convex NP-hard problem, and finding the optimal solution is neither practical nor tractable for the following reasons: (i) constraints (5.12b) and (5.12c) are finite sets with integer constraints; (ii) due to the interference, the objective function is still a non-convex function of digital BF vectors $\mathbf{f}_i$, even though the analog BF vectors are fixed; (iii) to find the optimal subset of users that will maximize the sum rate, the subset of users needs to be jointly selected with both analog BF and digital BF; this means an exhaustive search over all K users is required, which can lead to high computational complexity: high CSI acquisition overhead is needed at the AP to collect CSI from all potential users in order to identify the best user group.

The problem of finding joint optimal analog BF and digital BF (similar to $\mathcal{P}1$) has been studied before, in [24, 43, 44, 46]. However, the user selection problem has not been considered with the HBF algorithm when the number of users is larger than that of available

RF chains. To solve the challenges associated with the user selection problem, we propose a novel HBF-VG algorithm with a low-complexity user selection algorithm in Section 5.2. The aim of our proposed algorithm is to incorporate the user selection algorithm into the HBF algorithm while keeping computational complexity low and realizing satisfactory performance.

5.2 HBF-VG Algorithm

To reduce the high computational complexity associated with solving problem $\mathcal{P}1$, and to consider the user selection problem when $K >> N_f$, we employ a suboptimal three-step algorithm, summarized in Algorithm 3.

The analog BF, digital BF, and user selection are separately designed in the proposed HBF-VG algorithm. First, the AP and each user maximize their anticipated beam steering between one another using the analog BF, without considering the MUI. This step adopts the SLS BF training of the IEEE 802.11ay. Second, a user selection algorithm selects a subset of users based only on the information from the analog BF training realized in the first step. Thus, no additional full CSI feedback is required. Third, the final step adopts digital BF to mitigate the residual MUI, using an SINR maximization method.

5.2.1 First Step: Analog BF

The SLS BF training from the IEEE 802.11ay standard represents the analog beam pattern (analog BF). Analog BF vectors can only take finite values because of RF hardware constraints: the RF phase shifters only take quantized angles. The analog BF vectors can be selected from finite-size codebooks in (5.6) and (5.7), with both the AP and users selecting from these predefined analog beams.

Algorithm 3: HBF-VG Algorithm

Inputs: $\mathcal{F}_t$ and $\mathcal{F}_r$, the codebook sets of analog BF for each user and AP, respectively.

Outputs: $\mathbf{u}_i$, $\mathbf{v}_i$, $\mathbf{f}_i$, and $\mathcal{G}$.

First Step: Analog BF

Each user and AP selects $\mathbf{u}_i$ and $\mathbf{v}_i$ to determine the best beam pair, as in $\mathcal{P}2$. Then, the best SID pair is obtained through the sequential training method using SLS BF, as described in Subsection 3.1.3.

Second Step: Proposed User Selection

The AP divides the coverage area into VSs.
The VSs are divided into two semi-orthogonal groups: VG_{g1} and VG_{g2}.
The AP selects a subset of users based on the best SID reported in step 1.
The AP schedules multi-user transmission in separate time slots for each group.

Third Step: Digital BF

The AP estimates the effective channel, $\bar{\mathbf{h}}_i = \mathbf{V}^H \mathbf{H}_i \mathbf{u}_i, \forall i \in \mathcal{G}$, for each user$_i$.
The AP designs $\mathbf{f}_i$ in (5.18) for the i-th RF chain, with all effective CSI.
The AP normalizes $\mathbf{f}_i = \frac{\mathbf{f}_i}{\|\mathbf{f}_i\|}$ for i.

Each user and AP has to choose $\mathbf{u}_i \in \mathcal{F}_r$ and $\mathbf{v}_i \in \mathcal{F}_t$, the analog BF codebooks, to maximize channel gain and determine the best transmit and receive beam pair for each user:

$$\mathcal{P}2 : \max_{\mathbf{u}_i, \mathbf{v}_i} \quad \|\mathbf{v}_i^H \mathbf{H}_i \mathbf{u}_i\|^2 \tag{5.13a}$$

$$\text{s.t.} \quad \mathbf{u}_i \in \mathcal{F}_t, \forall i \in \Omega \tag{5.13b}$$

$$\mathbf{v}_i \in \mathcal{F}_r, \forall i \in \Omega \tag{5.13c}$$

An exhaustive search method requiring a search over the entire $\mathcal{F}_t \times \mathcal{F}_r$ of possible transmit and receive steering angles combinations (analog BF vectors combinations) can solve the above problem. However, this can increase analog BF training overhead significantly. The IEEE 802.11ad/ay standards use SLS BF training to handle this and reduce

the latency.

In this step, we adopt the SLS BF training in IEEE 802.11ad/ay. Since we use iterative bidirectional training with sequential time slots, the full CSI is not required. The SLS BF training can determine the best SID pair in the sequential training method, as explained in Subsection 3.1.3.

5.2.2 Second Step: User Selection Algorithm

In order to reduce computational complexity, the user selection algorithm is performed independently in the second step of the HBF-VG algorithm after analog BF training is completed. The proposed user selection does not require full CSI; it can be realized from only the analog BF information.

As described in Section 3.2, we propose a user selection algorithm in this step to divide users into two semi-orthogonal groups without the need to find an optimal set of users by collecting the CSI for all users. The coverage area is divided into VSs ($A = 8$ in the example in Fig. 3.3) and these sectors are further divided into two semi-orthogonal groups, VG_{g1} and VG_{g2}, such that multi-user transmission can be attained in separate time slots for each group. Divisions are based on the beam direction associated with the optimal SID, determined when the users report their SID during analog BF training. Therefore, to calculate the number of SIDs per VG_{g1} or VG_{g2}, groups VG_{g1} and VG_{g2} can be formulated as $\left(\frac{A+2pq-2p}{A}\right) \leq \text{SID} \leq \left(\frac{2pq-p}{A}\right)$ and $\left(\frac{A+2pq-2p}{A}\right) \leq \text{SID} \leq \left(\frac{2pq-p}{A}\right)$, respectively, where A is the total number of VSs, p is the total number of SIDs, and $q = \{1, 2, ..., A/2\}$. The details of the proposed user selection algorithm are shown in Algorithm 4.

Note that when more than one user is reported in the same VS, only the user with the highest SNR is selected for multi-user transmission. While we use the SNR reported during A-BFT as a selection metric, any other scheduling mechanism could be utilized. The details of the proposed user selection algorithm are as follows:

1. After the BF training is completed, the AP checks and examines the best SID information exchanged by all associated users.

2. If the best SID of the i-th user belongs to VG_{g1} or VG_{g2}, then the i-th user is selected and scheduled for simultaneous transmission at time slot t or $t+1$, respectively.

3. If there is more than one user in any VSs of VG_{g1} or VG_{g2}, then only the one user with the highest SNR is selected.

4. The unselected users are re-evaluated for simultaneous transmission by the algorithm until no user can be selected for VG_{g1} or VG_{g2}. Then, the AP schedules the unselected users in different time slots sequentially (not simultaneous transmission).

Algorithm 4: Proposed user selection algorithm

Input: The best SID information for each user.

Repeat

  for $SID = 1$ *to* p **do**

    if *the best SID of the i-th user belongs to* VG_{g1} $\left\{\left(\frac{A+2pq-2p}{A}\right) \leq SID \leq \left(\frac{2pq-p}{A}\right)\right\}$ **then**

      select user$_i$ and assign them to $\mathcal{G}$ at time slot t

    if *more than one user in the VSs of* VG_{g1} **then**

      select only the one user with the highest SNR

    if *the best SID of the i-th user belongs to* VG_{g2} $\left\{\left(\frac{A+2pq-p}{A}\right) \leq SID \leq \left(\frac{2pq}{A}\right)\right\}$ **then**

      select user$_i$ and assign them to $\mathcal{G}$ at time slot $t+1$

    if *there is more than one user in the VSs of* VG_{g2} **then**

      select only the one user with the highest SNR

Until there are no more users that can be selected **then**

the AP schedules the unselected users sequentially in advanced sequential time slots t.

5.2.3 Third Step: Digital BF Approach

After determining the subset of users ($\mathcal{G}$) in the second step of the HBF-VG algorithm, the AP can obtain digital BF vectors in order to cancel the remaining MUI from the selected users. By the time the second and third steps are complete, the AP is ready to simultaneously serve the selected users in $\mathcal{G}$ at each time slot (t). The interference mitigation of the ZF method, a common approach to digital BF, comes at the expense of energy inefficiency. Uplink scenarios should use an energy-efficient digital BF method because of limited power resources, e.g., on-board battery power. Therefore, we use an SINR maximization method instead of the more conventional ZF method in the digital BF step in order to increase energy efficiency.

For simplicity, let $h_{i,j} = \mathbf{v}_j^H \mathbf{H}_i \mathbf{u}_i \in \mathbb{C}^{1\times 1} \forall i \in \mathcal{G}$ be the effective channel gain between the i-th user and j-th RF chain at the AP. Furthermore, let $\bar{\mathbf{h}}_i = \mathbf{V}^H \mathbf{H}_i \mathbf{u}_i \in \mathbb{C}^{S\times 1}$ be the effective channel vector between the i-th user and the AP. Then, the SINR in (5.10) can be written as

$$\gamma_i = \frac{|\mathbf{f}_i^H \bar{\mathbf{h}}_i|^2}{|\mathbf{f}_i^H (\sum_{j\neq i}^{S} \bar{\mathbf{h}}_j + \frac{1}{\sqrt{P}} \bar{\mathbf{n}})|^2}, \tag{5.14}$$

where $\bar{\mathbf{n}} \triangleq \mathbf{V}^H \mathbf{n} \in \mathbb{C}^{S\times 1}$ is the processed noise vector.

The purpose of the digital BF step is to maximize the SINR when the digital BF is designed. To do this, an optimization problem can be formulated as follows:

$$\mathcal{P}3 : \max_{\mathbf{F}} \quad \gamma_i \tag{5.15a}$$

$$\text{s.t.} \quad \|\mathbf{f}_i\|^2 = 1, \forall i \in \mathcal{G}. \tag{5.15b}$$

To solve the above optimization problem, the objective function can first be simplified as follows. Let $\hat{\mathbf{H}}_i = [\bar{\mathbf{h}}_1, ..., \bar{\mathbf{h}}_{i-1}, \bar{\mathbf{h}}_{i+1}, ..., \bar{\mathbf{h}}_S] \in \mathbb{C}^{S\times S-1}$ be the extended effective channel

matrix that excludes $\bar{\mathbf{h}}_i$. Thus, the SINR in (5.14) can be written as

$$\gamma_i = \frac{\mathbf{f}_i^H \bar{\mathbf{h}}_i \bar{\mathbf{h}}_i^H \mathbf{f}_i}{\mathbf{f}_i^H (\hat{\mathbf{H}}_i \hat{\mathbf{H}}_i^H + \frac{\sigma^2}{P} \mathbf{I}_S) \mathbf{f}_i}. \tag{5.16}$$

Equation (5.16) is a Rayleigh quotient form. According to the Rayleigh-Ritz quotient theorem [87], the upper bound of γ_i is

$$\gamma_i \leq \lambda_{max}(\bar{\mathbf{h}}_i \bar{\mathbf{h}}_i^H, \hat{\mathbf{H}}_i \hat{\mathbf{H}}_i^H + \frac{\sigma^2}{P} \mathbf{I}_S), \tag{5.17}$$

where $\lambda_{max}(\mathbf{A}, \mathbf{B})$ is the largest eigenvalue of the matrix pair $\mathbf{A}$ and $\mathbf{B}$.

If $\mathbf{f}_i$ is the eigenvector equivalent to the largest eigenvalue, then equality can occur. Optimal $\mathbf{f}_i$ can then be written as $\mathbf{f}_i = \text{eigenvector}(\bar{\mathbf{h}}_i \bar{\mathbf{h}}_i^H, \hat{\mathbf{H}}_i \hat{\mathbf{H}}_i^H + \frac{\sigma^2}{P} \mathbf{I}_S)$. Finally, if the matrix $\hat{\mathbf{H}}_i \hat{\mathbf{H}}_i^H$ is invertible, the optimal $\mathbf{f}_i$ can be written as

$$\mathbf{f}_i = \text{eigenvector}((\hat{\mathbf{H}}_i \hat{\mathbf{H}}_i^H + \frac{\sigma^2}{P} \mathbf{I}_S)^{-1} \bar{\mathbf{h}}_i \bar{\mathbf{h}}_i^H). \tag{5.18}$$

The digital BF vector is then normalized, i.e., $\mathbf{f}_i = \frac{\mathbf{f}_i}{\|\mathbf{f}_i\|}$, because of the unit power constraint of digital BF.

Remark 1. *The SINR maximization method used in the digital BF step requires only low-dimensional effective CSI. Therefore, computational complexity can be reduced significantly. Furthermore, the SINR maximization method allows the digital BF design used above to attain a higher sum rate than designs that use ZF digital BF.*

5.3 Performance Analysis

The proposed user selection algorithm finds an indirect solution by selecting users with the most spatial separation in order to maintain decent semi-orthogonality between the effective channel vectors. Hence, the sum-rate performance for digital BF is better than with a random selection. This section describes first the impact of effective channel vectors of two-user on user selection in multi-user MIMO systems with digital BF, such as the ZF method. This underlines the importance of instantaneous channels among the selected users being orthogonal. Then, we analyze the impact of angle correlation and beam patterns on the proposed user selection algorithm and discuss its computational complexity.

5.3.1 Impact of Effective Channel Vectors of Two-User Using the ZF Method

This subsection investigates the impact of effective channel vectors on user selection when digital BF is adopted, using the ZF method, to mitigate the MUI. In the ZF method, to maximize the sum rate, the AP selects digital BF vectors $\mathbf{F}$ that can achieve the zero-interference condition $\sum_{j\neq i}^{S} \mathbf{f}_i^H \mathbf{H}_j = 0$. A common method to achieve zero interference is to use the pseudoinverse of the channel matrix of selected users in order to find the user that locally maximizes the total power projection. Finding the optimal solution to maximize the sum rate is challenging due to the computational complexity: it requires an exhaustive search over all K users. Thus, user selection that considers the channel state of the selected users is valuable.

We utilize the ZF method in this subsection for the sake of simplicity and traceability in the analysis. We will briefly review the relationship between the channel state of each selected user and the ZF digital BF technique, which nulls the effect of the other selected user by projecting the received signal in a direction orthogonal to that user. Following the

same analysis as in [37], consider a simple example with two users with single antennas that transmit simultaneously to a two-antenna AP. x_1 and x_2 are the symbols concurrently transmitted by user$_1$ and user$_2$, respectively. The signal received at the AP is given by

$$\mathbf{r} = \mathbf{H}_1 x_1 + \mathbf{H}_2 x_2 + \mathbf{n}, \tag{5.19}$$

where $\mathbf{r} = [r_1, r_2]$ is the received vector at the AP, and $\mathbf{H}_1 = [h_{11}, h_{12}]$ and $\mathbf{H}_2 = [h_{21}, h_{22}]$ are the channels vectors of user$_1$ and user$_2$, respectively. $\mathbf{n} = [n_1, n_2]$ is the noise vector, where $n_1, n_2 \sim \mathcal{CN}(0, N_0)$. We want to observe the effect of orthogonality and digital BF from the point of view of the SNR. Consider that the AP attempts to recover the symbol x_1. The interference from the other symbol x_2 can then be mitigated at the AP by projecting $\mathbf{r}$ in a direction orthogonal to $\mathbf{H}_2$. Then, the projected signal can be decoded. The estimate of x_1 is as follows:

$$\hat{x_1} = x_1 + \frac{h_{22}n_1 - h_{12}n_2}{h_{11}h_{22} - h_{21}h_{12}}. \tag{5.20}$$

By performing maximal-ratio combining [37], the SNR of x_1 when both symbols (x_1 and x_2) are transmitted simultaneously, denoted by SNR$_{Simult.}$, can be found as follows:

$$\begin{aligned} \text{SNR}_{Simult.} &= \frac{\mathbb{E}[\|x_1\|^2]}{\mathbb{E}[\|n_1\|^2]}, \\ &= \frac{\mathbb{E}[\|\mathbf{H}_1 x_1\|^2]}{N_0} \left(1 - \cos^2(\Theta)\right), \\ &= \text{SNR}_{prime} \left(1 - \cos^2(\Theta)\right), \end{aligned} \tag{5.21}$$

where SNR$_{prime}$ is the SNR of symbol x_1 when it is transmitted alone, and Θ is the Hermitian angle between the two channel vectors $\mathbf{H}_1$ and $\mathbf{H}_2$. This is defined as $0 \leq$

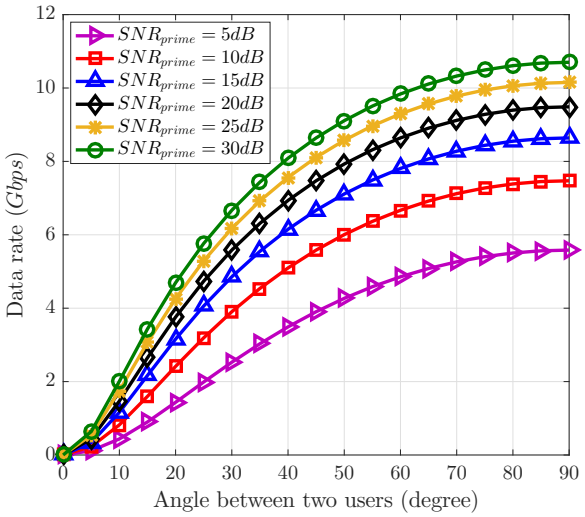

Figure 5.3: Data-rate performance versus different angles between two users.

$\Theta_H(\mathbf{H}_1, \mathbf{H}_2) \leq \pi/2$, such that

$$cos\Theta_H(\mathbf{H}_1, \mathbf{H}_2) = \frac{|\mathbf{H}_1 \cdot \mathbf{H}_2|}{\| \mathbf{H}_1 \| \| \mathbf{H}_2 \|}. \tag{5.22}$$

The Hermitian angle can be used to evaluate orthogonality and the spatial correlation between two channel vectors when non-orthogonal instantaneous channels among the selected users can result in MUI [88, 89].

We can observe from the above example that the angle between the two channel vectors of user$_1$ and user$_2$ can affect the SNR$_{Simult.}$ when they transmit simultaneously. Fig. 5.3 shows the data-rate performance using (5.21) versus the angles between users for different SNR$_{prime}$ values. Higher performance can be achieved when the angle between users is nearly orthogonal. Hence, SNR$_{Simult.}$ depends on the angle between the two users as well as on the ZF technique.

5.3.2 Impact of Angle Correlation on User Selection Algorithm

Angle correlation among the effective channel vectors of the selected users can affect the performance of the proposed algorithm after the digital BF stage. In order to justify the spatial separation or semi-orthogonality of the proposed user selection algorithm and analyze its benefit over the random user selection method, orthogonal vectors are first defined by adopting the ZF concept for traceability. Let $\mathbf{\Phi}_a \in VG_{g1}$ or VG_{g2} (where $a = \{1, 2, ..., A\}$) be the semi-orthogonal vectors shown in Fig. 5.4(a). The orthogonal directions Φ_1, Φ_3, Φ_5, and Φ_7 represent the simultaneous selection among users for the first group VG_{g1}, while Φ_2, Φ_4, Φ_6, and Φ_8 are the equivalents for VG_{g2}.

Subsequently, $\mathbf{\Phi}_a$ can be adopted to estimate if there are good spatial separations or alignments between $\mathbf{\Phi}_a$ and each $\mathbf{H}_i$. This is accomplished by calculating the angles between the channel gain vectors of each user in either VG_{g1} or VG_{g2} with respect to $\mathbf{\Phi}_a$. In other words, each user should be properly aligned with one of the defined semi-orthogonal vectors ($\mathbf{\Phi}_a$) in order to maintain spatial separation. For example, as shown in Fig. 5.4(b), we can assume that there is high orthogonality between user$_1$ ($\mathbf{H}_1$) and user$_4$ ($\mathbf{H}_4$) since they have the best alignment with $\mathbf{\Phi}_1$ and $\mathbf{\Phi}_2$, respectively. Thus, the semi-orthogonality selection criterion in the user selection algorithm allows better spatial separation and higher performance. Note that for generality, this analysis assumes that the beams focus only on one direction; the uniform antenna array beam pattern is neglected. The impact of the analog beam pattern is discussed in Subsection 5.3.3.

Proposition 1. *A higher SINR and better spatial correlation can be attained as long as the angle between two effective channel vectors is orthogonal or semi-orthogonal. Thus, MUI can be mitigated, and the sum rate can be improved.*

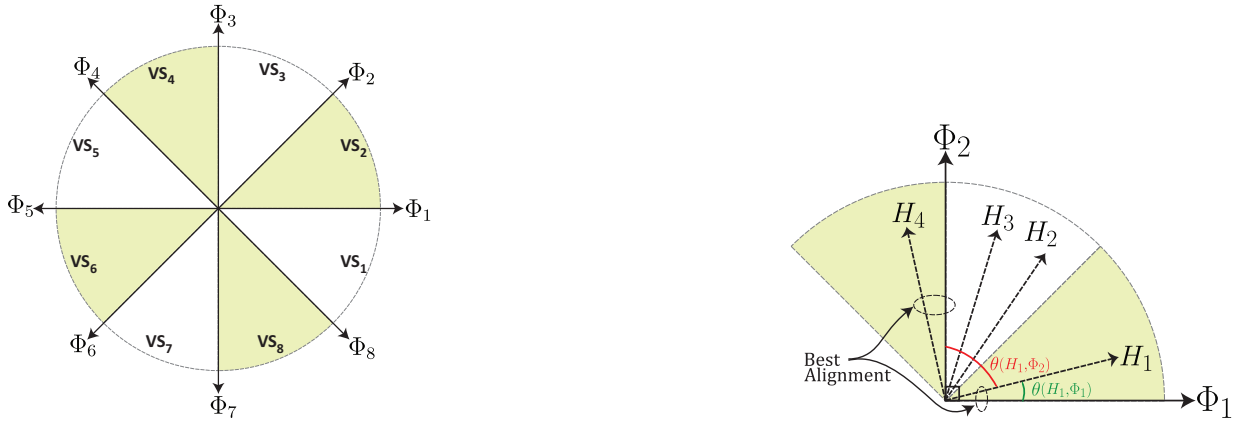

(a) $\mathbf{\Phi}_a$, when $A = 8$.

(b) Alignment metric example, when $A = 8$.

Figure 5.4: User selection using the predefined orthogonal-direction vectors.

Proof. Based on equation (5.14), the SINR of the i-th user can be written as

$$\begin{aligned}\gamma_i &= \frac{|\mathbf{f}_i^H \bar{\mathbf{h}}_i|^2}{\sum_{j\neq i}^{S} |\mathbf{f}_i^H \bar{\mathbf{h}}_j|^2 + \frac{\sigma^2}{P}} \\ &= \frac{||\bar{\mathbf{h}}_i||^2 |\mathbf{f}_i^H \tilde{\mathbf{h}}_i|^2}{\sum_{j\neq i}^{S} ||\bar{\mathbf{h}}_j||^2 |\mathbf{f}_i^H \tilde{\mathbf{h}}_j|^2 + \frac{\sigma^2}{P}},\end{aligned} \tag{5.23}$$

where $\tilde{\mathbf{h}}_i = \frac{\bar{\mathbf{h}}_i}{||\bar{\mathbf{h}}_i||}$, a unit vector of the effective channel vector $\bar{\mathbf{h}}_i$. The first term in the denominator represents interference from the other $S-1$ selected users, and the second term denotes the noise.

Let α denote the angle between $\mathbf{f}_i$ and $\bar{\mathbf{h}}_i$. Here, $\mathbf{f}_i$ can be decomposed as [88]

$$\mathbf{f}_i = (\cos\alpha)\tilde{\mathbf{h}}_i + (\sin\alpha)\mathbf{g}_i, \tag{5.24}$$

where $\mathbf{g}_i$ is a unit vector orthogonal to $\tilde{\mathbf{h}}_i$. Note we do not consider the detailed BF scheme for $\mathbf{f}_i$. Hence, the following analysis can be applied in various BF schemes.

Substituting (5.24) into (5.23), the SINR can be written as

$$\begin{aligned}\gamma_i &= \frac{||\bar{\mathbf{h}}_i||^2 \ \cos\alpha^2}{\sum_{j\neq i}^{S} ||\bar{\mathbf{h}}_j||^2 \left|\left((\cos\alpha)\ \tilde{\mathbf{h}}_i^H + (\sin\alpha)\ \mathbf{g}_i^H\right)\tilde{\mathbf{h}}_j\right|^2 + \frac{\sigma^2}{P}} \\ &= \frac{||\bar{\mathbf{h}}_i||^2 \ \cos\alpha^2}{\sum_{j\neq i}^{S} ||\bar{\mathbf{h}}_j||^2 \left|(\cos\alpha)\ \tilde{\mathbf{h}}_i^H\tilde{\mathbf{h}}_j + (\sin\alpha)\ \mathbf{g}_i^H\tilde{\mathbf{h}}_j\right|^2 + \frac{\sigma^2}{P}} \\ &= \frac{||\bar{\mathbf{h}}_i||^2 \ \cos\alpha^2}{\sum_{j\neq i}^{S} ||\bar{\mathbf{h}}_j||^2 \left|(\cos\alpha)\cos\theta_{i,j} + (\sin\alpha)\ \mathbf{g}_i^H\tilde{\mathbf{h}}_j\right|^2 + \frac{\sigma^2}{P}},\end{aligned} \tag{5.25}$$

where the last step is obtained from $\cos\theta_{i,j} = \tilde{\mathbf{h}}_i^H\tilde{\mathbf{h}}_j$, and $\theta_{i,j}$ denotes the angle between the two effective channel vectors $\tilde{\mathbf{h}}_i$ and $\tilde{\mathbf{h}}_j$. The above equation indicates that the SINR depends on the angles between the two effective channel vectors. If the angle ($\theta_{i,j}$) is small, i.e., close to 0, the interference can be significant because $\cos\theta_{i,j}$ is large, and the SINR can thus be reduced. To enhance the SINR, we need to select users such that the angles between channel vectors are semi-orthogonal. □

5.3.3 Impact of Beam Patterns on User Selection Algorithm

The analog beam patterns considered can affect the performance of the proposed user selection algorithm. In this subsection, we analyze the impact of the analog beam pattern of the uniform antenna array on the algorithm. As shown in Fig. 5.5(a), the analog beam pattern of the uniform antenna array is symmetrical with respect to the y-axis; there is almost an extra beam direction for each desired beam direction. This can affect the performance of the proposed user selection algorithm. For example, from Fig. 5.5(a), if SID 009 is selected for both user 1 and user 2, at 0° and 180°, respectively, then the beam separation is zero, which does not lead to orthogonal vectors. In addition, if SID 009 is selected for user 1 and either SID 008 or SID 010 is selected for user 2 at a mirror-opposite

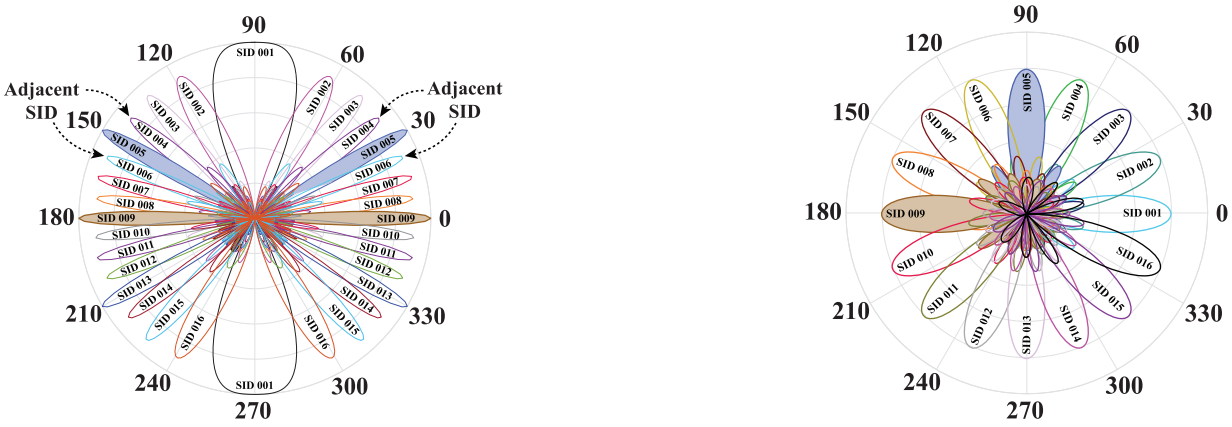

(a) Uniform linear array codebook.

(b) Circular codebook.

Figure 5.5: Antenna codebook beam patterns, where the number of beam patterns is 16.

position (0° or 180°), this can lead to minimal SID separation, and semi-orthogonality is not maintained. The same result holds for other beam patterns, such as SID 005.

Although the uniform antenna array can affect the performance of the proposed user selection, the probability (Q) of two selected users being simultaneously located at mirror-opposite positions or of one of the selected users being located at an SIDs adjacent to the other is very low when the number of beam patterns is large. Fig. 5.6 shows this probability (Q) for different numbers of beam patterns using the uniform antenna array. It can be seen that Q is very low for all scenarios where $A = 16$, $A = 8$, $K = 48$, and $K = 16$, and is almost zero when the number of beam patterns is 128. Therefore, the performance analysis and evaluation of the proposed user selection algorithm and HBF-VG algorithm here and in Section 5.4 will not be affected as long as the number of beam patterns considered is sufficiently large.

In general, while the proposed HBF-VG algorithm can operate in any codebook, performance depends on the analog beam pattern considered. Other predefined RF codebooks, such as the circular codebook [90], can be considered for future work in order to evaluate

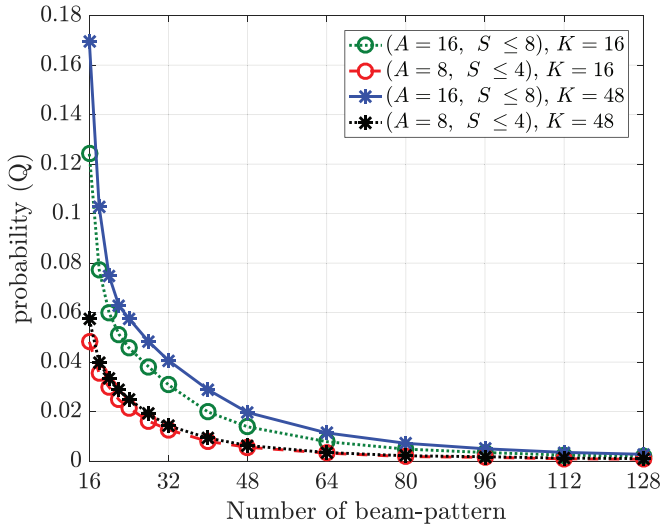

Figure 5.6: The probability (Q) for different numbers of beam patterns.

and compare algorithm performance. As shown in Fig. 5.5(b), the circular antenna array has beams that only focus on one direction, unlike the uniform antenna array [90]. In addition, the proposed user selection algorithm can be extended for future work to add a selection criterion that depends on the beam-pattern (separation of SIDs) at the AP.

5.3.4 Complexity Analysis of the User Selection

This subsection analyzes the computational complexity of the proposed user selection algorithm. To select a subset of users that locally maximizes the sum-power projection and hence grants zero interference, an exhaustive search is needed over a discrete set of size $\binom{K}{S}$ to find the optimal solution. The size and computation of the search space are prohibitively complex since mmWave propagation characteristics make a large number of antenna elements essential for mmWave communication. A large number of users (K) can also increase complexity since dense wireless networks are predicted in the near future. Therefore, the computational complexity of the optimal user selection solution is given by

$\mathcal{O}(K^S)$, a polynomial complexity [91]. However, a sub-optimal user selection solution is exploited by utilizing orthogonality as a selection metric. The computational complexity of the user selection of our proposed HBF-VG algorithm is hence reduced to $\mathcal{O}(A)$. In addition, the proposed user selection algorithm does not require collecting the perfect CSI for user selection. Traditional user selection methods in multi-user MIMO systems, including optimal and suboptimal schemes, do require this, thus creating significant overhead.

5.4 Performance Evaluation and Simulation Results

In this section, we conduct simulations to evaluate the performance of the proposed HBF-VG algorithm. First, the simulation set-up is introduced. Next, we evaluate the proposed algorithm with an optimal set of users in a simplified scenario. We then evaluate the average sum-rate performance of the proposed algorithm versus existing HBF algorithms. We also evaluate the energy efficiency performance of the proposed algorithm at the AP.

5.4.1 Simulation Setup

A Monte-Carlo simulation evaluates the proposed HBF-VG algorithm 50,000 times (simulating more than 2,000,000 BIs). For simplicity, our simulations do not account for the contention limitation of A-BFT; active users are assumed to always be available during A-BFT in every BI. The main performance criteria of this evaluation are the achievable sum rate of the selected users and the energy efficiency. The simulations adopt the channel model defined in [92, 93], a large-scale channel fading given by

$$PL(dB) = 20\log_{10}\left(\frac{4\pi D_0}{\lambda}\right) + 10n\log_{10}\left(\frac{D}{D_0}\right), \tag{5.26}$$

where D_0, D, and n are the free space reference distance, the propagation distance, and

Table 5.1: Simulation Parameters

Parameters	**Value**
Virtual sectors (A)	[8, 16]
Number of users (K)	8-64
AP antennas (N_r)	32-128
User antennas (N_t)	8-16
NLOS hall (n)	3.01
LOS hall (n)	2.17
LOS corridor (n)	1.64
Noise power spectral density	-134 dBm/MHz
System bandwidth	2.16 GHz
Central frequency (f)	60 GHz

the path loss exponent, respectively. Note that (5.26) holds for $D \geq D_0$. Users are uniformly distributed in the APs' coverage area. In this simulation, we consider various application scenarios, such as NLOS in a hall, LOS in a hall, and LOS in a corridor, based on the measurements of the mmWave indoor environment [84]. Table 5.1 summarizes the simulation set-up parameters used to derive the performance results. We use MATLAB software for the numerical analysis, executed on a computer with an Intel Core i7-8559U CPU and 32GB random access memory (RAM). The operating system is Windows 10.

We compare the proposed HBF-VG algorithm with an optimal set of users and the analog BF of the IEEE 802.11ad standard, denoted by HBF-Full-Search and Analog-BF, respectively. We also compare the existing HBF algorithms that employ the ZF method and do not consider the user selection algorithm (random selection) when the user population is large, such as [24], [44], [45] and [46]. For ease of representation, the existing HBF algorithm is denoted by HBF-Random.

Table 5.2: Simulation time in each run in seconds

Number of users (K)	HBF-VG $A = 8$, $S \leq 4$	HBF-VG $A = 16$, $S \leq 8$	HBF-Full-Search $S = 4$	HBF-Full-Search $S = 8$
8	0.19	0.19	0.29	0.17
16	0.21	0.21	2.10	32.05
24	0.22	0.22	11.23	1878.81
32	0.22	0.22	36.83	26062.27
40	0.22	0.22	93.16	203285.67 (2.35 days)
48	0.23	0.23	197.69	880930.79 (10.2 days)
56	0.23	0.23	372.15	not available
64	0.23	0.23	648.11	not available

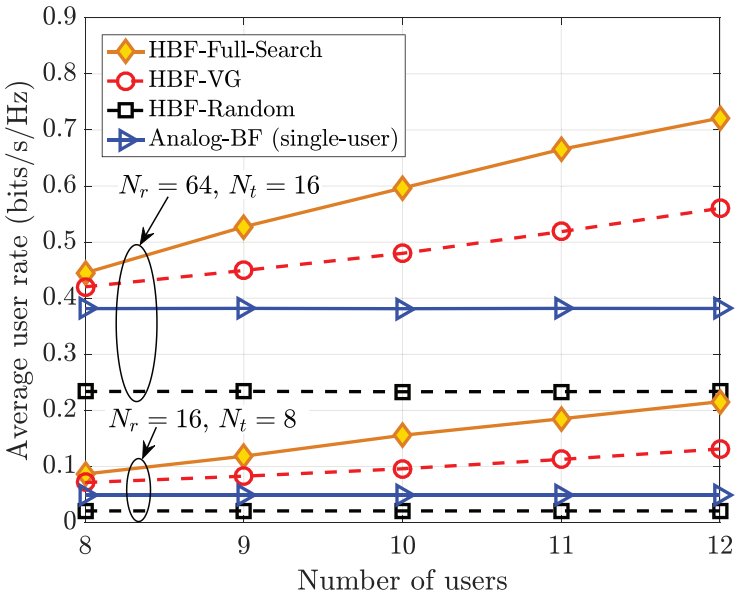

Figure 5.7: Average user rate versus the number of users ($n = 2.17$, SNR $=$ 30 dB, $S \leq 4$, $N_f = S$).

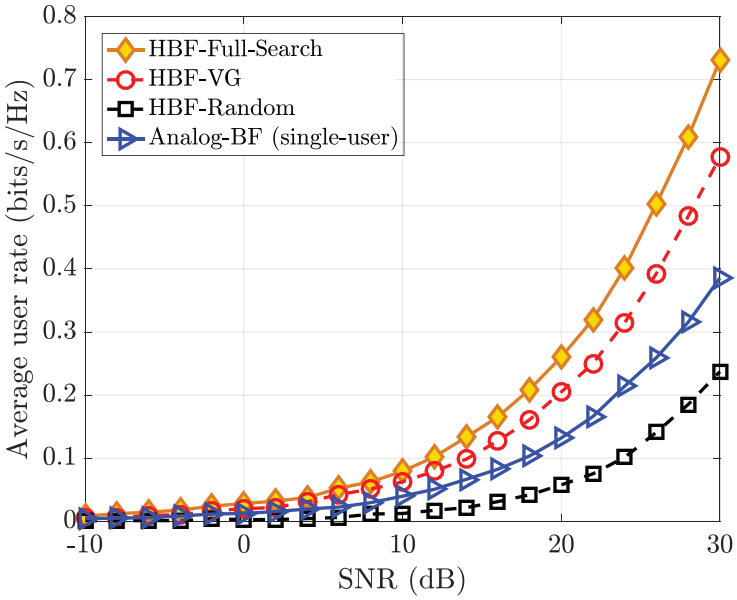

Figure 5.8: Average user rate versus the SNR ($K = 12$, $n = 2.17$, $N_r = 64$ $S \leq 4$, $N_f = S$).

5.4.2 Optimal Set of Users: Performance and Complexity Comparison

Our aim in this subsection is to benchmark the performance of the proposed HBF-VG algorithm in a simplified scenario against both HBF-Full-Search and Analog-BF. We also include HBF-Random in the performance comparison. The average user rate versus the number of users is shown in Fig. 5.7. We can see from this figure that HBF-Random is clearly outperformed by HBF-Full-Search, HBF-VG, and Analog-BF in both situations when $N_r = 64$, $N_t = 16$ and $N_r = 16$, $N_t = 8$. It can also be seen that HBF-Full-Search achieves the highest performance, as expected, at the cost of computational complexity. This performance gap is sacrificed for the low complexity of the proposed user selection algorithm. For example, for $K = 12$, $N_r = 64$, and $N_t = 16$, the proposed algorithm can achieve nearly 80% of the performance of HBF-Full-Search while performing much better than HBF-Random.

In Fig. 5.8, we show the average user rate versus SNR when $K = 12$. The proposed HBF-VG outperforms HBF-Random because of the proposed user selection algorithm and the SINR maximization approach used in digital BF. As expected, the user rate increases exponentially when SNR increases; better performance can be realized when the SNR is high. As with Fig. 5.7, HBF-Full-Search achieves the highest performance while HBF-Random has the lowest.

In Table 5.2, we illustrate the simulation time for each run in seconds. The simulation time of HBF-Full-Search is much higher than that of the proposed HBF-VG algorithm, and it increases significantly when the number of users increases. The simulation time becomes unfeasible, considering the capabilities of the device used, when the number of users is greater than 48 and $S = 8$. With these parameters, simulation time for HBF-Full-Search is more than 10 days, and up to 133 days, while the simulation time for the proposed algorithm is almost the same in all cases. Thus, the proposed algorithm run-time was not affected by the increased number of users in our experiments, and the computation time does not increase with the number of users.

5.4.3 Average Sum-Rate Performance

In this subsection, we compare the proposed HBF-VG with HBF-Random when $A = 16$ and $A = 8$. Different numbers of users are simulated in order to demonstrate the sum-rate performance in dense-deployment scenarios, as shown in Fig. 5.9. The proposed HBF-VG outperforms HBF-Random in both scenarios when the selected users are $S \leq 8$ and $S \leq 4$, and the sum-rate performance increases as K increases. Thus, higher performance can be achieved when K is large due to the higher probability of selecting users in the VG groups of the proposed user selection algorithm. Furthermore, a higher sum rate is obtained when $A = 16$ due to the higher spatial multiplexing gain, as discussed in Subsection 3.3.3.

Fig. 5.10 shows the impact of the number of antennas at the AP on sum-rate perfor-

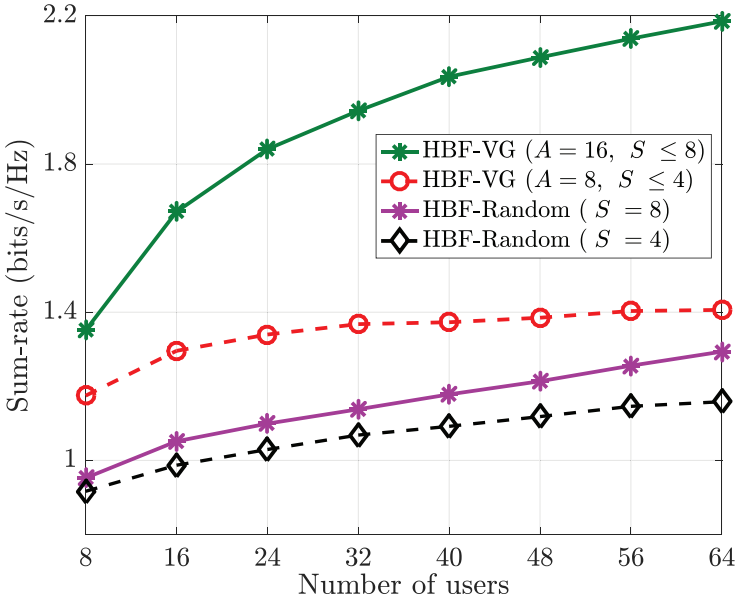

Figure 5.9: Sum rate versus the number of users ($N_r = 64$, $N_t = 16$, $n = 2.17$ SNR $=$ 30 dB, $N_f = S$).

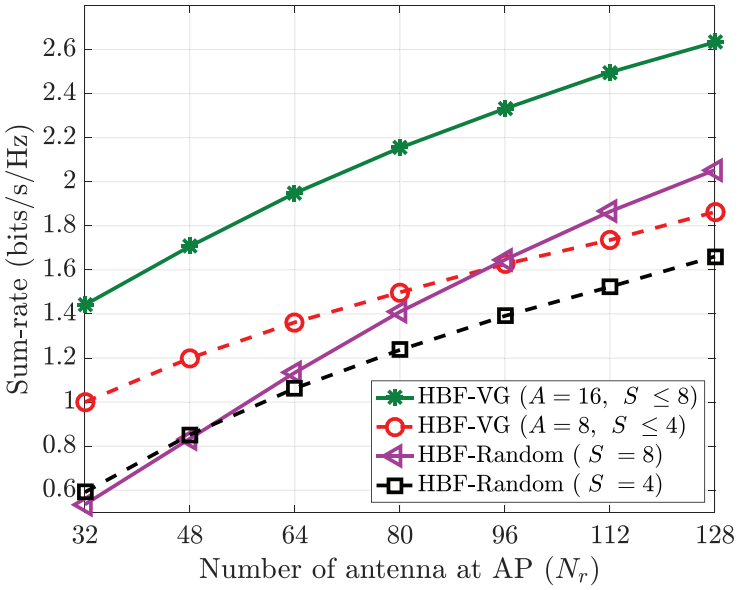

Figure 5.10: Sum rate versus the number of AP's antennas ($K = 32$, $N_t = 16$, $n = 2.17$ SNR $=$ 30 dB, $N_f = S$).

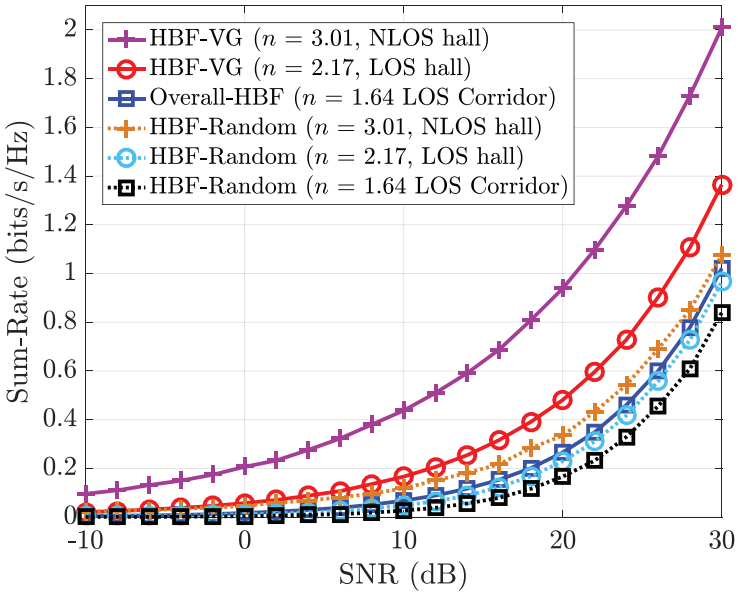

Figure 5.11: Sum rate versus SNR in different scenarios ($K = 32$, $S \leq 4$, $N_r = 64$, $N_t = 16$, $N_f = S$).

mance when $K = 32$. The proposed HBF-VG algorithm is compared with HBF-Random by considering both scenarios: when $S \leq 8$ and when $S \leq 4$. This figure shows that the proposed HBF-VG obtains the highest sum-rate performance, which increases as N_r increases. Furthermore, a higher sum-rate can also be obtained when the total number of VSs is 16, because of the spatial multiplexing gain.

In Fig. 5.11, we consider various path loss exponent scenarios based on mmWave measurements [84] in order to evaluate the sum-rate performance of our proposed HBF-VG algorithm versus SNR when $K = 32$ and $S \leq 4$. The proposed algorithm can achieve higher sum-rate performance than HBF-Random even with low SNR values due to the proposed user selection algorithm and the SINR maximization approach used in digital BF.

Table 5.3: Power consumption of the HBF and Analog BF architecture components

Component	Notation	Value
Combiner	P_C	19.5 mW
ADC	P_{ADC}	200 mW
Mixer	P_M	16.8 mW
Local oscillator	P_{LO}	5 mW
Low pass filter	P_{LPF}	14 mW
Power amplifier	P_{PA}	5 mW
Low noise amplifier	P_{LNA}	39 mW
Splitter	P_S	19.5 mW
Phase shifter	P_{PS}	2 mW

5.4.4 Energy Efficiency Performance

This subsection analyzes the energy efficiency performance of the proposed HBF-VG algorithm at the AP to demonstrate the impact of the power consumption of the analog-digital signal processing components of the HBF approach. The digital signal processing of the receiver components can consume a great deal of power due to the large number of antenna elements used in mmWave communication systems. Using a similar analytical approach as in [44] and [94], energy efficiency is defined as

$$E_{eff.} = \frac{R_{sum}}{P_{total}}, \tag{5.27}$$

where P_{total} is the total power consumption of the mmWave system at the AP. In order to compare total power consumption between HBF and analog BF, P_{total} represents the total power consumption at the AP of the HBF architecture approach (P_{total}^{HBF}) or of the

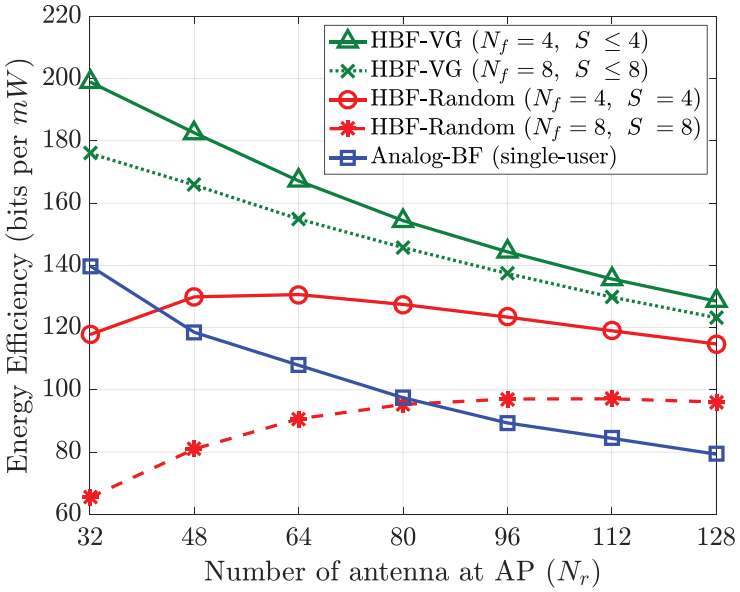

Figure 5.12: Energy efficiency performance at the AP versus the number of antennas ($K = 32$, $N_t = 16$, $n = 2.17$ SNR $= 30$ dB).

analog-only BF architecture approach (P_{total}^{ABF}).

$$P_{total}^{HBF} = N_f(P_1 + P_2 + P_4) + P_3 + P_5 \tag{5.28}$$

$$P_{total}^{ABF} = P_1 + P_2 + P_3 + P_4 \tag{5.29}$$

where $P_1 = P_C + 2P_{ADC}$ denotes the total power consumption in the baseband receiver, $P_2 = P_M + P_{LO} + P_{LPF} + P_{PA}$ denotes the total power consumption of each RF chain, $P_3 = N_r(P_{LNA})$ denotes the total power consumption of the low noise amplifiers (LNAs), $P_4 = N_r(P_{PS})$ denotes the total power consumption of the analog phase shifters, and $P_5 = N_r(P_S)$ denotes the total power consumption of the splitters. The power consumption components and their values are given in Table 5.3 [94, 95, 96, 97, 98, 99, 100].

In Fig. 5.12 and Fig. 5.13, the energy efficiency performance at the AP is shown by comparing the proposed HBF-VG algorithm, HBF-Random, and Analog-BF. Fig. 5.12

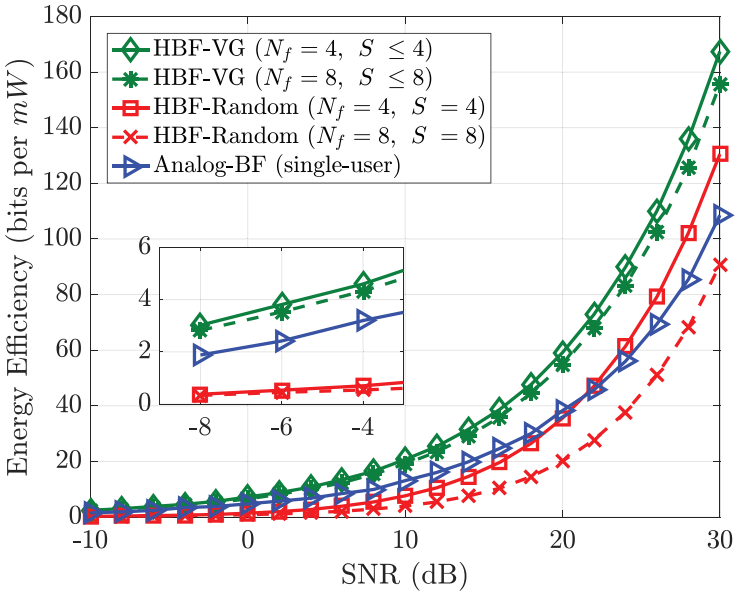

Figure 5.13: Energy efficiency performance at the AP versus the SNR ($K = 32$, $N_r = 64$, $N_t = 16$, $n = 2.17$).

shows energy efficiency versus the number of antennas (N_r) when $N_f = 4$ and $N_f = 8$ at SNR = 30 dB. We can see that the proposed HBF-VG algorithm outperforms both HBF-Random and analog BF. In addition, the analog BF offers higher energy efficiency than HBF-Random when the number of antennas (N_r) is small, since it only uses one RF chain. However, as N_r increases, the energy efficiency of analog BF decreases, and it offers the lowest energy efficiency when $N_r > 96$. It is worth noting that the number of RF chains and the number of antennas at the AP can impact energy efficiency as well as the SNR. Even though Analog-BF is independent of N_f, the proposed HBF-VG algorithm offers higher energy efficiency for both lower and higher SNRs, as shown in Fig. 5.13. Another observation from both Fig. 5.12 and Fig. 5.13 is that HBF-Random offers lower energy efficiency, especially in the low SNR region, where the interference mitigation of the ZF method comes at the cost of energy efficiency.

5.5 Summary

In this chapter, we have proposed a novel HBF-VG algorithm that incorporates user selection for uplink multi-user MIMO mmWave WLANs. A subset of users can be selected using semi-orthogonality, and the remaining interference among selected users can be canceled by optimizing the digital BF. Theoretical analysis shows that the computational complexity of the proposed algorithm can be reduced significantly. Simulation results show that the proposed HBF-VG algorithm can outperform existing solutions in terms of both average sum rate and energy efficiency. Even though the proposed algorithm is based on the IEEE 802.11ay, it can be generalized to work in other mmWave communication systems (e.g., 5G) that utilize analog BF and digital BF.

Chapter 6

Conclusions and Future Work

In this chapter, we summarize the research results and the contributions of the thesis and introduce several future research directions.

6.1 Conclusions

In this thesis, we proposed set of three efficient MAC layer algorithms, namely the VG, MHVG, and HBF-VG, for mmWave WLANs based on the IEEE 802.11ay system in order to meet the high throughput objective of the next generation wireless networks and to overcome the predicted global data traffic growth. The MAC layer algorithms were proposed to further improve the spectrum efficiency over mmWave bands by realizing simultaneous transmission and to mitigate the interference in different scenarios while keeping the computational complexity at a minimum level. The key contributions of this thesis are summarized as follows:

1. **Single-Hop Multi-User Transmission: MUI Perspective:** To realize simultaneous downlink transmission and to mitigate the MUI in a single hop, we proposed a

practical and efficient MAC protocol VG algorithm for IEEE 802.11ay in densely deployed WLAN scenarios. In this algorithm, the most perfect spatial users are selected based on analog BF information, where two methods were developed for the downlink transmission to avoid collecting the CSI. To investigate the successful simultaneous transmission, we evaluated the VG algorithm using the SINR, where the directed beamwidth angles of the simultaneous links are considered. It was shown that the proposed VG algorithm can achieve simultaneous downlink transmission and mitigate the MUI without adding extra feedback overhead to the system. The average throughput was improved while also reducing the transmission time allocation.

2. **Multi-Hop Multi-User Transmission: CCI Perspective:** To enhance the network performance while mitigating both the MUI within a single hop and CCI in a multi-hop scenario, we proposed an MHVG algorithm in a dense mDN. The interference is mitigated, and the complexity and overhead are kept at minimum levels by taking advantage of the spatial reuse in the MHVG algorithm, where the analog BF information is utilized instead of the of digital BF. To evaluate the performance of the MHVG algorithm, we analyzed the spatial multiplexing gain, which is the number of concurrent transmissions allowed over the same mmWave channel in a given area from the perspective of spatial reuse. The results of the evaluative simulations conducted demonstrate the superior performance offered by the proposed MHVG algorithm with respect to average throughput per time slot and spatial multiplexing gain.

3. **Low-Complexity Uplink Multi-User MIMO Algorithm:** To achieve uplink multi-user transmission in mmWave WLAN with a large user population, we proposed a low-complexity user selection algorithm, named HBF-VG, for IEEE 802.11ay. Three steps were developed in the HBF-VG algorithm. The user selection step is based on an orthogonality criterion of the VG algorithm to select simultaneous users

instead of collecting CSI from all potential users. To mitigate the residual interference among selected users, we optimized the digital BF. To study the impact of angle correlation and beam patterns on the achievable rate of the selected users, we have analytical validation for the proposed user selection algorithm and analyzed the computational complexity of the proposed algorithm. Moreover, to examine the effect of the RF chains implementation, we also evaluated the energy efficiency performance of the proposed HBF-VG algorithm. Extensive simulations were conducted to validate the proposed HBF-VG algorithm's performance with respect to both the average sum-rate of the system and energy efficiency in comparison to the existing HBF algorithms.

6.2 Future Research Directions

The proposed VG, MHVG, and HBF-VG algorithms in this thesis can be utilized to extend the research work in several directions. There are still several open research directions, including but not limited to the following.

6.2.1 Beam Tracking and Blockage Effect

The overhead generated from beam tracking is a challenge related to mmWave communication that arises because of the need for tracking the changes that occur in analog and baseband beams, e.g., due to mobility, RX rotation, or blockage. The blockage effect is also one of the main challenges associated with beam alignment in the mmWave communications, which can have many causes, including low-emissivity glass and high-density tree foliage. To overcome the challenges of beam tracking and the blockage effect, new and efficient beam tracking approaches are needed in order to guarantee the link robustness and quality of the user experience. Thus, in future work, the proposed VG algorithm

can be extended using a machine learning approach in order to find the optimal transmit-receive beam pair while keeping overhead at an acceptable level and by considering the beam alignment latency. In addition, employing analog tracking with limited digital baseband channel tracking can be investigated to develop an efficient mechanism to track beam changes between a TX and RX while reducing the complexity and overhead.

6.2.2 Interference and Energy Management for mmWave Distribution Networks

Maintaining efficient utilization of the mDN concept with ultra-dense deployment requires spatial and spectrum reuse, which negatively affects the end-user experience at cell boundaries due to CCI [25, 26, 27]. Furthermore, interference can be a crucial issue and can be difficult manage, especially for IEEE 802.11ay implementation, since it is a distributed network. Although the APs in an mDN essentially aim to serve applications that require high data rate and low latency, such as video streaming, some of these APs can be idle if there is no connection by users that require a high data rate. When APs are densely deployed in the mDN, scheduling idle APs to go into sleep mode can save energy. However, sleep scheduling can introduce a high cost if not managed well because the whole network needs to be considered. Therefore, the MHVG algorithm can be combined with a low-complex global optimization for managing interference, sleep scheduling, and radio resources in order to mitigate the interference and attain minimum energy consumption while improving the network performance.

6.2.3 Efficient Multi-User Uplink MIMO Transmission

MmWave communication requires advanced signal processing methods, such as the use of expensive power consuming wide-band ADCs or digital-to-analog converters (DACs)

for each antenna element. Thus, the high cost and power consumption of mmWave RF hardware elements are expected. As discussed in the thesis, it is true that the HBF design can be a solution to reduce the complexity of the mmWave multi-user MIMO transceivers; however, this hardware reduction is limited in the uplink scenario by the number of users that can be served. In the mmWave uplink multi-user MIMO, a large number of users is expected to be handled in denser deployment scenarios and applications, such as stadiums and airports, Internet of things (IoT), and vehicular communications.

Therefore, in future work, the proposed HBF-VG algorithm can be extended to have power selection allocation or priority-based resource allocation to handle large numbers of users in the multi-hop scenario and to reduce the energy consumption of the system while keeping the complexity at a minimum. The inter-cell interference problem also will be investigated for the uplink multi-user MIMO mmWave scenario when the coverages of several hops are overlapped by considering a clustering mechanism between a group of APs in a centralized or decentralized manner. Another possible solution for a large number of users in the uplink scenario is to combine the proposed HBF-VG algorithm with an orthogonal frequency division multiple access (OFDMA) mechanism in order to improve the resource allocation in dense deployment scenarios and to increase the per-user throughput by exploiting the frequency selective diversity gain. The OFDMA allocates different subsets of sub-carriers to different users and allows simultaneous multi-user transmission. OFDMA can be adapted in downlink and uplink communications, where interference mitigation among adjacent APs can be achieved through fractional frequency reuse. Thus, the question is how to design optimal beam selection, beam alignment, and resource allocation algorithms with low computation complexity when the proposed HBF-VG algorithm and OFDMA mechanism are combined.

References

[1] "Cisco visual networking index: Forecast and trends, 20172022," Cisco Systems Inc., San Jose, CA, White Paper, Updated: February, 2019. [Online]. Available: https://www.cisco.com/c/en/us/solutions/collateral/service-provider/visual-networking-index-vni/white-paper-c11-741490.pdf

[2] *IEEE Draft Standard for Information Technology–Telecommunications and Information Exchange Between Systems Local and Metropolitan Area Networks–Specific Requirements Part 11: Wireless LAN Medium Access Control (MAC) and Physical Layer (PHY) Specifications–Amendment: Enhanced Throughput for Operation in License-Exempt Bands Above 45 GHz*, IEEE P802.11ay/D2.0, July 2018, Standard.

[3] *Wireless LAN Medium Access Control (MAC) and Physical Layer (PHY) Specifications Amendment 3: Enhancements for Very High Throughput in the 60 GHz Band*, IEEE Std 802.11ad-2012, Standard, 2014.

[4] M. Marcus and B. Pattan, "Millimeter wave propagation: spectrum management implications," *IEEE Microwave Magazine*, vol. 6, no. 2, pp. 54–62, June 2005.

[5] W. Roh, J. Y. Seol, J. Park, B. Lee, J. Lee, Y. Kim, J. Cho, K. Cheun, and F. Aryanfar, "Millimeter-wave beamforming as an enabling technology for 5G cellular communications: theoretical feasibility and prototype results," *IEEE Communications Magazine*, vol. 52, no. 2, pp. 106–113, February 2014.

[6] T. S. Rappaport, J. N. Murdock, and F. Gutierrez, "State of the art in 60-GHz integrated circuits and systems for wireless communications," *Proceedings of the IEEE*, vol. 99, no. 8, pp. 1390–1436, August 2011.

[7] T. S. Rappaport, S. Sun, R. Mayzus, H. Zhao, Y. Azar, K. Wang, G. N. Wong, J. K. Schulz, M. Samimi, and F. Gutierrez, "Millimeter wave mobile communications for 5G cellular: It will work!" *IEEE Access*, vol. 1, pp. 335–349, May 2013.

[8] E. G. Larsson, O. Edfors, F. Tufvesson, and T. L. Marzetta, "Massive MIMO for next generation wireless systems," *IEEE Communications Magazine*, vol. 52, no. 2, pp. 186–195, February 2014.

[9] J. G. Andrews, S. Buzzi, W. Choi, S. V. Hanly, A. Lozano, A. C. K. Soong, and J. C. Zhang, "What will 5G be?" *IEEE Journal on Selected Areas in Communications*, vol. 32, no. 6, pp. 1065–1082, June 2014.

[10] "The zettabyte era: Trends and analysis," Cisco Systems Inc., San Jose, CA, White Paper, 2016.

[11] "iPass wi-fi growth map shows one public hotspot for every 20 people on earth by 2018," iPass Inc., Redwood Shores, CA, Tech. Rep., 2014.

[12] Z. Pi and F. Khan, "An introduction to millimeter-wave mobile broadband systems," *IEEE Communications Magazine*, vol. 49, no. 6, pp. 101–107, June 2011.

[13] J. Bae, Y. S. Choi, J. S. Kim, and M. Y. Chung, "Architecture and performance evaluation of MmWave based 5G mobile communication system," in *Proc. International Conference on Information and Communication Technology Convergence (ICTC)*, October 2014, pp. 847–851.

[14] C. Dehos, J. L. Gonzlez, A. D. Domenico, D. Ktnas, and L. Dussopt, "Millimeter-wave access and backhauling: the solution to the exponential data traffic increase in 5G mobile communications systems?" *IEEE Communications Magazine*, vol. 52, no. 9, pp. 88–95, September 2014.

[15] Y. Ghasempour, C. R. C. M. da Silva, C. Cordeiro, and E. W. Knightly, "IEEE 802.11ay: Next-generation 60 GHz communication for 100 Gb/s Wi-Fi," *IEEE Communications Magazine*, vol. 55, no. 12, pp. 186–192, December 2017.

[16] P. Zhou, K. Cheng, X. Han, X. Fang, Y. Fang, R. He, Y. Long, and Y. Liu, "IEEE 802.11ay-based mmWave WLANs: Design challenges and solutions," *IEEE Communications Surveys & Tutorials*, vol. 20, no. 3, pp. 1654–1681, third-quarter 2018.

[17] J. Wang, J. Liu, and L. Huang, "11ay DL MU-MIMO bf training and user selection," IEEE 802.11-16/0405r1, Tech. Rep., March 2016.

[18] Y.-C. Ko, M.-J. Kim, and J.-H. Lee, "Discussion on MU-MIMO based on hybrid beamforming system in 802.11ay," IEEE 802.11-15/0799r0, Tech. Rep., July 2015.

[19] K. JO, S. Park, H. Cho, J. Kim, S. Bang, and S.-G. Kim, "Multi beamforming in polarized channels for 11ay," IEEE 802.11-16/0092r1, Tech. Rep., January 2016.

[20] A. Maltsev, A. Pudeyev, I. Bolotin, and C. Cordeiro, "MU-MIMO schemes for NG60," IEEE 802.11-15/0356r0, Tech. Rep., March 2015.

[21] A. Alkhateeb, J. Mo, N. Gonzalez-Prelcic, and R. W. Heath, "MIMO precoding and combining solutions for millimeter-wave systems," *IEEE Communications Magazine*, vol. 52, no. 12, pp. 122–131, December 2014.

[22] M. N. Kulkarni, A. Ghosh, and J. G. Andrews, "A comparison of MIMO techniques in downlink millimeter wave cellular networks with hybrid beamforming," *IEEE Transactions on Communications*, vol. 64, no. 5, pp. 1952–1967, May 2016.

[23] O. E. Ayach, S. Rajagopal, S. Abu-Surra, Z. Pi, and R. W. Heath, "Spatially sparse precoding in millimeter wave MIMO systems," *IEEE Transactions on Wireless Communications*, vol. 13, no. 3, pp. 1499–1513, March 2014.

[24] A. Alkhateeb, G. Leus, and R. W. Heath, "Limited feedback hybrid precoding for multi-user millimeter wave systems," *IEEE Transactions on Wireless Communications*, vol. 14, no. 11, pp. 6481–6494, November 2015.

[25] E. Hossain, M. Rasti, H. Tabassum, and A. Abdelnasser, "Evolution toward 5G multi-tier cellular wireless networks: An interference management perspective," *IEEE Wireless Communications*, vol. 21, no. 3, pp. 118–127, June 2014.

[26] W. Nam, D. Bai, J. Lee, and I. Kang, "Advanced interference management for 5G cellular networks," *IEEE Communications Magazine*, vol. 52, no. 5, pp. 52–60, May 2014.

[27] A. Padaki, J. Mo, B. Ng, and C. Zhang, "Network simulations for FWA mesh distribution networks," IEEE 802.11-18/1086r0, Tech. Rep., July 2018.

[28] S. Singh, R. Mudumbai, and U. Madhow, "Interference analysis for highly directional 60-GHz mesh networks: The case for rethinking medium access control," *IEEE/ACM Transactions on Networking*, vol. 19, no. 5, pp. 1513–1527, October 2011.

[29] M. A. Maddah-Ali, A. S. Motahari, and A. K. Khandani, "Communication over MIMO X channels: Interference alignment, decomposition, and performance analysis," *IEEE Transactions on Information Theory*, vol. 54, no. 8, pp. 3457–3470, August 2008.

[30] R. W. Heath, N. Gonzlez-Prelcic, S. Rangan, W. Roh, and A. M. Sayeed, "An overview of signal processing techniques for millimeter wave MIMO systems," *IEEE Journal of Selected Topics in Signal Processing*, vol. 10, no. 3, pp. 436–453, April 2016.

[31] K. Aldubaikhy and X. Shen, "Simultaneous DL transmission in MmWave ultra dense networks: Inter-BSS interference prospective," in *Proc. IEEE International Conference on Communications Workshops (ICC Workshops)*, May 2018, pp. 1–6.

[32] X. Shen, K. Aldubaikhy, M. Wang, O. Aboul-Magd, K. S. Au, Y. Xin, and R. Sun, "Methods and systems for multi-user beamforming," UNITED STATES: Patent Application No. 15/360852, November 23, 2016.

[33] N. Anand, J. Lee, S. J. Lee, and E. W. Knightly, "Mode and user selection for multi-user MIMO WLANs without CSI," in *Proc. IEEE Conference on Computer Communications (INFOCOM)*, April 2015, pp. 451–459.

[34] X. Xie and X. Zhang, "Scalable user selection for MU-MIMO networks," in *Proc. IEEE Conference on Computer Communications (INFOCOM)*, April 2014, pp. 808–816.

[35] T. Yoo and A. Goldsmith, "On the optimality of multiantenna broadcast scheduling using zero-forcing beamforming," *IEEE Journal on Selected Areas in Communications*, vol. 24, no. 3, pp. 528–541, March 2006.

[36] W. L. Shen, K. C. J. Lin, S. Gollakota, and M. S. Chen, "Rate adaptation for 802.11 multiuser MIMO networks," *IEEE Transactions on Mobile Computing*, vol. 13, no. 1, pp. 35–47, January 2014.

[37] D. Tse and P. Viswanath, *Fundamentals of Wireless Communications*. Cambridge University Press, 2005.

[38] A. Zhou, T. Wei, X. Zhang, M. Liu, and Z. Li, "Signpost: Scalable MU-MIMO signaling with zero CSI feedback," in *Proc. the ACM International Symposium on Mobile Ad Hoc Networking and Computing*, vol. abs 1410.2609, June 2015, pp. 327–336.

[39] C. Wang and R. D. Murch, "Adaptive downlink multi-user MIMO wireless systems for correlated channels with imperfect CSI," *IEEE Transactions on Wireless Communications*, vol. 5, no. 9, pp. 2435–2446, September 2006.

[40] N. Czink, B. Bandemer, G. Vazquez-Vilar, L. Jalloul, C. Oestges, and A. Paulraj, "Spatial separation of multi-user MIMO channels," in *Proc. IEEE International Symposium on Personal, Indoor and Mobile Radio Communications (PIMRC)*, September 2009, pp. 1059–1063.

[41] K. Ko and J. Lee, "Low complexity multiuser MIMO scheduling with chordal distance," in *Proc. Conference on Information Sciences and Systems (CISS)*, March 2008, pp. 80–84.

[42] S. Kutty and D. Sen, "Beamforming for millimeter wave communications: An inclusive survey," *IEEE Communications Surveys Tutorials*, vol. 18, no. 2, pp. 949–973, Second-quarter 2016.

[43] Z. Wang, M. Li, X. Tian, and Q. Liu, "Iterative hybrid precoder and combiner design for mmwave multiuser MIMO systems," *IEEE Communications Letters*, vol. 21, no. 7, pp. 1581–1584, July 2017.

[44] X. Zhai, Y. Cai, Q. Shi, M. Zhao, G. Y. Li, and B. Champagne, "Joint transceiver design with antenna selection for large-scale MU-MIMO mmwave systems," *IEEE Journal on Selected Areas in Communications*, vol. 35, no. 9, pp. 2085–2096, September 2017.

[45] J. Choi, J. Mo, and R. W. Heath, "Near maximum-likelihood detector and channel estimator for uplink multiuser massive MIMO systems with one-bit ADCs," *IEEE Transactions on Communications*, vol. 64, no. 5, pp. 2005–2018, May 2016.

[46] J. Li, L. Xiao, X. Xu, and S. Zhou, "Robust and low complexity hybrid beamforming for uplink multiuser MmWave MIMO systems," *IEEE Communications Letters*, vol. 20, no. 6, pp. 1140–1143, June 2016.

[47] W. Wu, Q. Shen, K. Aldubaikhy, N. Cheng, N. Zhang, and X. Shen, "Enhance the edge with beamforming: Performance analysis of Beamforming-Enabled WLAN," in *Proc. IEEE International Symposium on Modeling and Optimization in Mobile, Ad Hoc and Wireless Networks (WiOpt)*, May 2018, pp. 1–6.

[48] P. Zhou, X. Fang, Y. Fang, Y. Long, R. He, and X. Han, "Enhanced random access and beam training for millimeter wave wireless local networks with high user density," *IEEE Transactions on Wireless Communications*, vol. 16, no. 12, pp. 7760–7773, December 2017.

[49] K. Johnsson and C. Cordeiro, "Scalable A-BFT," IEEE 802.11-16/1165r3, Tech. Rep., September 2016.

[50] Y. Xin, R. Sun, and O. Aboul-Magd, "Channel access in A-BFT over multiple channels," IEEE 802.11-16/0101r0, Tech. Rep., January 2016.

[51] M. Grigat, S. Sawhney, D. Tujkovic, S. Krauss, C. Lange, and O. Bonness, "mmWave distribution network usage model," IEEE 802.11-17/1019r2, Tech. Rep., July 2017.

[52] "Ieee 802.11 TGay use cases," IEEE 802.11-2015/0625r7, Tech. Rep., August 2017. [Online]. Available: https://mentor.ieee.org/802.11/dcn/15/11-15-0625-07-00ay-ieee-802-11-tgay-usage-scenarios.pptx

[53] B. Li, Z. Zhou, W. Zou, X. Sun, and G. Du, "On the efficient beam-forming training for 60GHz wireless personal area networks," *IEEE Transactions on Wireless Communications*, vol. 12, no. 2, pp. 504–515, February 2013.

[54] H. H. Lee and Y. C. Ko, "Low complexity codebook-based beamforming for MIMO-OFDM systems in millimeter-wave WPAN," *IEEE Transactions on Wireless Communications*, vol. 10, no. 11, pp. 3607–3612, November 2011.

[55] H. Shokri-Ghadikolaei, L. Gkatzikis, and C. Fischione, "Beam-searching and transmission scheduling in millimeter wave communications," in *Proc. IEEE International Conference on Communications (ICC)*, June 2015, pp. 1292–1297.

[56] J. Wang, Z. Lan, C. W. Pyo, T. Baykas, C. S. Sum, M. A. Rahman, R. Funada, F. Kojima, I. Lakkis, H. Harada, and S. Kato, "Beam codebook based beamforming protocol for multi-Gbps millimeter-wave WPAN systems," in *Proc. IEEE Global Telecommunications Conference (Globecom)*, November 2009, pp. 1–6.

[57] S. Hur, T. Kim, D. J. Love, J. V. Krogmeier, T. A. Thomas, and A. Ghosh, "Multilevel millimeter wave beamforming for wireless backhaul," in *Proc. IEEE Global Communications Conference Workshops (GC Wkshps)*, December 2011, pp. 253–257.

[58] L. Zhou and Y. Ohashi, "Efficient codebook-based MIMO beamforming for millimeter-wave WLANs," in *Proc. IEEE International Symposium on Personal, Indoor and Mobile Radio Communications (PIMRC)*, September 2012, pp. 1885–1889.

[59] *Amendment 2: Millimeter-wave-based Alternative Physical Layer Extension*, IEEE Std 802.15.3c-2009, Standard, 2009.

[60] S. Payami, M. Shariat, M. Ghoraishi, and M. Dianati, "Effective RF codebook design and channel estimation for millimeter wave communication systems," in *Proc. IEEE International Conference on Communication Workshop (ICCW)*, June 2015, pp. 1226–1231.

[61] G. Kwon, Y. Shim, H. Park, and H. M. Kwon, "Design of millimeter wave hybrid beamforming systems," in *Proc. IEEE Vehicular Technology Conference*, September 2014, pp. 1–5.

[62] Z. Zhou, J. Fang, L. Yang, H. Li, Z. Chen, and S. Li, "Channel estimation for millimeter-wave multiuser MIMO systems via PARAFAC decomposition," *IEEE Transactions on Wireless Communications*, vol. 15, no. 11, pp. 7501–7516, November 2016.

[63] T. E. Bogale, L. B. Le, A. Haghighat, and L. Vandendorpe, "On the number of RF chains and phase shifters, and scheduling design with hybrid analog digital beamforming," *IEEE Transactions on Wireless Communications*, vol. 15, no. 5, pp. 3311–3326, May 2016.

[64] "802.11ac MU-MIMO: Bridging the MIMO gap in wi-fi," Qualcomm Atheros, Inc., San Jose, CA, White Paper, January 2015.

[65] I. K. Son, S. Mao, M. X. Gong, and Y. Li, "On frame-based scheduling for directional mmWave WPANs," in *Proc. IEEE International Conference on Computer Communications (INFOCOM)*, March 2012, pp. 2149–2157.

[66] R. Mudumbai, S. K. Singh, and U. Madhow, "Medium access control for 60 GHz outdoor mesh networks with highly directional links," in *Proc. IEEE International Conference on Computer Communications (INFOCOM)*, April 2009, pp. 2871–2875.

[67] J. Qiao, X. Shen, J. W. Mark, and Y. He, "MAC-layer concurrent beamforming protocol for indoor millimeter-wave networks," *IEEE Transactions on Vehicular Technology*, vol. 64, no. 1, pp. 327–338, January 2015.

[68] Y. Niu, C. Gao, Y. Li, D. Jin, L. Su, and D. Wu, "Boosting spatial reuse via multiple-path multihop scheduling for directional mmWave WPANs," *IEEE Transactions on Vehicular Technology*, vol. 65, no. 8, pp. 6614–6627, August 2016.

[69] P. Xu and H. Chu, "A novel link scheduling strategy for concurrent transmission in mmWave WPANs based on beamforming information," in *Proc. IEEE Wireless Communications and Networking Conference (WCNC)*, April 2014, pp. 1709–1714.

[70] H. Yu, O. Bejarano, and L. Zhong, "Combating inter-cell interference in 802.11ac-based multi-user MIMO networks," in *Proc. Annual International Conference on Mobile Computing and Networking*, September 2014, pp. 141–152.

[71] K. Ishihara, T. Murakami, Y. Asai, Y. Takatori, and M. Mizoguchi, "Cooperative inter-cell interference mitigation scheme with downlink MU-MIMO beamforming for dense wireless LAN environment," *Wireless Personal Communications*, vol. 93, no. 3, pp. 661–674, April 2017.

[72] T. Murakami, R. Kudo, K. Ishihara, N. Honma, and M. Mizoguchi, "Cooperative interference management by beam tilt and power controls in an indoor multi-cell environment," in *Proc. European Conference on Antennas and Propagation (EuCAP)*, April 2013, pp. 643–647.

[73] R. Liao, B. Bellalta, M. Oliver, and Z. Niu, "MU-MIMO MAC protocols for wireless local area networks: A survey," *IEEE Communications Surveys Tutorials*, vol. 18, no. 1, pp. 162–183, First-quarter 2016.

[74] *802.11 Task Group ax (TGax)*. [Online]. Available: http://www.ieee802.org/11/Reports/tgax_update.htm

[75] T. Tandai, H. Mori, K. Toshimitsu, and T. Kobayashi, "An efficient uplink multiuser MIMO protocol in ieee 802.11 WLANs," in *Proc. IEEE International Symposium on Personal, Indoor and Mobile Radio Communications*, September 2009, pp. 1153–1157.

[76] H. Jin, B. C. Jung, H. Y. Hwang, and D. K. Sung, "Performance comparison of uplink WLANs with single-user and multi-user MIMO schemes," in *Proc. IEEE Wireless Communications and Networking Conference*, March 2008, pp. 1854–1859.

[77] K. Tan, H. Liu, J. Fang, W. Wang, J. Zhang, M. Chen, and G. M. Voelker, "SAM: Enabling practical spatial multiple access in wireless LAN," in *Proc. Annual International Conference on Mobile Computing and Networking*, September 2009, pp. 49–60.

[78] S. Wu, W. Mao, and X. Wang, "Performance study on a CSMA/CA-based MAC protocol for multi-user MIMO wireless lans," *IEEE Transactions on Wireless Communications*, vol. 13, no. 6, pp. 3153–3166, June 2014.

[79] W. L. Huang, K. B. Letaief, and Y. J. Zhang, "Joint channel state based random access and adaptive modulation in wireless LANs with multi-packet reception," *IEEE*

Transactions on Wireless Communications, vol. 7, no. 11, pp. 4185–4197, November 2008.

[80] S. Zhou and Z. Niu, "An uplink medium access protocol with SDMA support for multiple-antenna WLANs," in *Proc. IEEE Wireless Communications and Networking Conference*, March 2008, pp. 1809–1814.

[81] D. Jung, R. Kim, and H. Lim, "Asynchronous medium access protocol for multi-user MIMO based uplink WLANs," *IEEE Transactions on Communications*, vol. 60, no. 12, pp. 3745–3754, December 2012.

[82] *802.11 Task Group ay (TGay)*. [Online]. Available: http://www.ieee802.org/11/Reports/tgay_update.htm

[83] A. Maltsev, "Channel models for 60 GHz WLAN systems," IEEE 802.11-09-0344-07ad, Tech. Rep., March 2010.

[84] S. Geng, J. Kivinen, X. Zhao, and P. Vainikainen, "Millimeter-wave propagation channel characterization for short-range wireless communications," *IEEE Transactions on Vehicular Technology*, vol. 58, no. 1, pp. 3–13, January 2009.

[85] M. R. Akdeniz, Y. Liu, M. K. Samimi, S. Sun, S. Rangan, T. S. Rappaport, and E. Erkip, "Millimeter wave channel modeling and cellular capacity evaluation," *IEEE Journal on Selected Areas in Communications*, vol. 32, no. 6, pp. 1164–1179, Jun. 2014.

[86] Y. Shabara, C. E. Koksal, and E. Ekici, "Linear block coding for efficient beam discovery in millimeter wave communication networks," in *Proc. IEEE Conference on Computer Communications (INFOCOM)*, Apr. 2018, pp. 2285–2293.

[87] A. Tarighat, M. Sadek, and A. H. Sayed, "A multi user beamforming scheme for downlink MIMO channels based on maximizing signal-to-leakage ratios," in *Proc. IEEE International Conference on Acoustics, Speech, and Signal Processing (ICASSP)*, March 2005, pp. 1129–1132.

[88] T. Yoo, N. Jindal, and A. Goldsmith, "Multi-antenna downlink channels with limited feedback and user selection," *IEEE Journal on Selected Areas in Communications*, vol. 25, no. 7, pp. 1478–1491, September 2007.

[89] K. Scharnhorst, "Angles in complex vector spaces," *Acta Applicandae Mathematicae*, vol. 69, no. 1, pp. 95–103, October 2001.

[90] Wei Feng, Zhenyu Xiao, Depeng Jin, and Lieguang Zeng, "Circular-antenna-array-based codebook design and training method for 60GHz beamforming," in *Proc. IEEE Wireless Communications and Networking Conference (WCNC)*, Apr. 2013, pp. 4140–4145.

[91] D. Gesbert, M. Kountouris, R. W. Heath, C. Chae, and T. Salzer, "Shifting the MIMO paradigm," *IEEE Signal Processing Magazine*, vol. 24, no. 5, pp. 36–46, September 2007.

[92] G. R. MacCartney and T. S. Rappaport, "Rural macrocell path loss models for millimeter wave wireless communications," *IEEE Journal on Selected Areas in Communications*, vol. 35, no. 7, pp. 1663–1677, Jul. 2017.

[93] W. Wu, N. Zhang, N. Cheng, Y. Tang, K. Aldubaikhy, and X. Shen, "Beef up mmwave dense cellular networks with D2D-assisted cooperative edge caching," *IEEE Transactions on Vehicular Technology*, vol. 68, no. 4, pp. 3890–3904, Apr. 2019.

[94] W. B. Abbas, F. Gomez-Cuba, and M. Zorzi, "Millimeter wave receiver efficiency: A comprehensive comparison of beamforming schemes with low resolution ADCs," *IEEE Transactions on Wireless Communications*, vol. 16, no. 12, pp. 8131–8146, December 2017.

[95] R. Mndez-Rial, C. Rusu, N. Gonzlez-Prelcic, A. Alkhateeb, and R. W. Heath, "Hybrid MIMO architectures for millimeter wave communications: Phase shifters or switches?" *IEEE Access*, vol. 4, pp. 247–267, January 2016.

[96] Y. Yu, P. G. M. Baltus, A. de Graauw, E. van der Heijden, C. S. Vaucher, and A. H. M. van Roermund, "A 60 GHz phase shifter integrated with LNA and PA in 65 nm CMOS for phased array systems," *IEEE Journal of Solid-State Circuits*, vol. 45, no. 9, pp. 1697–1709, September 2010.

[97] Y.-H. Lin and H. Wang, "A low phase and gain error passive phase shifter in 90 nm CMOS for 60 GHz phase array system application," in *Proc. IEEE International Microwave Symposium (IMS)*, May 2016, pp. 1–4.

[98] M. Kraemer, D. Dragomirescu, and R. Plana, "Design of a very low-power, low-cost 60GHz receiver front-end implemented in 65nm CMOS technology," *International Journal of Microwave and Wireless Technologies*, vol. 3, no. 2, p. 131138, March 2011.

[99] N. Deferm and P. Reynaert, *CMOS Front Ends for Millimeter Wave Wireless Communication Systems*. Springer International, Jan. 2015.

[100] R. Mndez-Rial, C. Rusu, N. Gonzlez-Prelcic, A. Alkhateeb, and R. W. Heath, "Hybrid MIMO architectures for millimeter wave communications: Phase shifters or switches?" *IEEE Access*, vol. 4, pp. 247–267, Jan. 2016.

Appendix List of Publications

1. **K. Aldubaikhy**, W. Wu, N. Zhang, N. Cheng, and X. Shen, "MmWave IEEE 802.11ay for 5G Fixed Wireless Access," *IEEE Wireless Communications Magazine*, accepted.

2. **K. Aldubaikhy**, W. Wu, Q. Ye, and X. Shen, "Low-Complexity User Selection Algorithm for Multiuser Transmission in mmWave WLANs," *IEEE Transactions on Wireless Communications*, under minor review.

3. W. Wu, N. Zhang, N. Cheng, Y. Tang, **K. Aldubaikhy** and X. Shen, "Beef Up mmWave Dense Cellular Networks With D2D-Assisted Cooperative Edge Caching," *IEEE Transactions on Vehicular Technology*, vol. 68, no. 4, pp. 3890-3904, April 2019.

4. **K. Aldubaikhy**, W. Wu, and X. Shen, "HBF-PDVG: Hybrid beamforming and user selection for UL MU-MIMO mmWave systems," in *Proc. IEEE Global Communications Conference (Globecom)*, December 2018, pp. 1-6.

5. **K. Aldubaikhy** and X. Shen, "Simultaneous DL transmission in MmWave ultra dense networks: Inter-BSS interference prospective," in *Proc. IEEE International Conference on Communications (ICC)*, May 2018, pp. 1-6.

6. W. Wu, Q. Shen, **K. Aldubaikhy**, N. Cheng, N. Zhang, and X. Shen, "Enhance the edge with beamforming: Performance analysis of Beamforming-Enabled WLAN," in *Proc. IEEE International Symposium on Modeling and Optimization in Mobile, Ad Hoc and Wireless Networks (WiOpt)*, May 2018, pp. 1-6.

7. **K. Aldubaikhy**, Q. Shen, M. Wang, W. Wu, X. Shen, O. Aboul-Magd, Y. Xin, R. Sun, and E. Au, "MAC layer design for concurrent transmissions in millimeter wave WLANs," in *Proc. IEEE/CIC International Conference on Communications in China (ICCC)*, October 2017, pp. 1-6.

8. X. Shen, **K. Aldubaikhy**, M. Wang, O. Aboul-Magd, K. S. Au, Y. Xin, and R. Sun, "Methods and systems for multi-user beamforming," UNITED STATES: Patent Application No. 15/360852, November 23, 2016.